

# UNIVERSITÀ DI PISA



Università degli Studi di Pisa  
Facoltà di Scienze Matematiche Fisiche e Naturali  
Corso di Laurea Magistrale in Fisica

## In Silico Model of Neuron-Glia Interaction

**Supervisors:**

Dr. Alberto Mazzoni  
Prof. Angelo Di Garbo

**Tutor:**

Dr. Nicolò Meneghetti

**Candidate:**

Angelo Lasala

Academic Year 2021/2022

# Extended Abstract

Since their discovery at the beginning of the nineteen century, glial cells have been the subject of growing interest in the field of neuroscience, due to the number of biological processes that they perform and their high level of connectivity with neural cells. Among glial cells, a prominent role in the modulation of neural activity is played by astrocytes. However, our knowledge of the basic mechanism involved in the reciprocal modulation between astrocytes and neurons is not complete. The neuron-astrocyte network is a clear example of complex system in which the nonlinearity and coupling properties shape its whole dynamical behaviour.

The present thesis aims to fill the gap between microscopic and mesoscopic descriptions of the interplay between neurons and astrocytes.

The work is presented in five main chapters. The first one is a general overview of neural and glial physiology. More specifically, the neuron-glia interaction at the synaptic level and the regulation of the released neurotransmitters are the evidence that the non-neuronal cells must be included in the models for a more accurate description of the human brain functionality. In the second chapter, the adopted mathematical models of the brain's elements are described, as well as the method used to derive insight information of synaptic transmission and network dynamics.

Afterwards, we present the analysis of the microscopic and mesoscopic levels of description. Chapter 3 is dedicated to the tripartite synapses. At the beginning, it is reported the well-described scenario of simple bipartite and open-loop tripartite synapses. Starting from these results we investigate the effect of gliomodulation in homosynaptic connection and deduce a possible procedure to its mean field description. In Chapter 4 we focus on the network dynamics. For the sake of clarity, we describe both neuron and neuron-glia models to investigate the:

- effects of short-term plasticity in excitatory/inhibitory neural network;
- effects of a single activation of astrocyte in neuron-glia network;
- long-term effects induced by glial cells in neuron-glia network.

The original results obtained in this thesis concern the description of the mean field procedure of homosynaptic transmission, the modulation of excitatory/inhibitory balance and the regulation of network oscillations induced by persistent astrocytic activity. More specifically, we identify a glia-induced frequency filtering of periodic external input. In conclusion, we propose future perspectives that arise from the presented work aiming to improve the knowledge of the functional activity of human brain domains.

# Summary

## Background

It is commonly accepted that neurons are the main protagonist in the functional and anatomical organization of the human brain. However, they can not accomplish complex cognitive processes without the presence of another non-neuronal cell type: the glial cells. Glia is physically collocated in proximity to neurons and, due to elaborate anatomical and functional branches organization, performs vital biological tasks. These include but are not exhaustive in the homeostatic regulation of extracellular ions concentrations, blood vessel-neuron interface and related feeding mechanism, immune function and modulation/regulation of signalling transmissions among neurons [1]. In particular, the latter aspect might underline that glial cells are not simple onlookers in information transmission but, beside the neurons, be a unit process that takes part actively in the encoding mechanism of external stimuli. Nevertheless, in the field of neuroscience and especially computational neuroscience, the functional role of this type of cell is only partially explored. During the last twenty years, several models composed of several coupled ordinary differential equations are developed to dynamically describe the bidirectional coupling between the synaptic and glial activity [11, 15]. Despite the chance of a detailed microscopic portrait, the mesoscopic level of description still lacks an overview thereby glia are dealt with their physiological features.

The purpose of the present thesis is, following a bottom-up approach, to deeply investigate the neuron-glia interaction and try to build a bridge between the microscopic and mesoscopic levels of description. This link might shed light on a possible new mechanism of signalling transmission and explain some current incongruent results in computational neuroscience. Accordingly, the analyses lie in two interconnected steps. In the beginning, we characterize all the dynamic aspects of the unit element, the so-called tripartite synapse that embeds the bidirectional coupling between neuronal (in particular synaptic) and glial activity. Then, starting with these results, extend the description to the neuron-glia network, namely an ensemble of neurons where the connections are provided by tripartite synapse. In particular, in the first part, we use the methods of nonlinear dynamical theory to elucidate the behaviour induced by glial cells at the synaptic level. In the second part, we want to underline if these emerging features affect also the mesoscopic quantities in network dynamics. In both cases, numerical and approximation are suitable tools to accomplish the prefixed goals.

## Simulations and Analysis overview

We perform the simulation of the dynamical model with a suitable integration scheme, described in section 2.2. The conductance-based integrate and fire model (section 2.1.1) is

simulated by the second-order Rouge-Kutta algorithm with an integration step of 0.05 ms. The astrocytic dynamics (section 2.1.3), are reproduced with the same integration scheme with a time step equal to 0.01 s. For the latter one, we analyse the well-described picture of the model present in the literature to have a broad and overreaching comprehension of the underpinning phenomena. In particular, the bifurcation plot summarizes the dynamical features of a model concerning the variation of control parameters (section 1.2). The general framework to compute a bifurcation plot is the following: evaluate the dynamical variable for different values of control parameters, neglect from the data a transient time, select from the signal a particular value (extreme or null values) and finally plot this data regarding the value of control parameters.

In the case of noisy systems, we evaluate the values of interest for 30 different realizations of the noise. The respective quantities are represented as mean and standard error to quantify the variability induced by the noise term<sup>1</sup>. We use a similar procedure to evaluate the filter characteristic curve of bipartite and tripartite synapses. For each value of the input stimulus, we calculate the quantity of interest (sections 3.1 and 3.2) for 30 different trials. Then, we present the result as mean and standard error. In this case, we can also derive the mean filed description of the system (section 1.2).

The variable's time course and the bifurcation plots can be used to individuate periodic patterns in the signals. In this context, the spectral analysis provides a quantitative tool to validate the presence of dominant frequencies. Then, the oscillation periods are computed by taking the time interval between the presentation of the same value into the time series.

The aforementioned integration schemes are used also in the simulation of network dynamics. The mesoscopic quantities such as the firing rate and the Local Field Potential (section 1.3 and 4.1) are estimated from the activity of the neurons. The former signal is the average value of neural spikes activity in a time window of 5 ms, obtained from a Gaussian filter from the activity evaluated on the integration time steps of 0.05 ms. The latter is evaluated from the neuron dynamics recorded each 10 ms. In the first stage, the effect induced by glial cells is quantified as the variation over time of the mean values of these measurements. Then, the spectral analysis through Continuous Wavelet Transform (CWT) described in section 2.4.1 is computed to estimate the changes in the frequency domain. In detail, the activity is evaluated for a 100 s long time simulation. The CWT is applied to the whole signal. The astrocytes are activated after 15 s, this guarantees the separation in time of baseline (signal without astrocytic activity) and signal of interest (signal in the presence of astrocytic activity). Then, the time-frequency matrix from CWT is averaged on 5 – 15 s time window for the baseline, and 50 – 90 s for the signal of interest. Therefore, the modulation is quantified as the percentage decrease of the spectral power densities between the two signals (section 2.4.2). This procedure is employed for 5 different realizations to represent the power spectrum as mean and standard error.

---

<sup>1</sup>We perform the bifurcation analysis for several systems to highlight different behaviours. The parameters such as time simulation, transient time as well as measured quantities are presented in the caption of relative figures.

## Highlights

In the present thesis, we investigate the functional role of glial cells in the signalling transmission at the microscopic and mesoscopic levels of description.

In the first part, we built a numerical framework to analyse the model of the bipartite and tripartite synapses. This procedure ables us to point out the main mechanism of interplay between neurons and glial cells. More specifically, the astrocyte dynamics induce a degree of freedom in the basal release probability of simple short-term plasticity synapses. This is achieved by the release of neuroactive chemicals from the astrocytic processes, namely the gliotransmitters. In this scenario, the synapses can dynamically switch their transmission modality, changing from facilitating transmission to depressing one. In the former, the release of neurotransmitters increases with the incoming action potential, conversely in the latter one. In the first part of analysis, we underline how the strength of functional interaction and the characteristic time course of astrocyte affect the synaptic transmission:

1. the effect induced by astrocytic activity increases with a higher value of the gliotransmitter release. The facilitating transmission occurs on larger time windows for intense gliotransmitters release;
2. astrocytic parameters that regulate the modulation of basal release probability characterize how the system tends toward its baseline condition. Importantly, this time scales (order of tons of second) are larger than the neural one (order of milliseconds).

The functional relation between the release of neurotransmitters and the presynaptic action potential limps the physiological aspects of the tripartite synapse. The intricate coupling pathway of interaction makes the mathematical manipulation considerably demanding. However, starting from bifurcation analysis we propose a mean field description of homosynaptic connection that can reproduce the bell shape of the filtering characteristic curve.

In the second part, we extend the focus on the neuron-glia network. Once obtained the information regarding the synaptic level of description, the further step is to investigate the possible effect on network dynamics. In particular, to deeply characterize both neuron and neuron-glia networks, we consider a flexible model that makes the analysis dependent not only on dynamical properties but also on the network's structure. Interesting, the preliminary analysis suggests that the depletion induced by plasticity synapses increases the network activity at the baseline condition, i.e. without gliomodulation. Thereafter, the modulation due to the presence of astrocytic activity is investigated by looking at the mesoscopic quantities like population firing rate and Local Field Potential (LFP). According to the results of tripartite synapses, we perform the analysis for long-time simulation thereby we notice that:

1. a gliorelease event drops the firing activity of excitatory neurons;
2. the persistent astrocytic activity alters the recurrent excitatory current and the excitatory/inhibitory network balance.

The latter evidence might be considered a clue for a novel encoding mechanism performed by the neural domains. To validate this hypothesis we perform a spectral analysis on LFP

to spotlight possible changes in power spectral densities due to astrocytic activity. In this context, the original result concerns the modulation of periodic external stimuli regarding the amplitude. Specifically, the power spectrum for the input of 0.5 Hz and 20.0 Hz decreases in the presence of persistent astrocytic activity that occurs only for low amplitude values.

Overall, the framework presented in this thesis may be exploited to further investigation. Indeed, the results and the procedures might shed light on both the functional and pathological activity of human brain domains that are not completely understood in the context of the classical neuron paradigm.

# Contents

<b>Extended Abstract</b>	<b>i</b>
<b>Summary</b>	<b>ii</b>
<b>1 INTRODUCTION</b>	<b>1</b>
1.1 Functional role of Glial Cells . . . . .	1
1.2 Brain Cells as Dynamical Systems . . . . .	6
1.2.1 Bifurcation Theory . . . . .	8
1.2.2 Noisy Systems and Mean Field Description . . . . .	9
1.3 Spiking Neural Model . . . . .	11
<b>2 METHODS AND MODELS</b>	<b>15</b>
2.1 Brain cells and their mathematical models . . . . .	15
2.1.1 Neurons . . . . .	15
2.1.2 Synapses . . . . .	18
2.1.3 Astrocytes . . . . .	21
2.1.4 Gliotransmission modulation of synaptic release . . . . .	27
2.2 Numerical Method . . . . .	29
2.3 Poisson spike trains . . . . .	31
2.4 Spectral Analysis . . . . .	31
2.4.1 Continuous Wavelet Transform (CWT) . . . . .	31
2.4.2 Wavelet Power Spectrum and Modulation . . . . .	32
<b>3 RESULTS: INTERPLAY BETWEEN NEURONAL AND GLIAL CELLS</b>	<b>34</b>
3.1 Bipartite Synapse . . . . .	34
3.2 Tripartite Synapses . . . . .	36
3.2.1 Heterosynaptic Connection - open loop . . . . .	37
3.2.2 Homosynaptic Connection - closed loop . . . . .	41
3.2.3 Mean field description of homosynaptic connection . . . . .	48
<b>4 RESULTS: NEURON-GLIA NETWORKS</b>	<b>56</b>
4.1 Network Model . . . . .	56
4.1.1 Poisson Heterogeneity . . . . .	58
4.2 STP influence on E/I Network . . . . .	59
4.2.1 Heterogeneity of the external connectivity $s$ and degrees of balance $g$ . . . . .	61
4.3 Activation of Gliorelease events . . . . .	64
4.4 Long-Term effect of gliomodulation . . . . .	69
4.5 Network Oscillations . . . . .	71

<b>5 CONCLUSIONS</b>	<b>77</b>
<b>A Mean field approximation</b>	<b>80</b>
A.1 Validity of Mean Field Description . . . . .	80
<b>B Supplementary numerical material</b>	<b>82</b>
B.1 Description of the code . . . . .	82
B.2 Neuron-glia network implementation and simulation . . . . .	84
B.3 Integration steps . . . . .	86
<b>C Parameters</b>	<b>89</b>
C.1 Neurons ans Synapses . . . . .	89
C.2 Astrocyte . . . . .	90
<b>Bibliography</b>	<b>90</b>

# Chapter 1

## INTRODUCTION

In this chapter, we introduce the main physiological aspects of the glial cells and the theoretical framework used to study them. The important role of the glial cells, and especially astrocytes, emerges from the evidence of large biological tasks that these non-neuronal cells accomplish in the Central Nervous Systems (CNS). Among these mechanisms, we emphasize the functional role in signal transmission and the necessity to deal with the interplay between neurons and glia to represent the real encoding process of an external stimulus. From a physics point of view, brain elements are nonlinear dynamical systems that interact with each other. Accordingly, we sketch the theoretical setting to describe these coupled systems and the possibility to arise collective phenomenon from the interaction of several unit elements.

### 1.1 Functional role of Glial Cells

The functional and anatomical complexity makes the human brain one of the most complex systems in the universe. It continuously elaborates sensory stimuli from the environment, interfacing with it through several cognitive processes, and controls the internal activities of the entire body. Furthermore, it regulates high-level mechanisms such as consciousness and sensations. The study of the Central Nervous System (CNS), due to the intricate and variegated tasks accomplished by the brain, encompasses different levels of analysis, for instance, chemical, molecular, anatomical, and cognitive. Therefore it has always been an interdisciplinary subject to study.

The discovery of neural morphology by Santiago Ramón y Cajal, Nobel Prize in Medicine in 1906, has put the stage for current knowledge of neural systems through the common efforts from different fields such as anatomy, biochemistry, physics as well as medicine and psychology. Typically a neuron is composed of three functional parties: dendrites, the soma and the axon. Soma is the body of the neuron and contains the nucleus of the cell, dendrites are the extensions of the cell and carry input information to the neurons and the axons are the branches of output communication. In neurons, the ionic channels located on the soma, but also on dendrites and axons, provide the fluxes of ions through the cell membrane. The electrical potential difference across the membrane arises from these fluxes is called the membrane potential. Nowadays it is clear that neurons communicate with each other by the propagation of action potential, an abrupt increase of membrane potential due to the encoding mechanism of external inputs employed by the soma. Furthermore, a widely assumed premise is that most cognitive

processes emerge from the activity of ensembles of neurons, whose dynamics arise from complex interactions and connection involving single elements. The chemical synapses are the most common structure in the neural system that provide these interactions by the release of specific chemicals called neurotransmitters from the presynaptic neurons that bind with the receptors in the postsynaptic neurons causing either depolarization (decreasing of membrane potential) or hyperpolarization (increasing of membrane potential) of their membrane potential.

Sophisticated processing of sensory information and, more in general, the ability to respond to external stimuli is a feature that humans share with most animals, resulting from the development of the complex neural structure. From a phylogenetic perspective, as the nervous systems changed from simple net structure (invertebrates) to condensed centralized brains (vertebrates), a new cell type could be recognized in morphological studies: *glial cells* [2].

It is customary to credit pathologist Virchow with the discovery of glia. Following the idea that only connective tissue is capable of becoming inflamed, he found a connective tissue not only beneath the ependyma, but penetrating the mass of the brain, filling all interstices among nerve cells and their fibres, and also separating nervous tissue from blood vessels. In the collection of Virchow's papers published in 1856, there is the first use of the term neuroglia. [4]. Other illustrious researchers at the beginning of the nineteen century brought paramount contributions to the glia cause: Golgi led to the recognition of multipolar glial cells, and also their intimate relationship to blood vessels, the same Ramón y Cajal legitimated neuroglia as the "third element" of the nervous system, and Rio-Hortega in 1920 crystallizing the still-accepted classification of glia [3].

Interestingly, the glial cells are the main type of both neuronal and non-neuronal cells in the fully developed human brain, indeed they account for ~ 90 percent of total cells [1]. The most numerous glial cells appear to fall into three different types: oligodendrocytes, microglia and astrocytes. Despite the different origins, both cells type share a common feature, that is physical proximity to neurons by an elaborated breaches anatomy that interweaves with neuronal processes, which allows performing several biological tasks. Oligodendrocytes, for example, are responsible for the myelination of axons, which is essential to support the signal transmission over long distances [5] otherwise, microglia are responsible for immune function including the mechanism of neural protection [6].

Astrocytes, literally star-like cells, are the most numerous and diverse glial cells in the CNS. There is a common agreement regarding their crucial roles in controlling the homeostasis of surrounding neurons, with a fundamental role in energy metabolite supply and neurons-vascular interface [7]. One of the first possible recognized functions of astrocytes is their importance in the maintenance of extracellular K<sup>+</sup> concentration. Electrophysiological recordings in vivo, indeed, implicate modulation of K<sup>+</sup> by astrocytes in the regional controls of neural excitability in the healthy brain [8, 9]. The resting membrane potential of neurons depends on intra- and extracellular concentrations of different ions, thus changes in extracellular K<sup>+</sup> concentration can alter neuronal excitability.

This is only one possible pathway where astrocytes could have an active role in the signalling transmission. In this regard, Figure (1.1) illustrates the intricate portrait of

neuron-astrocyte interplay at synaptic level. Besides the homeostatic functions, astrocytes display dynamic signalling with neurons and synapses. For a cell to be considered an active element in the brain coding network, it should be able to: (i) receive incoming information; (ii) integrate and code that information; and (iii) transfer the information to other cells. Neurons have the ability to perform these actions due to their anatomical characteristics and intrinsic electrical properties. Because glial cells are notorious electrically passive, their code must rely on mechanisms not involving membrane potential fluctuations.

Despite the lack of excitability, they show intricate cellular signaling proprieties originating from membrane receptors in the cytosol, this is the case of second messengers like inositol 1,4,5-trisphosphate ( $IP_3$ ) and intracellular calcium. The oscillations of these chemicals provide the encoding mechanism of external input in the astrocytes instead of membrane potential fluctuations. In these regards, they fulfil the three requirements by a glia code based on second messenger oscillations. Among these, calcium signalling is the most studied one, arguably because of the availability of indicators to monitor intracellular calcium concentration as well as for its recognized function as an intracellular messenger in a multitude of other cells [10].

Astrocytes, therefore, can sense the synaptic activity induced by several neurotransmitters such as glutamate, GABA, acetylcholine and ATP, that trigger intracellular processes causing variation in  $Ca^{2+}$  concentration. Decoding these signals is a necessary step for any mechanism that uses this code to perform a downstream action. In this sense, the ability to release neuroactive molecules, called gliotransmitters, when calcium overcomes a threshold value makes the astrocytes able to influence neuronal activity and synaptic transmission. This feature takes the name of *gliotransmission* and bears the widest implication in information processing.

All these features can be regarded as evidence of the purpose of glia for being an integral part of both structure and function of neural networks. The recognition that glia cells could be much more than passive elements has therefore been accepted as a revolution of the classical Neuron paradigm of the brain in favor of a more comprehensive Neuron-Glia paradigm [11]. There is no other concept that epitomizes the Neuron-Glia paradigm better than the *tripartite synapses*, whereby the astrocyte is the third active element in synaptic communication between the pre- and postsynaptic neurons by sensing synaptically-released neurotransmitters by a variety of mechanisms, and signalling back to the synapse by gliotransmission.

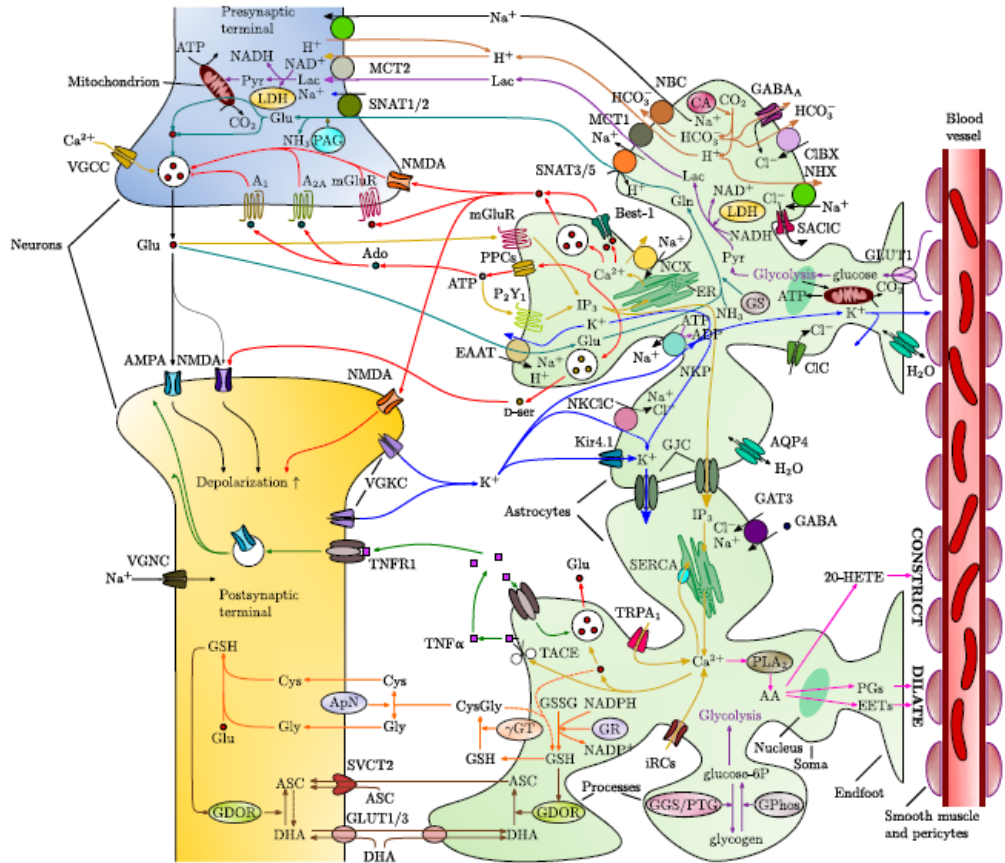


Figure 1.1: **Common interaction between astrocytes and glutamatergic synapses.** Simplified illustration of the main pathways of the interaction of astrocytes with neurons at glutamatergic synapses. The transmission between the presynaptic button (blue element) and the postsynaptic one (yellow element) is affected by the astrocytic processes (green elements). Each coloured line stands for the interaction pathway regarding a particular chemical that can regulate the opening mechanism of both synaptic and astrocytic membrane receptors (symbol on the edge of synapse and astrocyte). In this illustration is also reported the gap junction between adjacent astrocytes and the neural-blood vessel interface (red element). The intimate and intricate relationship between the two neural and non-neural cells is clearly visible. Taken from De Pittà (2020) [2].

Since their discovery, astrocytes have been the subject of growing interest, nonetheless, their active role in the framework of neuronal network theory has only been partially explored. Neglecting the glia pathway of interaction might lead to a warped description of the functional brain physiology because the modulation of neural excitability and synaptic transmission by glia could regulate network activity dramatically.

The important role of theoretical and computational modelling lies in this framework. In the field of neuroscience, instead, it is not always possible to record all the measurements needed to understand a study case and the difficulty in brain activity measurements and recordings *in vivo* leads to adopting both mathematical and computational approaches to overcome experimental issues. One of the central tasks of computational neuroscience is to bridge different levels of description, i.e. from a single ionic channels to an entire neural network, by simulation and mathematical theory. The link can be built in two different directions, from microscopic to macroscopic scales (bottom-up) or from behavioural target functions to properties of components (top-down) [26].

During the years, the joint effort of theoretical neuroscientists has led to improving the computational modelling of neural networks to the point of simulating well-recorded neural population electrical activities such as asynchronous irregular firing or oscillatory firing [30, 31, 32]. We want to stress that this is not a mere theoretical challenge since, reproducing real physical phenomena through equations, approximations and simplifications mean fully understanding the systems and extrapolating among all possible mechanisms only that drive the dynamics.

In the context of the neuron-glia network, there are only a few available mathematical models that tackle the role of astrocytes. For instance, the model by Ullah [35] considers the homeostasis regulation of extracellular  $K^+$  and  $Na^+$ , while Stavachennko et al consider the effect of gliotransmission by glutammatergic synapses. Interesting, in the latter case, the author dealt with a neural network based on the well-tested hippocampal cells and found that the depression of synapses within an astrocytic domain correlates with a decrease in neuronal firing and synchronization [36]. However, they mimicked the astrocytic modulation, namely they did not consider a theoretically plausible feedback effect associating neuronal firing frequency with astrogliial actions.

The possibility to build a Neuro-Glia network with fundamental physiological mechanisms is the first step toward the application of such a modelling framework to investigate pathological behaviours related to the dysfunctional activity of glial cells.

Like other types of human cells, the astrocytes are affected by ageing changes. Morphological alteration of the astrocytic processes have been shown in older individual: long and slender processes in young subjects turn into short and stubby processes in older ones. The number and the density instead show region-dependent changes with ageing. No changes were observed in the hippocampus whereas an increase is present in the cortex and hypothalamus. Overall, ageing of the human brain is mainly observed as structural alterations that are most notably accompanied by cognitive decline. Several studies have shown that neuronal count does not change with age. Therefore, the search for what was responsible for the structural changes became an active area of research [1, 37].

Besides these structural changes, we need to take into account also the possible functional modifications in the astrocytic activity induced by a specific disease. Precisely, these types of modifications are present in the development of some classes of tumours that affect the glial cells, the gliomas. Gliomas are tumours of the nervous system, which develop from glial cells, and they account for the majority of primary brain neoplasias. Biologically, gliomas express several systems which adapt them to grow and expand within the CNS environment. The lack of free space due to the intricate CNS architecture does not allow the free growth of cancer mass as in the other non-brain organs. Therefore, the gliomas must clear the space by actively eliminating the surrounding healthy cells, and actively propagating neoplastic cells through the brain matter. To accomplish this task, a huge non-physiological glutamate concentration is released from cancer cells triggering an effect called excitotoxicity. Roughly speaking, the excitotoxicity involving a high level of neurotransmitters in the extracellular space involves a sustained activity of the membrane receptors. This activity allows the  $Ca^{2+}$  influx and activates several enzymes that go on to damage cell structures [39].

Among gliomas, the most violent without any doubt is glioblastoma multiforme (GBM). Glioblastoma is the most commonly occurring primary brain tumour, representing 77%-81% of all primary malignant tumours of the CNS. GBM is an aggressive brain tumour

that alters the balance of inhibitory and excitatory neurotransmission and disrupts neural circuits. Nowadays, the few available therapeutic options make survival rates disappointingly low despite medical and surgical advances [40]. A Neuron-Glia network that embedded the main physiological aspect of the interplay between neurons and astrocytes might be a suitable tool to find novel diagnosis techniques as well as therapeutic treatments. Indeed, the simulation of non-pathological dynamics is the first step toward a better and more detailed comprehension of bidirectional coupling between glioblastoma and neurons. For example, such numerical data could set the benchmark for comparison with pathological data coming from experimental observations.

In this regard, the present thesis aims to follow a bottom-up approach to filling the gap between microscopic and macroscopic aspects of neuron-glia interaction and underline the possible dynamical changes that arise both at the synaptic and network level.

From the point of view of Physics, neurons, synapses and astrocytes are nonlinear dynamical systems that intricately interact with each other, whereby we follow the framework of Dynamical Systems Theory to shed light on interacting pathways of tripartite synapse and signalling transmission. In particular, the theory of bifurcation and, more in general, the qualitative description of the dynamics of complex systems are the theoretical tools allow us to explain the effect of gliomodulation.

Thereafter, we develop a spiking network model in order to explain the possible implication of the presence of glia in the network dynamics. At this level of detail, it is possible to build a structured network of hundreds or thousands of elements coupled together in different fashions. Most importantly, in this way, we can take into account the dynamics of every element, thereby maintaining a well-detailed description of microscopic processes and simultaneously portraying the important macroscopic phenomena.

In the following paragraphs, we describe in detail the theoretical tools in nonlinear dynamical theory and underline the limits and constraints of this procedure when it is applied to complex biological systems. Then we introduce the framework of neural networks, namely interacting neurons, to elucidate how collective phenomena could arise and monitor by macroscopic observables.

## 1.2 Brain Cells as Dynamical Systems

The world is an ensemble of systems that evolve in time and interact with each other. Although the study of these dynamical systems is now a multidisciplinary subject, physics has built over the century the right mathematical setting to deal with them. The study of the gravitational two-body problem by Newton in the middle of 1600 through ordinary differential equations (ODEs) gave rise to the theory of dynamical systems. Despite the possibility of reaching an analytical solution for this system, the extension of the three-body problem turned out to be essentially impossible to solve.

The breakthrough came with the work of Poincaré in the late 1800s [41] where he introduced a new method based on qualitative rather than quantitative descriptions to deal with the celestial motion. Poincaré's powerful approach is completely general and can be applied also to complex nonlinear dynamical systems, like biological ones. This was a turning point because, in contrast to linear systems, nonlinear ones cannot be separated into different parts, and the principle of superposition fails spectacularly.

In general, dynamical systems could be described by an autonomous ODE of this form<sup>1</sup>:

$$\frac{d\mathbf{x}}{dt} = f(\mathbf{x}, \boldsymbol{\mu}) \quad (1.1)$$

with  $\mathbf{x} \in U \subset \mathbb{R}^n$ ,  $t \in I \subseteq \mathbb{R}$ , and  $\boldsymbol{\mu} \in W \subset \mathbb{R}^p$  where  $U$  and  $W$  are respectively open set in  $\mathbb{R}^n$  and  $\mathbb{R}^p$ . The vector  $\mathbf{x}$  represents the state of the system, and the space of dependent variables in  $\mathbb{R}^n$  is the *phase space*. Typically, the vector  $\boldsymbol{\mu}$  stands for the ensemble of *parameters* that characterize the systems, whereas the independent variable  $t$  is often referred to as *time*. In contrast, nonautonomous ordinary differential equations have explicit depend on time: the vector field  $f$  read as  $f(\mathbf{x}, t, \boldsymbol{\mu})$ .

In the field of neuroscience, most mathematical models concern the dynamics of voltage or second messenger to describe the cell's intrinsic properties. Due to their electrical features, neurons are typically modeled using an equivalent electric circuit. The membrane is made by a lipid bilayer that behaves as a passive capacitor  $C_m$ . Ionic channels creating ionic currents acts as dynamical resistances  $R$  and the difference between membrane potential  $V$  and resting potential  $E_l$  represents a voltage source. This is the setting for Hodgkin and Huxley's pioneering work in modelling neuronal excitability. They discovered that the principal membrane ionic currents were due to sodium and potassium diffusion. Accordingly, they developed a remarkable and detailed biophysical model in 1952 [49] describing the time evolution of the membrane potential of neurons that is still widely used nowadays. The model is based on 4 differential equations:

$$\begin{aligned} C_m \frac{dV}{dt} &= -[\bar{g}_{N_a} m^3 h(V - E_{N_a}) + \bar{g}_K m^4 (V - E_K) + \bar{g}_l (V - E_l)] \\ \tau_m \frac{dm}{dt} &= m_\infty(V) - m \\ \tau_h \frac{dh}{dt} &= h_\infty(V) - h \\ \tau_n \frac{dn}{dt} &= n_\infty(V) - n \end{aligned} \quad (1.2)$$

in particular, the first equation describes the time evolution of membrane potential. The variation of  $V$  depends on the sum of the three currents on the right side of the equation: the aforementioned sodium and potassium ionic currents, defined respectively by conductance  $\bar{g}_{N_a}$  and  $\bar{g}_K$ , and the leakage current that drives the system to its resting potential  $E_l$ . This model embeds specific electrophysiological properties and reproduces experimental data about action potential generation of giant squid's axon.

On the other hand astrocytes, the main type of glial cells in the brain, do not generate action potentials as neurons do, yet they can transfer information to other cells and encode information in response to external stimuli by employing "excitable"-like rich second messengers dynamics. Many models of a general chemical  $A$ , are based on the interpretation of essential fluxes and described using the language of differential equations. The rate of change of the concentration of  $A$  [ $A$ ] in the cytosol,  $A(t)$ , depends on a combination of fluxes contributing positively ( $J_{in}$ ) and negatively ( $J_{out}$ ):

$$\frac{dA}{dt} = J_{in} + J_{out} \quad (1.3)$$

---

<sup>1</sup>Here we briefly summarize the main aspect of dynamical systems present in this thesis, for detailed and rigorous treatment we refer to [42, 45, 43]

where the fluxes depends on the open-close mechanism of endoplasmatic receptors regulating the concentration of second messengers in astrocytic cytosol.

A solution  $\mathbf{x}(t)$  of equations (1.1) is a function  $\mathbf{x}(t) : I \rightarrow \mathbb{R}^n$  with  $I \subseteq \mathbb{R}$  satisfying:

$$\frac{d\mathbf{x}(t)}{dt} = f(\mathbf{x}(t), \boldsymbol{\mu}). \quad (1.4)$$

Abstractly, the goal will be to understand the geometry of solution curves in phase space. Therefore, following the qualitative approach introduced by Poincaré, we will not be interested in the exact solution of equation (1.4). The general approach, for autonomous differential equations, starts to individuate the *steady states* (or fixed points), namely the solutions that do not change in time ( $f(\mathbf{x}, \boldsymbol{\mu}) = 0$ ). Once we find these peculiar states, it is natural to try to determine the nature of their stability. Roughly speaking, a steady state  $\bar{\mathbf{x}}$  is *stable* if solutions close to  $\bar{\mathbf{x}}$  at a given time remain close to  $\bar{\mathbf{x}}$  for all later time, otherwise, if the neighbouring trajectories run far away from  $\bar{\mathbf{x}}$  the fixed point is *unstable*. The stability of steady states gets the first important clues regarding the fate of the variables' time evolution, nevertheless this is not the end of the story. One of the most fascinating aspects of autonomous and nonlinear systems is the multitude type of dynamical regimes that we can appreciate in the phase space. In general, depending on the stability of fixed points and the geometry properties of vector field  $f(\mathbf{x}(t), \boldsymbol{\mu})$  in the phase space, we can observe periodic, aperiodic and even chaotic orbits. Interesting, the stability of fixed points can depend on the value of parameters space  $\boldsymbol{\mu}$  induced a switch into the observable dynamical regimes. Therefore, the study of vector field properties concerning the value of parameters is a mandatory step to point out the features of dynamical systems.

### 1.2.1 Bifurcation Theory

The natural question we ask is how the stability or instability of stationary states or other solutions is affected as  $\mu$  is varied. In other words, what is the sort of the dynamics concerning the variations of one or more parameters. The theorem of bifurcation of fixed points gives us an important clue about the answer. In the textbook by Wiggins [43] is present a definition for the one-dimensional and one-parameter family vector field:

**Bifurcation of fixed points:** let's consider one-dimensional autonomous vector field

$$\frac{dx}{dt} = f(x, \mu) \quad (1.5)$$

where  $f$  is a  $\mathbf{C}^r$ <sup>2</sup> function on some open set in  $\mathbb{R}^1 \times \mathbb{R}^1$ . A fixed point of one-parameters vector field  $(\bar{x}, \bar{\mu}) = (0, 0)$  is said to undergo a *bifurcation* at  $\bar{\mu}$  if the flow for  $\mu$  near 0 and  $x$  near 0 is *not* qualitative the same as the flow near  $(\bar{x}, \bar{\mu}) = (0, 0)$ .

This definition is not more general: the vector field must have a precise smooth conditions, the fixed point lies in the origin of phase space, and the phrase "qualitative the same" is only adequate for the study of the bifurcation of one-dimensional dynamical systems<sup>3</sup>. Nevertheless, Meiss in his book [44] gives an alternative definition:

---

<sup>2</sup>Usually  $\mathbf{C}^5$  will be sufficient

<sup>3</sup>The phrase "qualitative the same" is a bit vague and it can be made precise only in the context of one-dimensional vector field by substituting the term  $\mathbf{C}^0$ -equivalent.

**Bifurcation:** A bifurcation is a *qualitative* change in dynamics occurring upon a small change in a parameter.

According to the approach described by Poincaré, both the definition emphasize the role of qualitative dynamical changes, however, the second puts the bifurcation into a wide sense framework: it is an extremely general theory that stands for the ensemble of techniques to qualitatively understand how the control parameter drives the dynamics.

However, knowing physiologically proprieties does not suffice to determine what the cell is doing and why it is doing it. Both neurons and glial cells, indeed, can exhibit different responses in terms of their code by varying one or more characteristics of their inner proprieties. Neurons, for example, can exhibit completely different spiking activity to the same injecting current [50], whereas astrocytes respond with amplitude or frequency modulation to periastrocytic neurotransmitter concentration [18]. In this regard bifurcation is the most suitable tool for a systematic study of the relationship between physiology and the computational properties of brain cells. Izhikevich, in the preface of his book, brilliantly summarized the above considerations with the following sentence:

"Information-processing depends not only on the electrophysiological properties of neurons but also on their *dynamical properties*. Even if two neurons in the same region of the nervous system possess similar electrophysiological features, they may respond to the same synaptic input in very different manners because of each cell's bifurcation dynamics."

Izhikevich, preface of *Dynamical Systems in Neuroscience: The Geometry of Excitability and Bursting* [45]

### 1.2.2 Noisy Systems and Mean Field Description

Unfortunately, in the real world, most (if not all) physical phenomena can not be described by a set of deterministic ODEs like (1.1), most of the time indeed, the noise sources can not be neglected for a faithful description of reality. Several noise sources affect all aspects of nervous system function and neuron activity at different time and space scales, from the open-closed mechanism of ionic channels to the signalling transmission over long distances as illustrated in Figure (1.2).

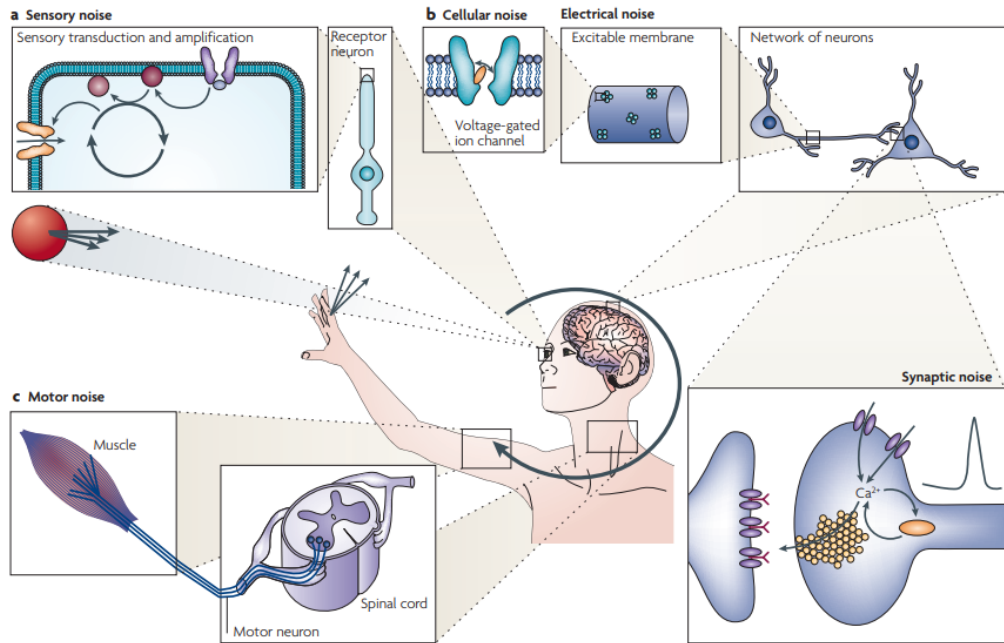


Figure 1.2: **Overview of the behavioural loop and the stages at which noise is present in the nervous system.** How noise permeates every level of the nervous system, from the perception of sensory signals to the generation of motor responses, and poses a fundamental problem for information processing. Taken from Faisal (2008) [54].

Accordingly, the recording of some measurable quantities, such as spike timing and membrane potential, show that such quantities exhibit fluctuation. In particular, analysis of physiological data suggests that both neurons and astrocytes *in vivo* fire irregularly [55, 56]. Trial-to-trial variability can arise from two distinct sources. We have already mentioned the deterministic variability of neuron activity due to dynamical properties. The other type of variability is strictly related to the noise: the spikes trains of a single neuron vary from one trial to the other by repeating an experiment several times, namely when external stimuli, such as the sensory input or task goal, are kept as equal as possible across different trials. To take into account the latter kind of variability the deterministic description is not enough and we explicitly need to consider a noise term in the system's equation:

$$\frac{d\mathbf{x}}{dt} = f(\mathbf{x}, \boldsymbol{\mu}) + \text{noise source} \quad (1.6)$$

Equation (1.6) represents a stochastic differential equation (SDE) with additive noise term<sup>4</sup>. The most important consequence is that by fixing the parameters space  $\boldsymbol{\mu}$  (therefore the vector field  $f$ ) and the initial condition  $\mathbf{x}_0$ , the time course of variables  $\mathbf{x}$  is different over several noise realizations, hence the system examines a widespread region of accessible phase space. To elucidate this point let's consider a generic dynamical system white noise  $\xi(t)$  defined by mean and autocorrelation function respectively equal to  $\langle \xi(t) \rangle = 0$  and  $\langle \xi(t) \xi(l) \rangle = \delta(t - l)$ :

$$\frac{dx}{dt} = f(x, \boldsymbol{\mu}) + A \xi(t) \quad (1.7)$$

<sup>4</sup>The world of SDE is a minefield. Here we consider only the most general noise term to treat trial-to-trial variability in neurons model. However, more complex situations like multiplicative noise might be present.

where  $A$  is a constant value. The function  $\xi(t)$  is not a simple deterministic perturbation but, as described above, is characterised by the moments of its probability distribution. This means that, for each representation of the noise perturbation, the variable  $x$  shows different time evolution. In this sense, we can consider the equation (1.6) as an infinity sample of the equations depending on the probabilistic proprieties of the noise source.

It is pleonastic to point out that the study of a nonlinear dynamical system with infinite phase space is quite undemanding, even in the context of qualitative description. In this regard, a statistical approach is mandatory to get insights into the noisy system dynamics.

From the experimental and computational point of view, the goal is to record an ensemble of data about the same system with identical initial conditions and parameter space, and then estimate the dispersion of the dynamical variables around their mean values. Accordingly, with a large data set, it is possible to have a robust portrait of underpinning deterministic rules driving the variables' time evolution, and the dispersion effect induced by noise terms.

Another typical approach is the mean field approximation, a general analytic method that returns the dynamics of mean quantities. Starting from the analytic approximation, we can understand which of all parameters drive the variable time evolution and extrapolate, among all the possible underpinning mechanisms, only the most influential ones. The reasoning of the mean field is summarized by the following steps:

1. Consider an ensemble of  $n_S$  equation (1.6) with the different realization of noise with the same statistical proprieties.
2. Compute trial averaged dynamics in terms of mean quantities  $\bar{\mathbf{x}} = \frac{1}{n_S} \sum_l^{n_S} \mathbf{x}_l$
3. Write down the ODEs for mean quantities  $\bar{\mathbf{x}}$  using the statistical proprieties of noise.

The above computational and analytical approaches share the effort to "clear" the results to stochasticity, thus we expect that the former are in good agreement with the latter ones. More precisely, all the mathematical approximations and hypotheses (if correct) have to bring a solution as close as possible to the real-world data, i.e. computational one, otherwise, these assumptions can not be considered correct and must be changed.

In conclusion, the bifurcation intended as the qualitative study concerning the small variation of a control parameter and the numerical/analytical mean field description are two powerful tools to shed light on the dynamical features of a system. Importantly, these tools are not mutually exclusive. Indeed, how the mean quantities are affected by a small variation of a control parameter is a legitimate question in the field of random motions, and the answer lies in the wide sense bifurcation framework.

### 1.3 Spiking Neural Model

The neuron is the unit element of processing information in the nervous system however, it does not accomplish alone the multitude of elaborate cognitive functions. The brain contains millions of neurons which are organized in a hierarchical organization of connected populations. In this sense, the brain is interpreted as a complex system in which the connection of nonlinear elements brings out collective phenomena. Neural populations, indeed, show a multitude of dynamical behaviours from asynchronous to synchronous

activity. The latter is elicited from the cooperative organization of neurons that show a synchronization not presented in single elements. Network oscillations are common and prominent features that are involved in cognitive and sensory processes, for example, oscillations in the  $\gamma$ -band (30-100 Hz) are robustly triggered by sensory stimuli in the cortex, whereas the  $\beta$  oscillation (13-30 Hz) are involving in somatosensory processing and motor control [38]. Such cooperative many-body systems are characterized by rich phase space and high-dimensional dynamics used to continuously interact with the external environment [62]. Importantly, the behaviour of a population is deeply characterized by the dynamical model of neurons and the type of connectivity.

In the general framework, let's consider a population of  $N$  neurons in which the state of a single unit evolves according to an equation of type (1.6), thus the ensemble of these states describes the time evolution of the entire population:

$$\Omega_N = \{\mathbf{x}_1, \mathbf{x}_2, \dots, \mathbf{x}_N\} \quad (1.8)$$

Neuronal code is based on the timing of action potentials that can be thought as the times at which the membrane potential at the soma reaches the firing threshold. Thus, there is a sequence of action potentials containing information about the membrane potential at the neuronal cell body, and it is the information carried by the train of action potentials that provides information at the projection targets for the neurons. This train of action potentials, the *spike train*, is the element of a neural code [63]. Accordingly, the activity of neuron  $j$  is a sum of point events in time:

$$\rho_j(t) = \sum_k \delta(t - t_{j_k}) \quad (1.9)$$

where the Delta function  $\delta(t - t_{j_k})$  stand for the generation of the  $k$ -th spike of neuron  $j$ . The response of the neuron  $i$  in the population  $\Omega_N$  depends on the activities  $\{\rho_j|_{j=1,\dots,N_i}\}$  of its  $N_i$  coupled neurons:

$$\frac{d\mathbf{x}_i}{dt} = f(\mathbf{x}_i, t, \boldsymbol{\mu}_i) + \sum_{j=1}^{N_i} s(\rho_j) \quad (1.10)$$

Equation (1.10) limps all the characteristics that drive the population dynamics. The time evolution of the state  $\mathbf{x}_i$  is affected by the adopted model used to describe the dynamics of single neurons  $i$ , i.e. the vector field  $f(\mathbf{x}_i, t, \boldsymbol{\mu}_i)$ , and by the the activity of the other coupled neurons  $j$  through the sum of  $s(\rho_j)$ . This latter aspect points out the importance of connectivity links to understand the network dynamics

In most neural networks, the connection is provided by chemical synapses which elaborate the input spikes train from the so called presynaptic neuron to the postsynaptic one. From a biological point of view, the involved mechanism of synaptic communication is the release of neurotransmitters from the presynaptic bottom at the arrival of an action potential, hence we can deal with synapses as a dynamical system with finite characteristic timescales which shape the time-evolution of pulse-like action potential communication. More precisely, a simple way of describing the time course of synaptic input is as a decaying exponential:

$$s(\rho_j(t), t) = \sum_k \frac{1}{\tau_{syn}} \exp\left(-\frac{t - t_{j_k}}{\tau_{syn}}\right) \Theta(t - t_{j_k}) \quad (1.11)$$

where  $\Theta(t - t_{j_k})$  is the Heaviside function and therefore every exponential term is considered only starting from the spike arrivals  $t_{j_k}$  and  $\tau_{syn}$  is the characteristic decay time constant. The limited experimental data make demanding to determine the real connectivity in several layers of the brain. At least, some plausible estimates of connection probabilities exist, for example in some cases the connection probability is considered distance-dependent or assumes randomly within and between populations. Despite the existence of different schemes, from a computational and modelling perspective, the connectivity is represented by a square matrix involving a number of rows and columns equal to the number of neurons in the network. The value of the entry  $C_{i,j}$  of the connectivity matrix is 1 (0) if the  $i$ -th postsynaptic neuron receives (does not receive) synaptic input from the  $j$ -th presynaptic neuron. In these regards, equation (1.10) becomes<sup>5</sup>:

$$\frac{dx_i}{dt} = f(\mathbf{x}_i, \boldsymbol{\mu}_i) + \sum_{j=1}^N C_{i,j} w_{i,j} s(\rho_j(t), t) + I_{ext_i}(t) \quad (1.12)$$

where  $w_{i,j}$  stands for the strength of connection and  $I_{ext_i}(t)$  is the external input from environment. Besides the microscopic variability introduced above, if the matrix  $C_{i,j}$  is random and sparse, we insert other degree of variability due to the structural arrangement of the network.

In this sense, we cannot neglect any source of noise for an accurate description of the neural time course. Indeed, the variability of the neural response causes the time between two consecutive spikes, namely the inter-spike intervals (ISI), to have a certain distribution. A statistical approach is mandatory to obtain the right picture of signalling transmission. Given a spike at time  $t_0$ , we have to find the probability to observe another one at time  $t_1$ , i.e.  $P(n+1, t_1|n, t_0)$ . These probability distributions characterize the spike activity of a neuron  $j$  and, as illustrated in equation (1.12), the dynamics of all neurons  $i$ . The knowledge of spike train distribution allows us to compute the average number of action potentials per unit of time, namely the *firing rate*  $\nu(t)$ . The recording data suggest that both *in vivo* and *in vitro*, neurons fire reminiscent of a Poisson process for which the timing of an action potential is independent of the previous one.

Once the time evolution of a single neuron in the interacting population is known, it is natural finding some global measurements to quantify the activity of  $\Omega_N$ . Moreover, in the context of computational neuroscience, the network dynamic has to describe as clear as possible the physiological aspects of the human brain domain. In this way, we can compare the numerical results with the experimental data. A common non-invasive technique is Electro-Encephalography (EEG). This method aims to record the electrical activity on the scalp that represent the macroscopic activity of the large brain region of the surface layers. Nevertheless, the EEG signals must propagate through various media, such as cerebrospinal fluid, cranium, and skin, and are therefore subject to filtering and diffusion phenomena across these media.

More invasive techniques allow us to record the activity of limited and depth regions of the brain. Indeed, using deep electrodes, we can monitor electric potential in the extracellular space due to the activity of surrounding neurons in the sphere of 1 mm or by a few hundred microns [64]. This spatial-constraint potential takes the name of Local Field Potential (LFP) and includes the dynamics and structural arrangement of neurons,

---

<sup>5</sup>We consider here only the action of inputs on a single variable  $x_i$  of the model. The variable affected by synaptic activity might for instance be either the membrane potential or the membrane capacitance.

synapses and dendrites of the investigated region. Because multiple neuronal processes contribute to the LFP, the signal is inherently ambiguous and more difficult to interpret than spikes train as well as its relation to single neuron variables like synaptic currents and membrane potentials. The situation is further complicated if we consider a spiking neural model where the space compartmental structure is neglected in order to focus on dynamical properties.

The purpose of modelling the spiking neural model is to link the microscopic dynamics with the mesoscopic behaviour of one or more populations. Therefore, the main goal is to get the relation between neurons' variables and global quantities. Once obtained these signals, statistical and data analysis tools like spectrum analysis could shed light on possible synchronous activities and, more importantly, how the single elements are involved in this collective phenomenon.

# Chapter 2

## METHODS AND MODELS

We present in this chapter all the methods adopted in this thesis. The mathematical models of neurons, synapses and astrocytes are present with their physiological meaning. Moreover, for the mechanism underpinning the release of neuroactive chemicals, we describe the relative mean field derivation. In this context, the main results reported in the literature are reproduced to have a complete and understandable comprehension of the core of future analyses. Afterwards, we describe the generation of Poisson processes, spectral analysis and numerical methods.

### 2.1 Brain cells and their mathematical models

In section 1.2 we introduce the general framework to deal with biological cells as dynamic systems. In the following paragraphs, we describe the adopted dynamical model used for further analysis. We want to emphasize that any choice we made is justified by the aim to describe neuron-glia interaction and its role in the corresponding networks dynamics. For the modelling point of view it is crucial to understand the physiological mechanism driving the behavior of the studied neural population. Therefore, starting from experimental data, the goal is to extrapolate knowledge about the underlying system and to encode this information into the dynamical equations such that, the time evolution of variables in that model nicely reproduces the experimental results. Thus, the choice of the model reflects the level of detail we want to achieve for the microscopic description of synaptic transmission and the mesoscopic behaviour of both neuronal and neuro-glia networks. According to this, we adopt the Integrate and Fire model to describe the neuron dynamics and a more physiological detailed model for synapses and astrocytes, such that Tsodyks-Markram for short-term plasticity and G-ChI for astrocytes. These theoretical approach allow us to describe the time evolution of neurotransmitter and gliotransmitter concentration in extracellular space. The main disadvantage of these choice comes from the huge number of parameters that regulate in particular the astrocytes dynamics. However, due to their directly physiological meaning, it is easy to individuate the paramount parameters that could affect neuronal communication.

#### 2.1.1 Neurons

As already mentioned in section 1.2, the Hodgkin-Huxley (HH) model describes the dynamics of the membrane potential in terms of sodium and potassium ionic channels. Over

the years, with the improvement of computational power, other ionic currents were included in the HH model in such to have a more realistic description of the generation of action potential. However, the growth of complexity suffers some limitations. Indeed, the essential nature of neuronal dynamics broadly remains hidden behind a multitude of factors and this is strictly related to huge parameter space that makes tedious any meaningful exploration of available phase space. The method of dimension reduction moves in the opposite direction, it tries to adapt models containing the minimal neurophysiological properties to reproduce experimental data with the lowest possible number of variables and parameters. In this regard, models like FitzHugh-Nagumo [51] and Morris-Leclar [52] consistently describe the neuron dynamics with only two variables: membrane potential and recovery variable.

Despite the complexity inherent in the generation of action potentials through the multitude of ionic currents, in many cases, the conditions required for their initiation can be characterized quite straightforwardly. As we have already mentioned, the action potential is, roughly speaking, an abrupt increase of membrane potential. This increase starts in correspondence with a cert threshold value. Accordingly, we can simulate an action potential following this procedure: when the membrane potential reaches a certain threshold, a spike is initiated. In this setting lies the family of the Integrate-and-Fire models (IF). IF models only describe the sub-threshold membrane potential  $V(t)$  and when  $V(t)$  crosses the threshold  $V_\theta$ , the neuron fires causing the following consequences: the neuron potential is reset at a value  $V_r$  and the neuron cannot fire again for a refractory time  $\tau_r$ . In our model, all the neurons are described by leaky integrate-and-fire (LIF), where the term *leaky* stands for the exponential decay of  $V$  with a characteristic time scale. In the framework of RC equivalent electric circuit, the sub-threshold time course of membrane potential is described by the following ODE:

$$C_m \frac{dV}{dt} = g_l(E_l - V) + I_{syn}(t) + I_{ext}(t) \quad (2.1)$$

where  $C_m$  is the membrane capacitance and  $g_l$  is the membrane conductance. In addition, the model can take to account the synaptic current coming from the activity of other neurons  $I_{syn}(t)$  and the possible external current  $I_{ext}(t)$ . More precisely, a simple way of describing the time course of synaptic current is as a decaying exponential

$$I_{syn}(t) = \bar{I}_{syn} s(t) \quad (2.2)$$

where  $s(t)$  is the synaptic activity described in (1.11) and  $\bar{I}_{syn}$  stand for a current depending on the membrane potential of the presynaptic neuron  $V(t)$ . In particular,  $\bar{I}_{syn}$  can be represented as:  $\bar{I}_{syn} = g_{syn}(V(t) - E_{syn})$ , where  $g_{syn}$  and  $E_{syn}$  are respectively the synaptic conductance and the reversal potential of the synapses. The synaptic current read as:

$$I_{syn}(t) = g_{syn} (V(t) - E_{syn}) s(t) \quad (2.3)$$

Depending on  $E_{syn}$  the synaptic current can be excitatory ( $E_{syn} > E_l$ ) or inhibitory ( $E_{syn} < E_l$ ).

Finally, considering the possibility of excitatory and inhibitory input, the complete conductance-based integrate-and-fire model with  $N_e$  excitatory and  $N_i$  inhibitory ones reads as:

$$\begin{aligned}
 C_m \frac{dV}{dt} &= g_l(E_l - V) + g_e(E_e - V) + g_i(E_i - V) + I_{ext}(t) \\
 \frac{dg_e}{dt} &= -\frac{g_e}{\tau_e} + w_e \sum_{m=1}^{N_e} \sum_k \delta(t - t_{m_k}) \\
 \frac{dg_i}{dt} &= -\frac{g_i}{\tau_i} + w_i \sum_{n=1}^{N_i} \sum_k \delta(t - t_{n_k})
 \end{aligned} \tag{2.4}$$

where  $g_e$  and  $g_i$  are respectively the excitatory and inhibitory synaptic conductance with exponential time constant  $\tau_e$  and  $\tau_i$ . An arrival of spike at time  $t_{m_k}$  ( $t_{n_k}$ ) from presynaptic excitatory (inhibitory) neurons  $m$  ( $n$ ) causes an increase of postsynaptic conductance by  $w_e$  ( $w_i$ ). Figure (2.1) illustrates an IF neuron described by equation (2.4)

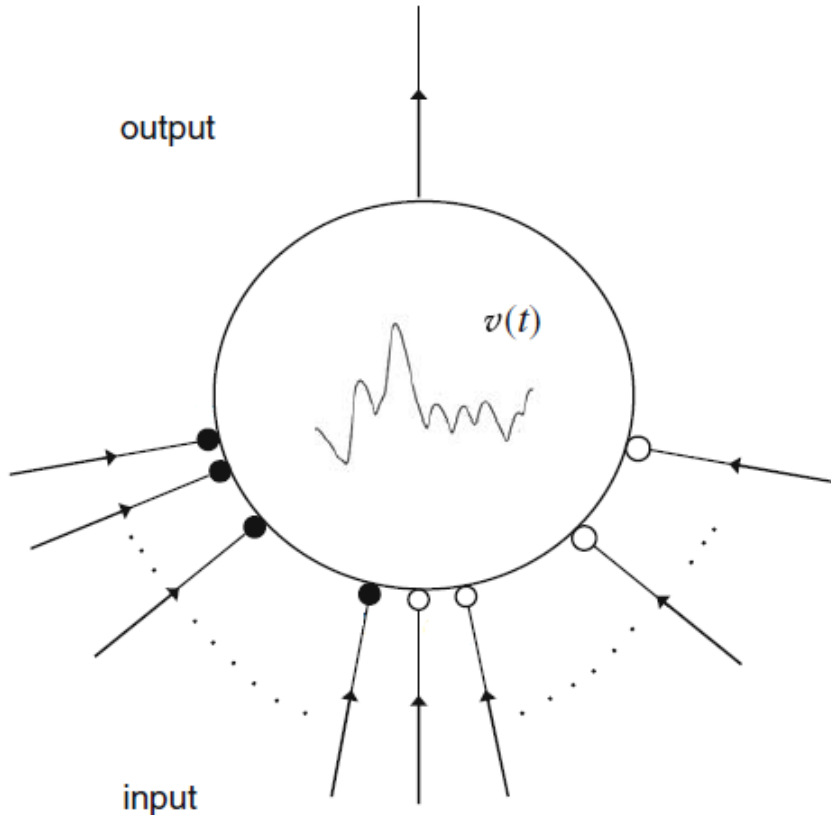


Figure 2.1: **Schematization of IF neuron.** Cartoon visualization of equation (2.4) with  $N_e$  excitatory (filled circles) and  $N_i$  inhibitory (open circles) current synapses. Each excitatory (inhibitory) synapse receives an input spike  $\delta(t - t_{m_k})$  ( $\delta(t - t_{n_k})$ ). Taken from Burkitt (2008) [53].

The integrate-and-fire neuron model is a single compartment model in which the spatial structure of the neuron associated with the dendrites, soma and axon are neglected. However, it is useful in understanding the basic properties of large networks of neurons and the implementation of synaptic plasticity is straightforward.

### 2.1.2 Synapses

In most model of neuronal systems, neurons are connected by chemical synapses, elements of the nervous system that allow the transmission of signals from one neuron to another by releasing signaling molecules called neurotransmitters. The events leading to the synapses communication involve several steps. The action potential travels down the axon and terminates at many presynaptic sites, called synaptic terminals (or presynaptic buttons). These terminals contain a presynaptic releasable vesicle pool, namely the ensemble of "capsules" that allow the release of neurotransmitters. The arrival of an action potential on the presynaptic button leads to calcium entry through voltage-gated calcium channels which may result in a vesicle fusing with the presynaptic membrane and releasing neurotransmitters into the synaptic cleft. The neurotransmitters diffuse in the cleft and binds with postsynaptic receptors. Then, the activation of postsynaptic receptors induces a postsynaptic current that can either depolarize or hyperpolarize the postsynaptic neuron depending on the nature of the chemicals and receptors.

Neurotransmitters release can become quite complex to describe due to its probabilistic nature and the multitude types of membrane receptors. Furthermore, presynaptic stimulation can lead to more vesicles becoming docked to the membrane, thus on the next presynaptic spike more transmitters is released than on the first spike. This increase is called potentiation or *synaptic facilitation*. Additionally, after several presynaptic spikes, the transmitter release per spike can decrease through various means, such as depletion, and take some time to recover. Decrease of transmitter over successive firings of action potentials is called *synaptic depression* [47].

To describe the dynamics of facilitation and depression of synaptic transmission, we adopt the phenomenological description of short-term plasticity first introduced by Tsodyks and Markram [59], by now indicated as TM model.

The TM model describes synaptic release ( $r_S$ ) by the product of two factors: (i) the probability of neurotransmitter-containing vesicles to be available for release ( $x_S$ ), and (ii) the probability of such vesicles to be effectively released by a presynaptic action potential ( $u_S$ ), which correlates with  $\text{Ca}^{2+}$  levels in the presynaptic button and the ensuing state of occupancy (activation) of the  $\text{Ca}^{2+}$  sensory of synaptic neurotransmitter exocytosis.

The variable  $u_S$  is zero at rest, when intrasynaptic  $\text{Ca}^{2+}$  concentration is low and the sensor for neurotransmitter exocytosis is only little bound, whereas it increases upon an action potential arriving at time  $t_k$ , mimicking increased of the fraction of binding synaptic sensor. In this interpretation the model assumes that a fraction  $u_0$  of  $1 - u_S$  of free binding sites of the sensor is instantaneously occupied by incoming  $\text{Ca}^{2+}$  ions and is following recovered at rate  $\Omega_f$ . Thus, the dynamics of  $u_S$  is driven by

$$\frac{du_S^-}{dt} = -\Omega_f u_S^- + u_0 \sum_k (1 - u_S^-) \delta(t - t_k) \quad (2.5)$$

where the Dirac delta function  $\delta(t - t_k)$  denotes the presynaptic spikes train and  $u_S^- = u_S(t_k^-)$  denotes the values immediately before a generic action potential at time  $t_k$ .

Neurotransmitter resource in the presynaptic terminal are assumed limited and only a fraction of  $x_S(t)$  of them is available for release. At rest, all resources are available, i.e.  $x_S = 1$ . When an action potential arrives, a fraction  $u_S^+ = u_S^- + u_0(1 - u_S^-)$  of the resources is released into the cleft and is following reintegrated at rate  $\Omega_d$ . The differential equation

for time course of available neurotransmitter reads as

$$\frac{dx_S^-}{dt} = \Omega_d(1 - x_S^-) - \sum_k u_S^+ x_S^- \delta(t - t_k) \quad (2.6)$$

Accordingly, the fraction of neurotransmitter resources ( $r_S$ ) that is released by an action potential arriving at  $t_k$  is given by

$$r_S = u_S(t_k^+) x_S(t_k^-) = u_S^+ x_S^- \quad (2.7)$$

Time evolution of variables is present in Figure (2.2)

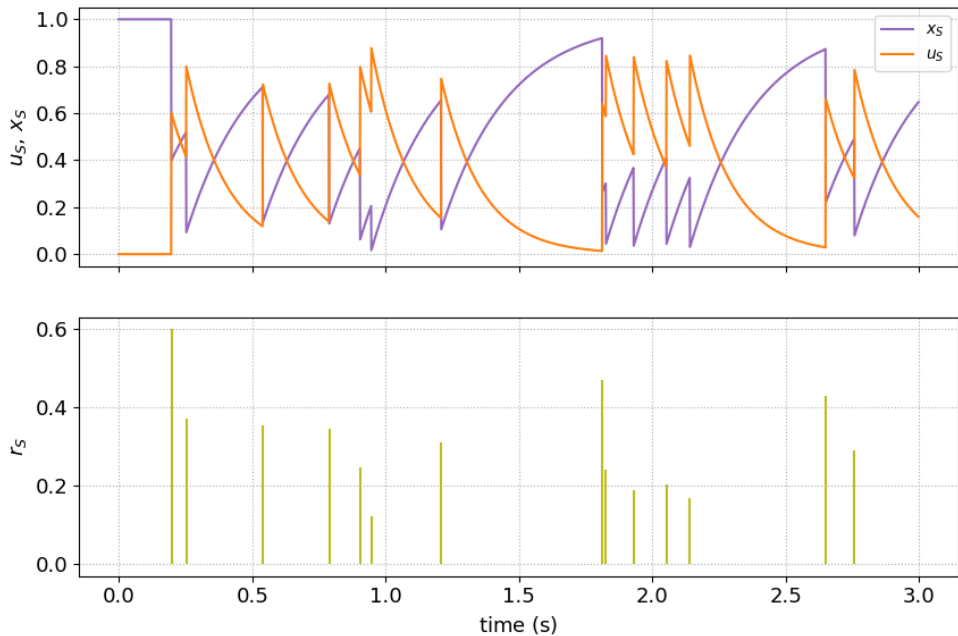


Figure 2.2: **Dynamical behavior of variables in TM model.** (Top panel) Time evolution of  $x_S$  (purple) and  $u_S$  (orange) for Poisson presynaptic firing rate of 4 spk/s. (Bottom panel) Released neurotransmitter resources (yellow). Time simulation covers 3 second, integration steps is 1 ms. Parameters as in table in Appendix C.1

Equations (2.5) and (2.6) compose the TM model where the parameter  $u_0$  coincides with the value that  $u_S$  reaches at resting condition immediately after first action potential of a series. When presynaptic firing rate is low than facilitation and depression time constant, i.e.  $\nu_S \ll \Omega_f, \Omega_d$ , synaptic variables reach their initial values and, as a consequence, the dynamics is equal to the total absence of plasticity. Then, in this case, the release probability from synapses equals  $u_0$ . On the other hand, intense presynaptic firing rate provides strong depletion of resources that drastically reduce neurotransmitter exocytosis.

The neurotransmitter's time course in the synaptic cleft must be taken into account to complete our description of synaptic transmission. We assume a total vesicular neurotransmitter concentration of  $Y_T$ , thus the released concentration in the synaptic cleft is equal to  $Y_{rel}(t_i) = \rho_c Y_T r_S(t_k)$ , where  $\rho_c$  represents the ratio between vesicular and

synaptic cleft volumes. The time course of synaptically released neurotransmitters in the cleft ( $Y_S$ ) depends on several mechanisms, including clearance by diffusion, uptake and degradation. In the simplest approximation, the contribution of these mechanisms to glutamate time course in the cleft may be modelled by a first-order degradation reaction of characteristic time  $\Omega_c$  so that [17]:

$$\frac{dY_S}{dt} = -\Omega_c Y_S + \sum_k Y_{rel} \delta(t - t_k) \quad (2.8)$$

### Mean field description of Neurotransmitters release

The TM model of bipartite synapse can be used to study the way the activity of a large population of presynaptic neurons is transmitted to the postsynaptic target. The dynamics driven by generic spikes train is completely described by the following set of equations:

$$\begin{aligned} \frac{du_S^-}{dt} &= -\Omega_f u_S^- + u_0 \sum_k (1 - u_S^-) \delta(t - t_k) \\ \frac{dx_S^-}{dt} &= \Omega_d (1 - x_S^-) - \sum_k u_S^+ x_S^- \delta(t - t_k) \\ u_S^+ &= u_S^- + u_0 (1 - u_S^-) \end{aligned} \quad (2.9)$$

that is a nonlinear dynamical system of two ODEs. Substituting the third expression into the first leads to more useful form for next steps of mean field derivation:

$$\begin{aligned} \frac{du_S^+}{dt} &= \Omega_f (u_0 - u_S^+) + u_0 \sum_k (1 - u_S^+) \delta(t - t_k) \\ \frac{dx_S^-}{dt} &= \Omega_d (1 - x_S^-) - \sum_k u_S^+ x_S^- \delta(t - t_k) \end{aligned} \quad (2.10)$$

To simplify the notation, the variables are redefined without the apexes. Let's consider  $n_S$  trials of stimulation of a synapse by trains of action potentials of equal length and same statistics, delivered to the synapse at identical initial conditions. The trial-averaged synaptic dynamics is described by equations (2.10) in term of mean quantities  $\bar{u}_S = 1/n_S \sum_{l=1}^{n_S} u_{S_l}$  and  $\bar{x}_S = 1/n_S \sum_{l=1}^{n_S} x_{S_l}$ :

$$\begin{aligned} \frac{d\bar{u}_S}{dt} &= \Omega_f (u_0 - \bar{u}_S) + \frac{u_0}{n_S} \sum_{l=1}^{n_S} \sum_k (1 - u_{S_l}) \delta(t - t_{l_k}) \\ \frac{d\bar{x}_S}{dt} &= \Omega_d (1 - \bar{x}_S) - \frac{1}{n_S} \sum_{l=1}^{n_S} \sum_k u_{S_l} x_{S_l} \delta(t - t_{l_k}) \end{aligned} \quad (2.11)$$

where  $\delta(t - t_{l_k})$  represents the arrival of the  $k$ -th spike of trial  $l$ . In a small time interval  $\Delta t$ , the above equations can be rewritten in terms of finite differences as:

$$\begin{aligned} \bar{u}_S(t + \Delta t) - \bar{u}_S(t) &= \Omega_f (u_0 + \bar{u}_S) \Delta t + \frac{u_0}{n_S} \sum_l^{n_S} (1 - u_{S_l}) \Delta_l(\Delta t) \\ \bar{x}_S(t + \Delta t) - \bar{x}_S(t) &= \Omega_d (1 - \bar{x}_S) \Delta t - \frac{1}{n_S} \sum_l^{n_S} u_{S_l} x_{S_l} \Delta_l(\Delta t) \end{aligned} \quad (2.12)$$

where  $\Delta_l(\Delta t) = \sum_k \delta(t - t_{l_k})\Delta t$  is the number of spikes in the time interval  $\Delta t$  for the  $l$ -th trial and it is a stochastic quantity. In sections 1.2.2 and 1.3, we have already mentioned that individual neurons *in vivo* fire irregularly at all rates, reminiscent of a Poisson process. Mathematically, the Poisson assumption means that, at each moment, the probability that a neuron fires equal the neuron's instantaneous firing rate and is independent of the timing of previous action potentials. Then, assuming that the  $n_S$  trains are different realizations of the same Poisson process with average rate  $\nu_S(t)$ , equations (2.12) can be averaged in time over a proper  $\Delta t$ . In particular, thanks to the Poisson hypothesis, the variable  $u_S$ ,  $x_S$ ,  $u_S x_S$  and  $\Delta_l(\Delta t)$  can be considered independent and thus be averaged independently. Therefore, taking  $\Delta t$  of a order of several intervals between spikes, but shorter than longest time scale in the system ( $1/\Omega_d$  and  $1/\Omega_f$ ), the time average, denoted by  $\langle \cdot \rangle$ , of  $\Delta_l(\Delta t)$  can be estimate by  $\Delta_l(\Delta t) = \nu_S(t)\Delta t$ . Accordingly,

$$\begin{aligned} \langle \bar{u}_S(t + \Delta t) \rangle - \langle \bar{u}_S(t) \rangle &= \Omega_f(u_0 - \langle \bar{u}_S \rangle)\Delta t + \frac{u_0}{n_S} \sum_l^{n_S} (1 - \langle u_{S_l} \rangle) \nu_S(t) \Delta t \\ \langle \bar{x}_S(t + \Delta t) \rangle - \langle \bar{x}_S(t) \rangle &= \Omega_d(1 - \langle \bar{x}_S \rangle) - \frac{1}{n_S} \sum_l^{n_S} \langle u_{S_l} x_{S_l} \rangle \nu_S(t) \Delta t \end{aligned} \quad (2.13)$$

Finally, divided by  $\Delta t$  yields

$$\begin{aligned} \frac{d\langle \bar{u}_S \rangle}{dt} &= \Omega_f(u_0 - \langle \bar{u}_S \rangle) + u_0(1 - \langle \bar{u}_S \rangle) \nu_S(t) \\ \frac{d\langle \bar{x}_S \rangle}{dt} &= \Omega_d(1 - \langle \bar{x}_S \rangle) - \langle \bar{u}_S \rangle \langle \bar{x}_S \rangle \nu_S(t) \end{aligned} \quad (2.14)$$

that is a nonautonomous set of two ODEs describing the dynamics of average synaptic variables.

### 2.1.3 Astrocytes

Among all possible second messengers in astrocytic cytosol,  $\text{Ca}^{2+}$  and inositol 1,4,5-trisphosphate ( $\text{IP}_3$ ) are the most studied ones and are the core of most glio-computational models. For  $\text{Ca}^{2+}$ , influx usually occurs via two principal pathways: inflow from the extracellular medium through  $\text{Ca}^{2+}$  channels located in the cell membrane and release from internal stores (as endoplasmatic reticulum) via  $\text{IP}_3\text{R}$  receptor, i.e. when the  $\text{IP}_3$  binds  $\text{IP}_3\text{R}$  a calcium channel on the membrane pf the store opens and calcium flows from the store to the cytosol. Removal of  $\text{Ca}^{2+}$  from the cytosol also occurs in two principal ways: it is pumped out of a cell and is sequestered back into the internal store. In addiction,  $\text{Ca}^{2+}$  ions can also passively leak from the internal store into the cytosol.

In astrocytes, the primary mechanism underlying the influx is the  $\text{IP}_3$ -dependent  $\text{Ca}^{2+}$  release from endoplasmatic reticulum (ER). Morover  $\text{IP}_3$  concentration into the cytosol strongly depends on  $\text{Ca}^{2+}$ , thus this mechanims is called  $\text{Ca}^{2+}$ -induced  $\text{Ca}^{2+}$ -release (CICR). Classical models for a biophysically realistic cytosolic  $\text{Ca}^{2+}$  oscillation was developed by De Young and Keizer [57]. It mimics the molecular subunit configuration of the  $\text{IP}_3\text{R}$  to reflect the activation/inactivation sequence of the channel resulting from the binding of  $\text{Ca}^{2+}$  and  $\text{IP}_3$ . In particular, the model assumes that the  $\text{IP}_3\text{R}$  is composed of three independent and identical subunits, each state of the subunit is given by  $X_{ikj}$  wiht  $i, k, j = 0, 1$ , where the first index refers to the  $\text{IP}_3$  binding site, the second to the  $\text{Ca}^{2+}$ -activated site and the third to the  $\text{Ca}^{2+}$ -inactivated site. Therefore the

model consists of six ODEs, one for each subunit, and one differential equation for  $\text{Ca}^{2+}$  dynamics:

$$\begin{aligned}\frac{dX_{110}}{dt} &= [k_1 IX_{010} - k_1 X_{110}] + [k_{-2} X_{111} - k_4 CX_{110}] + [k_5 CX_{100} - k_{-5} CX_{110}] \\ &\dots \\ \frac{dX_{000}}{dt} &= [k_{-1} X_{100} - k_1 IX_{000}] + [k_{-4} X_{001} - k_4 CX_{000}] + [k_{-5} X_{010} - k_5 CX_{000}] \\ \frac{dC}{dt} &= \rho_A (\Omega_C X_{110}^3 + \Omega_L) (C_{ER} - C) - O_P \mathcal{H}_2(C, K_P)\end{aligned}\tag{2.15}$$

where  $C_{ER} = (C_T - C)/\rho_A$  denotes  $\text{Ca}^{2+}$  in the ER,  $\rho_A$  is the volume ratio between the ER and the cytosol, and  $C_T$  is the total concentration of  $\text{Ca}^{2+}$ , whereas  $k_{-i}$  ( $k_i$ ) are the rate (rate/moles) of reactions.

The complexity of the DYK model consisting of huge phase space provides motivation to simplify the model with the retention of its essential properties. One simplification was suggested by Li and Rinzel [58] who have shown that the original full model can be reduced to just two ODEs. The dimension reduction is based on experimental evidence that  $\text{IP}_3$  and  $\text{Ca}^{2+}$  bind quickly to the activating sites giving rise to the assumption that the receptor is in a quasi-steady-state with respect to  $\text{IP}_3$  binding and  $\text{Ca}^{2+}$  activation. Therefore it could be possible to mathematical treat Equations (2.15) and write down the reduced model with one differential equation for  $\text{Ca}^{2+}$  dynamics ( $C$ ) and other one for inactivation variable ( $h$ ) accounting for the three gating reactions, respectively,  $\text{IP}_3$ -binding, activating  $\text{Ca}^{2+}$ -binding and  $\text{Ca}^{2+}$ -dependent inactivation of the receptor [12]:

$$\begin{aligned}\frac{dC}{dt} &= J_r + J_l - J_p \\ \frac{dh}{dt} &= \frac{h_\infty - h}{\tau_h}\end{aligned}\tag{2.16}$$

where  $h_\infty = \frac{Q_2}{Q_2 + C}$ ,  $\tau_h = \frac{1}{O_2(Q_2 + C)}$  and  $Q_2 = d_2 \frac{I+d_1}{I+d_3}$  and  $d_i$  is intimately related with  $k_i$  and  $k_{-i}$  (see Appendix C for details about parameters)

According to above consideration, calcium dynamics is described by three different fluxes.  $J_l(C)$  stands for nonspecific leak current that is assumed to depend on the  $\text{Ca}^{2+}$  gradient across the ER membrane and on  $\Omega_L$ , the maximal rate of  $\text{Ca}^{2+}$  leakage from the ER:

$$J_l(C) = \Omega_L (C_T - (1 + \rho_A)C)\tag{2.17}$$

$J_p(C)$  represents the SERCA pump flux and can be taken as an instantaneous function of  $C$  by assuming Michaelis-Menten kinetics description [60] with exponent 2:

$$J_p(C) = O_P \mathcal{H}_2(C, K_P)\tag{2.18}$$

where  $O_P$  is the maximal rate of  $\text{Ca}^{2+}$  uptake by the pump and  $K_P$  is the SERCA  $\text{Ca}^{2+}$  affinity, that is the  $\text{Ca}^{2+}$  concentration at which the pump operates at half of its maximal capacity, and  $\mathcal{H}_2(C, K_P)$  is the Hill function<sup>1</sup>.

---

<sup>1</sup>The binding reaction of  $n$  molecules of a ligand  $A$  to a receptor is well described by a Hill function  $\mathcal{H}_n(A, B) = \frac{A^n}{A^n + B^n}$  where  $n$  is the Hill coefficient that quantifies the cooperativity among multiple ligand-binding sites and  $B$  is the receptor affinity for the ligand.

$J_r(C, h, I)$  is the current through the  $\text{IP}_3\text{R}$  channels and Li and Rinzel proposed the following equation for this terms:

$$J_r(C, h, I) = \Omega_C m_\infty^3 h_\infty^3 (C_T - (1 + \rho_A)C) \quad (2.19)$$

with the channel opening probability given by  $m_\infty^3 h_\infty^3$ , where  $m_\infty^3 = \mathcal{H}(I, d_1)\mathcal{H}(I, d_1)$ . The power of 3 was directly suggested by experimental data.  $I$  stands for the intercellular  $\text{IP}_3$  concentration and  $\Omega_C$  is the maximum channel permeability. The dynamics of the inactivation variable  $h$  is reminiscent of that of the gating variables in the Hodgkin-Huxley model and its dependence on  $C$  is embedded into the parameters  $h_\infty$  and  $\tau_h$  in highly nonlinear fashion.

It is important to point out that the main benefit of Li-Rinzel model is the ability to reproduce the same dynamical behavior of DeYoung-Keizer model and the same kind of physiological oscillation [19]. In particular, the reduced model of Li and Rinzel can reproduce two typical dynamical regimes of astrocytic signalling: amplitude (AM) and frequency (FM) modulation. Following the procedure described in [19], in the Figure(2.3) and Figure(2.4) these two types of dynamical behaviour are simulating concerning different parameters defining the SERCA affinity.

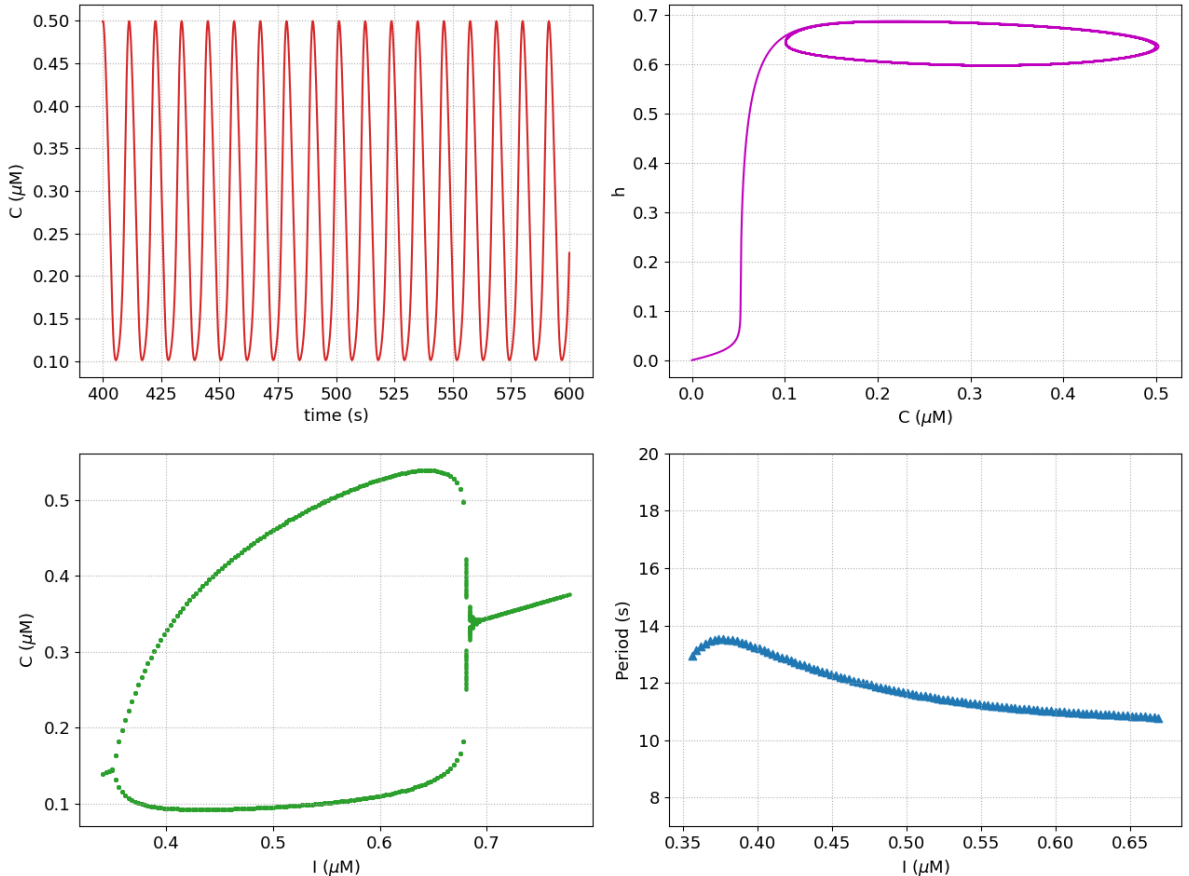
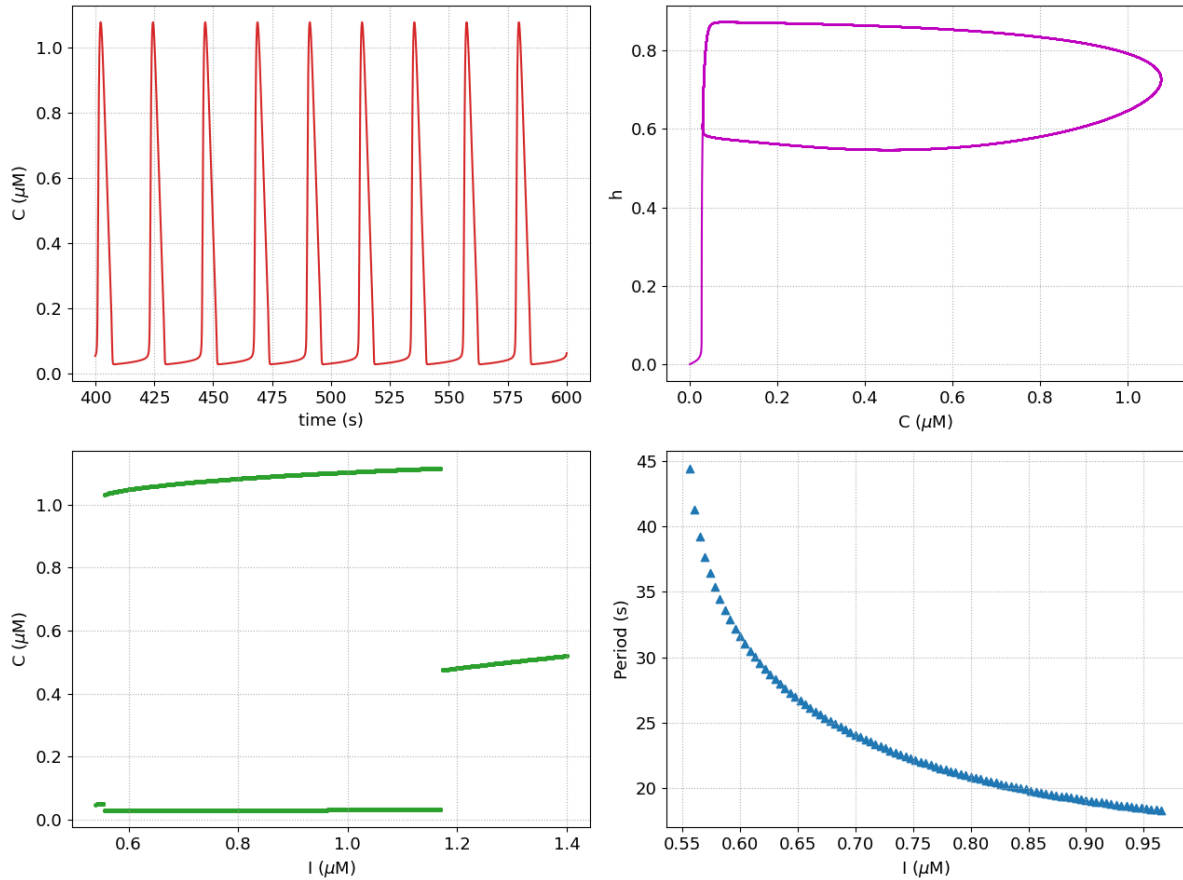


Figure 2.3: **Amplitude modulation (AM) encoding mode generated by the Li-Rinzel model.** For  $I = 0.40 \mu\text{M}$  (top left panel) the shape of calcium oscillation is quasimodulusoidal and the phase portrait (top right panel) shows a single limit circle. Changing the parameters  $I$ , qualitatively changes of dynamical is illustrated in bifurcation plot (bottom left panel) where the steady state changes its nature through Hopf bifurcations [19]. Time simulation is 600 s with relaxation time of 400 s; integration step is 0.01 s. Parameters as in table in Appendix C.2



**Figure 2.4: Frequency modulation (FM) encoding mode generated by the Li-Rinzel model.** For  $I = 0.75 \mu\text{M}$  (top left panel) the shape of calcium oscillation has a pulse-wise fashion. The number of stable fixed points change with the values of  $I$  according to the saddle-node bifurcations [19] as illustrated in bifurcation plot (bottom left panel). The nature of frequency modulation is clear looking at the range of periods with respects to  $I$  (bottom right panel). Time simulation is 600 s with relaxation time of 400 s; integration step is 0.01 s. Parameters as in table in Appendix C.2

The limitation of Li-Rinzel model is that assumes  $\text{IP}_3$  does not vary with time nor depend on the other dynamical variable, i.e. in Equation (2.16) its concentration is a parameter of the model as emphasized in above dynamical behavior analysis. Evidences suggest  $\text{IP}_3$  concentration depends on both intracellular  $\text{Ca}^{2+}$  and extracellular chemicals. For instance, glutamate concentration at the extracellular side of the astrocyte membrane determines the degree of activation of mGluRs, membrane channels directly linked to intracellular  $\text{IP}_3$  concentration. Accordingly,  $\text{IP}_3$  should be an additional variable in the model.

To update the Li-Rinzel model according to above remark, it is need taking to account both endogenous and exogenous production as well as its degradation mechanism, only such modeling can provide a realistic account of astrocytic  $\text{Ca}^{2+}$  variations induced by nearby synaptic inputs.

Astrocytic  $\text{IP}_3$  concentration is regulated by the complex  $\text{Ca}^{2+}$ -modulated interplay of enzymatic production by  $\text{C}\beta$  ( $J_\beta$ ) and  $\text{C}\delta$  ( $J_\delta$ ) and degradation by  $\text{IP}_3$  3-kinase ( $J_{3K}$ ) and inositol polyphosphatase 5-phosphatase ( $J_{5P}$ ) [19]. To reproduce experimental observations, two possible ways to trigger  $\text{IP}_3$  production must be taking into account. One is by synaptic stimulation of astrocytic metabotropic receptors which starts phospholipase  $\text{C}\beta$ -mediated  $\text{IP}_3$  production, modeled by making  $J_\beta$  proportional to the activated fraction of

these receptors (denoted hereafter by  $\Gamma_A$ ). The other way is to include a further  $J_{ex}$  term for constant  $IP_3$  production by an exogenous source of stimulation such as, for example,  $IP_3$  uncaging or intracellular diffusion from subcellular regions far from the CICR site. Mass balance equation for  $IP_3$  concentration  $I(t)$  reads as:

$$\frac{dI}{dt} = J_\beta + J_\delta - J_{3K} - J_{5P} + J_{ex} \quad (2.20)$$

For our purpose we used biophysical modeling approach fully described in [13] based on the assumption of Michaelis-Menten enzyme kinetics to effectively describe the wide range of complex chemical reactions that leads to  $IP_3$  synthesis. Each fluxes in Equation (2.20) are described by the following nonlinear expression:

$$\begin{aligned} J_\beta &= O_\beta \Gamma_A \\ J_\delta(I) &= O_\delta (1 - \mathcal{H}_1(I, \kappa_\delta)) \mathcal{H}_2(C, K_\delta) \\ J_{5P} &= \Omega_{5P} I \\ J_{3K} &= O_{3K} \mathcal{H}_4(C, K_D) \end{aligned} \quad (2.21)$$

The dynamics of the fraction of bound receptors needs to complete this description.  $\Gamma_A$  is defined as  $\Gamma_A = [R^*]/[R]_T$ , with  $[R]_T = [R] + [R^*]$  being the total receptor concentration at the site of  $IP_3$  production, thus its dynamics depends on the cascade of reactions driving  $[R]$  and  $[R^*]$  [13].

Finally, putting together (2.16), (2.20) and (2.21) leads to the so called *G-ChI model* [15, 19] for  $IP_3/Ca^{2+}$  signaling:

$$\begin{aligned} \frac{d\Gamma_A}{dt} &= O_N Y_S (1 - \Gamma_A) - \Omega_N (1 + \zeta \mathcal{H}_1(C, K_{KC})) \Gamma_A \\ \frac{dC}{dt} &= J_r(C, h, I) + J_l(C) - J_p(C) \\ \frac{dh}{dt} &= \frac{h_\infty(C, I) - h}{\tau_h(C, I)} \\ \frac{dI}{dt} &= J_\beta(\Gamma_A) + J_\delta(C, I) - J_{3K}(C, I) - J_{5P}(I) \end{aligned} \quad (2.22)$$

where  $Y_S$  stands for the neurotransmitter concentration in the periastrocytic space. Figure (2.5) illustrates G-ChI model can reproduce, like LR one, calcium oscillation in the sinusoidal-like fashion modality.

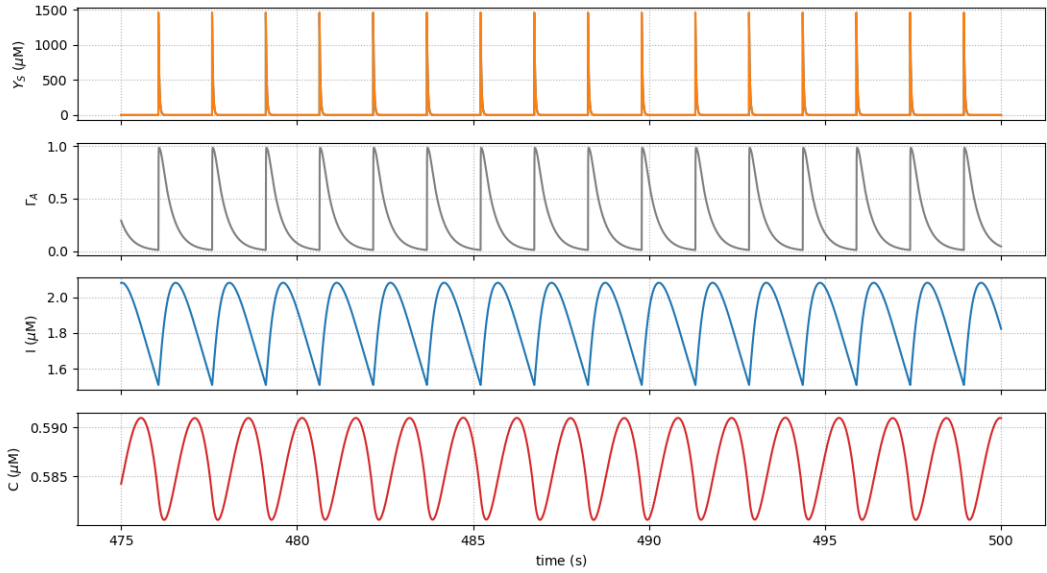


**Figure 2.5: Astrocytic variables dynamics in G-ChI model.** Synaptically activated astrocyte described by G-ChI model. Constant presynaptic firing rate of 0.6 Hz drives the neurotransmitter release and, according to TM model, its concentration upon each action potential arrivals (Top panel) notably, there are present either depression neither facilitation because of the regular inter-spike interval (ISI). The time course of astrocytic membrane receptors  $\Gamma_A$  deeply effects the time evolution of  $I$ . Importantly, for this combination of parameters,  $\text{Ca}^{2+}$  oscillations (bottom panel) are clearly visible as in AM of LR model in figure(2.3). Time simulation covers 500 seconds, only data after 475 seconds are plotted, with integration steps of 0.01 s. Parameters as in table in Appendix C.2,  $O_\beta = 3.2 \mu\text{M}$  and  $O_\delta = 0.6 \mu\text{M}$

This is the starting point to describe and analyze the neuron-glia interaction at the microscopic level. However, equation (2.22) provides only the synaptic activation of the astrocytic variable and, to consider also the gliomodulation of synaptic activity, we must describe the exocytosis and the time course of gliotransmitters in the synaptic cleft.

A large amount of evidence suggest that gliotransmitter exocytosis from astrocytes share several specialized similarities with its synaptic homologous [22, 23]. Astrocytes indeed possess vesicular compartments that are competent for exocytosis of glutamate. Fusion with plasma membrane, trafficking and recycling of glutamate-containing vesicles have also been observed in astrocytes which are indicative of quantal exocytotic release of these gliotransmitters [24, 25]. The mathematical modelling of these processes, adopted here, is based on the model of gliotransmitter exocytosis from astrocytes proposed by De Pittà in [15]. Astrocytic glutamate exocytosis is modeled akin to synaptic glutamate release, assuming that a fraction  $x_A(t)$  of gliotransmitter resources is available for release at any time. Then, every time  $t_j$  that astrocytic  $\text{Ca}^{2+}$  increases beyond a threshold concentration  $C_\theta$ , a fraction of readily releasable astrocytic glutamate resources, that is  $r_A(t_j) = U_A x_A(t_j^-)$ , is released into the extracellular space (ECS) and later reintegrated at rate  $\Omega_A$ . Hence  $x_A$  evolves according to:

$$\frac{dx_A}{dt} = \Omega_A(1 - x_A) - \sum_j r_A \delta(t - t_j) \quad (2.23)$$

where the Delta function denotes a gliotransmitter release event (GRE) at time  $t_j$ . Note that  $U_A$  in  $r_A(t_j) = U_A x_A(t_j^-)$  is the astrocytic analogous of the synapse's basal

release probability in (2.5).

Similarly to synaptic case, it is possible to estimate the contribution to glutamate concentration in the ECS ( $G_A$ ), resulting from a quantal glutamate release event by the astrocyte at  $t = t_j$ , as  $G_{rel}(t_j) = \rho_e G_{TrA}(t_j)$ , where  $G_T$  represents the total vesicular glutamate concentration in the astrocyte and  $\rho_e$  is the volume ratio between glutamate-containing astrocytic vesicles and periastrocytic space. Then, assuming a clearance rate of glutamate of  $\Omega_e$ , the time course of astrocyte-derived glutamate in the ECS comprised between the astrocyte and the surrounding synaptic terminals is given by:

$$\frac{dG_A}{dt} = -\Omega_e G_A + \sum_j G_{rel}\delta(t - t_j) \quad (2.24)$$

### 2.1.4 Gliotransmission modulation of synaptic release

*Gliotransmission modulation* (or gliomodulation) is the phenomenon by which glial activity influences the release of neurotransmitters from the presynaptic terminal. This modulation can be regarded as a two-steps processes. As we have already described, the first one is the release of gliotransmitters from the astrocytic processes into the ECS. The second is the activation of receptors located in the presynaptic terminal by the gliotransmitters. This activation translates the astrocytic signals into modulation of synaptic transmission. More precisely, depending on the gliotransmitters (such as glutamate or ATP) and the presynaptic receptors, the effects induced by gliomodulation can increase or decrease the release of neurotransmitters from the presynaptic neuron [21]. It is important to note that this kind of modulation does not require synaptic activation by action potentials and is observed even in basal conditions.

Based on this argument, an ansatz can be made whereby gliotransmitter modulation of synaptic release can be introduced in the TM synaptic model, making the variable  $u_S$  in (2.5) dependent on gliotransmitter dynamics in the ECS, i.e.  $G_A$  in equation (2.24). This model, adopted in the further analysis, is fully reviewed in [15]. For the sake of clarity, we reported here the main steps to mathematical introduce the gliomodulation in the short-term plasticity synapses.

It may be assumed that basal synaptic release probability  $u_0$  is not constant, but rather it is a function of  $G_A$  through the fraction  $\Gamma_S$  of presynaptic receptor that are activated by released gliotransmitter molecules

$$u_0 \equiv u_0(G_A) = u_0(\Gamma_S(G_A)) \quad (2.25)$$

In the absence of quantitative physiological data, the function  $u_0(\Gamma_S)$  can be taken analytic around zero that its first-order expansion is considered accordingly:

$$u_0(\Gamma_S) \simeq u_0(0) + u'_0(0)\Gamma_S + O(\Gamma_S^2) \quad (2.26)$$

The zeroth-order term  $u_0(0) = U_0^*$  corresponds to the value of  $u_0$  in the absence of astrocyte, hence this approximation falls back to the classic TM model. To express  $u'_0(0)$  instead, it may be noted that both  $u_0(\Gamma_S)$  and  $\Gamma_S$  are defined in the interval  $[0, 1]$ , so that  $u_0(\Gamma_S)$  must either increase or decrease with  $\Gamma_S$  depending on whether gliotransmission stimulates or inhibits synaptic release. In the simplest scenario, the choice of  $u_0 = \alpha - U_0^*$  can be made so that, neglecting the terms of  $O(\Gamma_S^2)$  in equations (2.26) ultimately provides

$$u_0(\Gamma_S) = U_0^* + (\alpha - U_0^*)\Gamma_S \quad (2.27)$$

The parameter  $\alpha$  in the above equation lumps in a phenomenological way information on the effect of gliotransmission on synaptic release. For  $0 \leq \alpha < U_0^*$ ,  $u_0$  decreases with  $\Gamma_S$ , consistently with the *release-decreasing* effect of gliotrasmission on synaptic release. This could be the case of astrocytic glutamate targeting presynaptic kainate receptors or group II/III metabotropic receptors [61]. For  $U_0^* < \alpha \leq 1$ ,  $u_0$  increase with  $\Gamma_S$ , consistent with a *release-increasing* effect of gliotrasmission on synaptic release, like in the case of glutamate in association with presynaptic NMDA receptors of group I metabotropic receptors . Finally, for  $\alpha = U_0^*$ , it is  $u_0 = U_0^*$ , independently of  $\Gamma_S$ . This case corresponds to *occlusion*, that is no net effect of gliotransmission on synaptic release due to the simultaneous activation of stimulatory and inhibitory receptors that may be co-expressed at the same synaptic terminal.

Finally, the presynaptic receptor dynamics are assumed to complete the model. The pool of presynaptic receptors target with gliotransmitters is composed of a fraction of bound receptors  $\Gamma_S$  and a complementary fraction  $1 - \Gamma_S$  of available ones, thus  $\Gamma_S$  evolves according to

$$\frac{d\Gamma_S}{dt} = O_G G_A (1 - \Gamma_S) - \Omega_G \Gamma_S \quad (2.28)$$

where  $O_G$  and  $\Omega_G$  denote rate constants loosely related with rise and decay of the modulation of synaptic release by gliotransmitters.

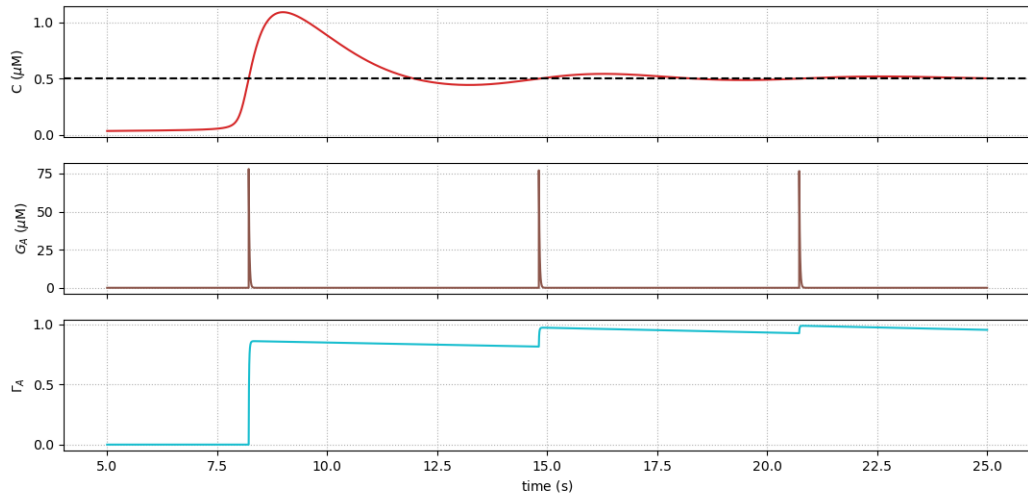


Figure 2.6: **Gliorelease event (GRE).** (Top panel) Astrocytic calcium oscillation (red solid line) across the threshold values (black dashed line) drives the release of gliotransmitters. Time course of gliotransmitters in extracellular (middle panel) space and presynaptic receptors (bottom panel). The sawtooth-shaped  $\Gamma_S$  increase is a consequence of the large difference between timescales of rise and decay of the gliotransmitter effect on synaptic release, since  $O_G G_A \ll \Omega_G$ . Time simulation covers the time window 5.0 - 25.0 seconds, with integration steps of 0.01 s. Parameters as in table in Appendix C.2,  $O_\beta = 0.5 \mu\text{M}$  and  $O_\delta = 1.2 \mu\text{M}$

### Mean field description of Gliotrasmission modulation

A mean field description of gliorelease events could be found following the same procedure of neurotransmitter release, noting that a release event by an astrocyte is described by

the same model of synaptic release in TM model of synaptic release. With this aim, the first important observation is the exocytosis of gliotransmitters may be approximated by a Poisson process with time-dependent frequency  $\nu_A(t)$ , as the neuron counterpart. Importantly, the exact expression of the GRE rate is not crucial for the validity of mean-field derivation, what is crucial is the Poisson assumption. The mean field equivalent of equations (2.23) and (2.24) reads as

$$\begin{aligned}\frac{d\langle\bar{x}_A\rangle}{dt} &= \Omega_A(1 - \langle\bar{x}_A\rangle) - U_A\langle\bar{x}_A\rangle\nu_A(t) \\ \frac{d\langle\bar{G}_A\rangle}{dt} &= -\Omega_e\langle\bar{G}_A\rangle + \rho_e G_T U_A\langle\bar{x}_A\rangle\nu_A(t)\end{aligned}\quad (2.29)$$

in particular, experimental data suggest that the timescale of gliotransmitter modulation is much slower than the time course of the gliotransmitter in the ECS. Accordingly, it may be assumed that  $\Omega_G \ll \Omega_A, \Omega_e$ , and only the timescale slower than  $1/\Omega_e$  can be considered in second equations (2.29) so that

$$\langle\bar{G}_A\rangle \approx \frac{\rho_e G_T}{\Omega_e} U_A\langle\bar{x}_A\rangle\nu_A(t) \quad (2.30)$$

substituting the above equation in (2.28), and averaging the latter, provides

$$\begin{aligned}\frac{d\langle\bar{\Gamma}_S\rangle}{dt} &= J_S U_A\langle\bar{x}_A\rangle(1 - \langle\bar{\Gamma}_S\rangle)\nu_A(t) - \Omega_G\langle\bar{\Gamma}_S\rangle \\ J_S &= \rho_e \frac{O_G G_T}{\Omega_e}\end{aligned}\quad (2.31)$$

the above equations can generally be used to reliably estimate the mean field dynamics of basal release probability

$$\langle\bar{u}_0\rangle = U_0^* + (\alpha - U_0^*)\langle\bar{\Gamma}_S\rangle \quad (2.32)$$

In conclusion, in these sections, we have presented the main physiological and computational aspects of the two pathways of interaction between neurons (more precisely the synapses) and astrocytes. Moreover, we have introduced the mathematical setting of mean field derivation that will be the main topic of the following chapter.

## 2.2 Numerical Method

An ordinary differential equation (ODE) is defined by equation:

$$\frac{dx}{dt} = f(x, t) \quad (2.33)$$

To numerically solve the equation (2.33), we have to discretize the time and evaluate on this grid the solution  $x(t)$  from the initial condition  $x_0 = x(0)$ . Therefore, we define a time step  $h$  and expand  $x(t)$  using Taylor approximation:

$$\begin{aligned}x(t+h) &= x(t) + \dot{x}(t)h + \frac{1}{2}\ddot{x}(t)h^2 + O(h^3) = \\ &= x(t) + f(x, t)h + \frac{1}{2}\dot{f}(x, t)h^2 + O(h^3)\end{aligned}\quad (2.34)$$

According to this expansion, we can iteratively evaluate the solution at time  $t+h$  knowing the solution at time  $t$  and the vector field  $f(x, t)$  (and eventually its derivate). A particular integration scheme is obtained from the truncation of this expansion at the selected order. The truncation order defines the numerical error of the iterative method following the equation (2.34). The Euler method is the lower integration scheme (first-order) and it is defined as:

$$x(t+h) = x(t) + f(x, t)h \quad (2.35)$$

One way to improve the numerical accuracy is to take into account more terms in Taylor's expansion. The Runge-Kutta methods provide an iterative procedure to improve the numerical accuracy up to the selected error. We can formally write the solution at time  $t+h$  as:

$$x(t+h) = x(t) + h \sum_i^m \alpha_i k_i \quad (2.36)$$

where the coefficient  $\alpha_i$  and the variable  $k_i$  are evaluated by comparing equations 2.34 and 2.36. Interesting, fixing the order  $m$ , the combination of parameters is not unique<sup>2</sup>. The midpoint second-order and four-order Runge-Kutta methods are described by the following set of the equations:

$$\begin{aligned} k_1 &= f(x, t)h \\ k_2 &= f(x + \frac{1}{2}k_1, t + \frac{1}{2}h)h \\ k_3 &= f(x + \frac{1}{2}k_2, t + \frac{1}{2}h)h \\ k_4 &= f(x + k_3, t + h)h \\ x(t+h) &= x(t) + (k_1 + 2k_2 + 2k_3 + k_4)/6 \end{aligned} \quad (2.37)$$

Given a total time simulation  $T$ , we obtain an approximation solution  $x_n$  defined on a spatial grid  $t_n$  with  $n = 0, \dots, T/h$ .

Let us consider now an ODE with delta function driving terms:

$$\frac{dx}{dt} = f(x, t) + c_x \delta(t - t_k) \quad (2.38)$$

where  $c_x$  is a constant value. The general adopted method to simulate equation (2.38) is described by the following steps:

- starting from the value  $x_n$  at time  $t_n$ , we evaluate the value  $\tilde{x}_{n+1}$  at the time  $t_{n+1}$  through one of the above integration schemes;
- if  $t_{n+1} = t_k$  then the value  $x_{n+1} = \tilde{x}_{n+1} + c_x$ , otherwise  $x_{n+1} = \tilde{x}_{n+1}$ .

---

<sup>2</sup>For detailed derivation we refer to [70]

For the G-ChI model and the conductance-based integrate and fire model we adopt the second-order Runge-Kutta integration scheme. This integration scheme provides the right trade-off between computational time (four-order Runge-Kutta) and the truncation approximation error (Euler)<sup>3</sup>.

## 2.3 Poisson spike trains

The variability of neural response is the noise source in the spikes train. We consider a generic rate  $\nu(t)$ , each event in the spikes train is isolated and the mean number of events follows a Poisson distribution. Given  $n$  spike at time  $t$  the probability to have  $n+k$  spike at time  $t + \Delta t$  is equal to:

$$P(n+k, t + \Delta t | n, t) = e^{-\langle \nu \rangle} \frac{\langle \nu \rangle^k}{k!} \quad (2.39)$$

where  $\langle \nu \rangle$  is the average value of the rate  $\nu(t)$  in the interval  $\Delta t$ , namely  $\int_t^{t+\Delta t} \nu(t') dt'$ . The statistical independence between consecutive events arises from equation (2.39). The probability to observe a new event in a small time interval is proportional to the rate  $\nu(t)$

$$P(n+1, t + \Delta t | n, t) \approx \nu(t) \Delta t \quad (2.40)$$

The statistical independence and equation (2.40) suggest a method to generate a sequence of events defined on the integration time grid with step  $h$ . Draw a random number  $r$  from uniform distribution  $U_{(0,1)}$  for each interval and place an event in the interval when  $r \leq \nu(t)h$  [71]. The approximation for a small time-step is valid in the limit  $\nu(t)h < 1$ . For  $h = 0.05$  ms, the above constraint implies  $\nu(t) < 20$  kHz.

The network's neurons receive an external stimulus from a Poissonian spikes train with rate  $\nu_{ext}(t)$ . To avoid the above constraints on firing rate, we exploit an important property of Poisson process. Let  $X$  and  $Y$  be independent Poisson random variables with parameters  $\nu_1$  and  $\nu_2$  and  $Z$  the process defined as the sum of  $X$  and  $Y$ . Then  $Z$  is a Poisson random variable with  $\nu = \nu_1 + \nu_2$ . Accordingly, it is possible to connect  $N_{ext}$  different spikes train with rate  $\nu_{ext}/N_{ext}$  to generate an external input of  $\nu_{ext}$ . Each signal satisfies the above constraint and the network's neurons receive a right poissonian spikes train.

## 2.4 Spectral Analysis

### 2.4.1 Continuous Wavelet Transform (CWT)

Spectral analysis is a technique that allows us to discover the underlying periodicities in the time series. The Fourier transform is the ordinary tool to convert a signal in the frequency domain:

$$\tilde{x}(\omega) = \frac{1}{\sqrt{2\pi}} \int_{-\infty}^{+\infty} x(t) e^{-i2\pi\omega t} dt \quad (2.41)$$

However, under the Fourier transform, the time information is lost, being hard to distinguish transient relations or identify structural changes. Wavelet analysis emerges

---

<sup>3</sup>See Appendix B.2

as an alternative. Wavelet analysis estimates the spectral properties of a time series as a function of time, revealing how its different periodic components change over time [69]. The main differences between the wavelet transform and the Fourier transform are that, in the Fourier case, we do not have a time localization parameter and we have cosine and sine functions instead of a wavelet function. More precisely, starting with a mother wavelet  $\psi$ , a family  $\psi_{\tau,s}$  of wavelet daughters can be obtained by simply scaling and translating  $\psi$ <sup>4</sup>.

$$\psi_{\tau,s} = \frac{1}{\sqrt{s}} \psi \left( \frac{t - \tau}{s} \right) \quad (2.42)$$

where  $s$  is a scaling or dilation factor that controls the width of the wavelet and  $\tau$  is a translation parameter controlling its location. Given a signal  $x(t)$ , its Continuous Wavelet Transform (CWT) with respect to the wavelet  $\psi$  is a function of two variables,  $W_{x,\psi}(\tau, s)$ :

$$W_{x,\psi}(\tau, s) = \int_{-\infty}^{+\infty} x(t) \frac{1}{\sqrt{s}} \psi \left( \frac{t - \tau}{s} \right) dt \quad (2.43)$$

The position of the wavelet in the time domain is given by  $\tau$ , whereas its position in the frequency domain is given by  $s$ . The wavelet transform, by mapping the original series into a function of  $\tau$  and  $s$ , gives us information simultaneously on time and frequency.

The relation between the period  $s$  and the frequency  $\omega$  is not straightforward and depends on the mother functional form of the mother wavelet. The starting point to derive this relation is the definition of the location in the frequency of the mother wavelet, namely the mean of the probability density function. In the frequency domain the centre in frequency  $\mu_{\omega,\psi}$  of a mother wavelet  $\psi$  is given by the following expression:

$$\mu_{\omega,\psi} = \frac{1}{\int_{-\infty}^{+\infty} |\tilde{\psi}(\omega)|^2 d\omega} \int_{-\infty}^{+\infty} \omega |\tilde{\psi}(\omega)|^2 d\omega \quad (2.44)$$

where  $\tilde{\psi}(\omega)$  is the Fourier transform of  $\psi$ . From equation (2.44), we can interpret the scale as frequency by using the formula

$$\omega(s) = \frac{\mu_{\omega,\psi}}{s} \quad (2.45)$$

In our study, we adopt the Morlet wavelet function, a one-parametric wavelet family given by

$$\psi_{\omega_0}(t) = K \cos(\omega_0 t) e^{-\frac{t^2}{2}} \quad (2.46)$$

#### 2.4.2 Wavelet Power Spectrum and Modulation

In analogy with the terminology used in the Fourier analysis, the Local Wavelet Power Spectrum is defined as

$$WPS_{x,\psi}(\tau, s) = |W_{x,\psi}|^2 \quad (2.47)$$

The wavelet power spectrum may be averaged over time for comparison with classical spectral methods. When the average is taken over all times, we obtain the Global Wavelet Power Spectrum (GWPS)

---

<sup>4</sup>For detailed mathematical description assumptions underpinning wavelet functions we refer to [69]

$$GWPS_{x,\psi}(s) = \int_{-\infty}^{+\infty} WPS_{x,\psi}(\tau, s) d\tau \quad (2.48)$$

From the equation (2.48) we can evaluate the frequencies spectrum in the selected time windows. As with other types of transforms, CWT applied to a finite length time series suffers from border distortions due to the fact that the values of the transform at the beginning and the end of the time series involve missing values of the series which are artificially prescribed. Since the support of the wavelet at scale  $s$  is proportional to  $s$ , these edge-effects increase with  $s$ . The region affected by these edge effects is called the Cone of Influence (COI). To avoid the data affected by this error, we consider a time window that must be neglected both at the beginning and the end of the signal.

With GWPS we can compare the power spectrum in two different time windows. We denote the benchmark signal as the baseline and the other one as the signals of interest. The percentage modulation of frequencies is computed as the ratio between the difference between the spectrum of two signals and the baseline one. The modulation  $M$  reads as:

$$M(s) = \frac{GWPS(s)_{\text{signal}} - GWPS(s)_{\text{baseline}}}{GWPS(s)_{\text{baseline}}} \quad (2.49)$$

# Chapter 3

## RESULTS: INTERPLAY BETWEEN NEURONAL AND GLIAL CELLS

The present chapter illustrates the signalling transmission modalities through the chemical synapses and how the frequency of incoming spike trains drives the release of neuromodulators into the synaptic cleft. Accordingly, to have a broad and overreaching comprehension of these phenomena, we start to analyse the well-described picture of bipartite synapses in the presence of short-term plasticity [28, 29] and the gliomodulation effects in the heterosynaptic connection [15]. Thereafter we investigate the more realistic scenario of bidirectional coupling between astrocyte and neurons, the homosynaptic connection. In this context, we present an original procedure to deduce the mean field description of homosynaptic connection exploiting methods of nonlinear dynamics.

### 3.1 Bipartite Synapse

In section 2.1.2, we have already presented the derivation of mean field description of TM model. This mathematically manipulation can be exploited to get quantitative insights into the synaptic transmission. In general, it is possible to solve analytically the first equations of the set (2.14) and then, from this result, obtain the solution of the whole system from the second equation [15]. However, when the presynaptic firing rate is constant in time, namely in the case of a homogeneous Poisson process with rate  $\nu_S$ , the system becomes autonomous and it is possible to evaluate the steady states. In particular, the intersection of nullclines provides the fixed points (or stationary states) for the system:

$$\begin{aligned}\langle \bar{u}_S \rangle &= \frac{u_0(\Omega_f + \nu_S)}{\Omega_f + \nu_S u_0} \\ \langle \bar{x}_S \rangle &= \frac{\Omega_d}{\Omega_d + \langle \bar{u}_S \rangle \nu_S}\end{aligned}\tag{3.1}$$

then, the mean value of release probability is given by the product of the components of the steady state (3.1)

$$\langle \bar{r}_S \rangle = \frac{u_0 \Omega_d (\Omega_f + \nu_S)}{(\Omega_f + \nu_S u_0)(\Omega_d + \langle \bar{u}_S \rangle \nu_S)}.\tag{3.2}$$

This approximated solution can be employed to estimate the behaviour for low and high value of  $\nu_S$ . For low firing rate, i.e.  $\nu_S \rightarrow 0$ , the probability of release tends to  $u_0$

and the available neurotransmitter resources tends to 1, thus  $r_S \rightarrow 1 \cdot u_0 = u_0$ . Conversely for high firing rate, i.e.  $\nu_S \rightarrow +\infty$ ,  $u_S$  tends to 1 and  $x_S$  tends to 0, therefore the average values of neurotransmitter is 0 (solid line in Figure (3.1)).

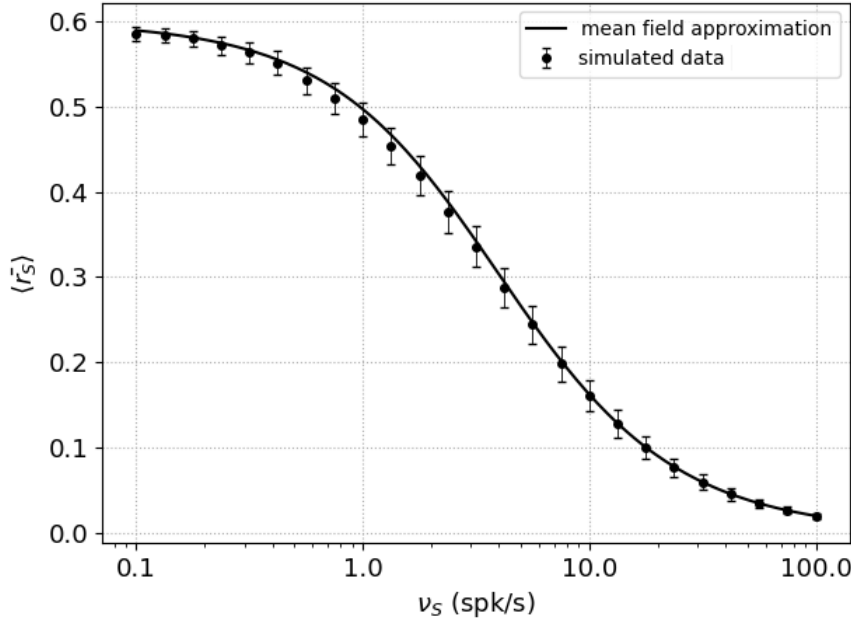


Figure 3.1: **Average release probability for TM model and mean field approximation solution.** Mean field approximation (3.1) and simulated data of  $r_S$ . Mean field approximation satisfying fit numerical data:  $\chi^2 = 0.91$ . Mean and standard error are computed over 30 different runs with the same initial condition for all  $\nu_S$  values. Time simulation cover 200 s, only data after 50 s are taken to evaluate mean and standard error. Integration steps of 1 ms. Parameters as in table in Appendix C.1

Both numerical data and approximated solution help to give important insights about synaptic release in the presence of short-term plasticity. When presynaptic firing rate is low than facilitation and depression time constant, i.e.  $\nu_S \ll \Omega_f, \Omega_d$ , synaptic variables reach their initial values and, as a consequence, the dynamics is equal to the total absence of plasticity. On the other hand, intense presynaptic firing rate provides strong depletion of resources that drastically reduce neurotransmitter exocytosis and, as a consequence, the synaptic strength.

Despite its apparent simplicity, The TM model can generate surprisingly complex dynamics due to the presence of the combination of facilitation and depression. With the mathematical background of mean field derivation, we can investigate the nature of a TM synapse and in particular the nature of transitions between facilitating and depressing responses. The slope of (3.2) with respect to input frequency  $\nu_S$  can be used to distinguish between facilitating and depressing synapse. Indeed, a negative slope implies that the increment of  $r_S$  decreases regarding the input frequencies, hence the occurrence of depression, otherwise a positive slope reflects ongoing facilitation. Notably, for the limit of small input frequency [20], the slope is equal to

$$\langle \bar{r}_S \rangle' (\nu_S \rightarrow 0) = \frac{\Omega_d - (\Omega_d + \Omega_f)u_0}{(\Omega_f \Omega_d)^2} \quad (3.3)$$

which can be either positive or negative depending on the sign of the numerator, therefore

the threshold value of basal release probability reads as

$$u_\theta = \frac{\Omega_d}{\Omega_d + \Omega_f} \quad (3.4)$$

Depending on whether  $u_0$  is respectively below or above the threshold value  $u_\theta$ , the synaptic transmission switch from depressing to facilitation and vice versa: the depressing synapse is defined by the condition  $u_0 > u_\theta$ , facilitating one by  $u_0 < u_\theta$ . That is the crucial point because the gliomodulation introduces new degrees of freedom on basal release probability. Therefore,  $u_0$  is no more a simple parameter, but it becomes a variable in the model. The time evolution allows the system to cross dynamically the threshold value  $u_\theta$ . Accordingly, we can appreciate a transition between the two regime mode of synaptic transmission due to astrocytic activity.

## 3.2 Tripartite Synapses

In line with the description of gliomodulation introduced in section 2.1.3, the tripartite synapses could be seen as a three compartmental model: (i) bipartite synapse with short-term plasticity (2.9), (ii) astrocytic calcium-dependent gliotransmitter and (iii) neurotransmitters and gliotransmitter time course in the ECS. For the sake of clarity, we report here the equations of G-ChI model

$$\begin{aligned} \frac{d\Gamma_A}{dt} &= O_N Y_S (1 - \Gamma_A) - \Omega_N (1 + \zeta \mathcal{H}_1(C, K_{KC})) \Gamma_A \\ \frac{dC}{dt} &= J_r(C.h, I) + J_l(C) - J_p(C) \\ \frac{dh}{dt} &= \frac{h_\infty(C, I) - h}{\tau_h(C, I)} \\ \frac{dI}{dt} &= J_\beta(\Gamma_A) + J_\delta(C, I) - J_{3K}(C, I) - J_{5P}(I), \end{aligned} \quad (3.5)$$

and the time course of chemicals in ECS:

$$\begin{aligned} \frac{dY_S}{dt} &= -\Omega_c Y_S + \sum_k Y_{rel} \delta(t - t_k) \\ \frac{dG_A}{dt} &= -\Omega_e G_A + \sum_j G_{rel} \delta(t - t_j). \end{aligned} \quad (3.6)$$

The synaptic modulation can be presented in two different situations relating to the interaction pathway among these elements. In the *homosynaptic* scenario of gliomodulation, the gliotransmitter exocytosis is modulated by the same synapses that are regulated by the astrocyte. In this type of tripartite synapse the bidirectional coupling, namely astrocyte-to-synapse and synapse-to-astrocyte, drives the dynamics of the system. Otherwise, if we consider only the gliomodulation of presynaptic release induced by astrocytic activity, we deal with a *heterosynaptic* scenario. The latter kind of connection, where the astrocytic activity is independent of the synaptic one, is used to describe how the gliotransmitters could change the synapse's short-term plasticity in the simplest situation. Then, the extension to the more realistic closed-loop is straightforward taking to account the additional term of astrocytic activity dependence on the extracellular space. We want

to stress that one of the peculiar aspects of neuron-glia interaction is the different time scales of neuronal (of the order of milliseconds) and glial (tons of seconds) dynamics. This difference will play a paramount role both in the microscopic and mesoscopic description.

### 3.2.1 Heterosynaptic Connection - open loop

In heterosynaptic connection (or open-loop circuit), the onset of  $\text{Ca}^{2+}$  oscillations depends only on endogenous  $\text{IP}_3$  production, namely in equation (3.5) the  $J_\beta$  flow is not present. The one-directional pathway simplifies the interaction, only the astrocyte influences the synaptic release. Therefore, in this condition, we restrict our focus on the modulation of presynaptic release probability  $r_S$  induced by astrocytic activity. In this context, the equation (2.27) embedded all the properties regarding the release-decreasing effect, in particular with  $\alpha$  is equal to 0, the time course of  $u_0$  becomes

$$u_0(t) = (1 - \Gamma_S(t))U_0^*. \quad (3.7)$$

In the simple bipartite scenario, the presynaptic receptors are totally silent due to the absence of gliotransmitters in ECS, hence the model falls back to a short-term plasticity one with  $u_0 = U_0^*$ . Otherwise, at the arrival of a GRE, a cert amount of gliotransmitters are released and detected by presynaptic receptors. Therefore  $\Gamma_S$ , according to the first ODE in (3.5), grows exponentially at the rate  $O_G G_A$  and then decreases in the same trend at the rate  $\Omega_G$ . The increasing mechanism leads to the decreasing of  $u_0$  which is generally lower than in the simple synapses, from this the name release-decreasing effect, whereas the exponential inactivated process of receptors provides an increase of basal release probability during two consecutive GREs. Figure (3.2) illustrates the above considerations and, in particular, we can merely appreciate modulation effects for time observation in the order of several seconds. The bottom panels show that the time scales of activation and inactivation mechanism are profoundly different from each other. In particular, the activation rate is two orders faster than inactivation one <sup>1</sup>.

---

<sup>1</sup>As reported in Appendix B.3, for typical astrocytic activity  $\nu_A = 0.2$  gre/s, the rate of activation  $O_G G_A$  is equal to 0.1 Hz whereas the inactivation rate is  $\Omega_G = 0.0083$  Hz.

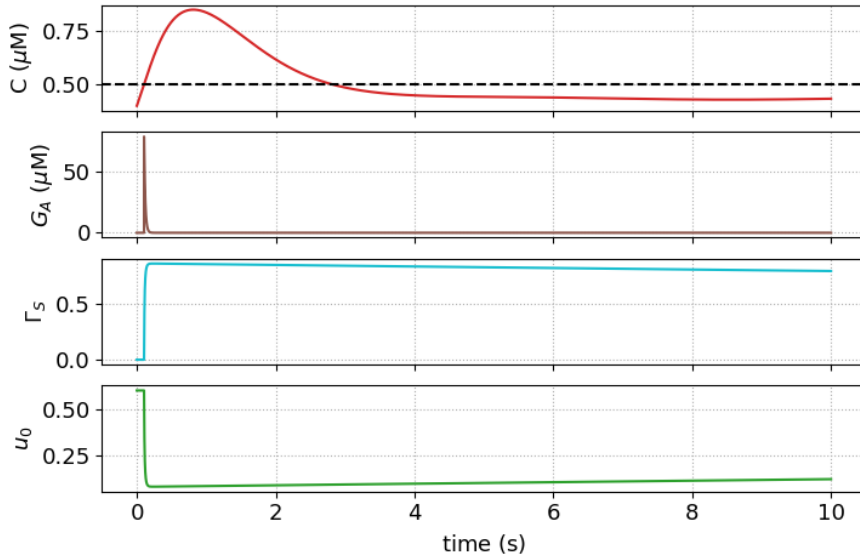


**Figure 3.2: Modulation of basal released probability on open-loop scenario.** Astrocytic calcium oscillation in open-loop scenario (red trace) drives the release of gliotransmitter in ESP (brown trace). Gliotransmitter release at time 97.55 ms triggers an increase of  $\Gamma_S$ , (light blue trace) with the notable effects in the decreasing of basal release probability  $u_0$ . According to the characteristic time scale, the modulation effects are visible for observation time in the order of several seconds. Time simulation of 10 seconds. Parameters as in table in Appendix C.

Notably, these considerations arising from the heterosynaptic connection are completely general and might be present also in the more realistic homosynaptic connection. The core is the activation and inactivation processes of the presynaptic receptor regardless of the selected model. Indeed, the meaningful result of the astrocytic activity is the extension of the phase space, the basal release probability is not further a constant but is a dynamical variable of the model. The natural question is how this new degree of freedom changes the synaptic transmission.

Counterintuitively, the release-decreasing effect does not provide only the drop of neurotransmitter's exocytosis, but also the gliotransmitter-induced facilitation effect.

We have already reported the facilitation effect in bipartite synapses in section 2.1.2 where it is the mechanism by which the concentration of released neurotransmitters increases with the incoming action potentials. We might appreciate a facilitation event in correspondence to an increase of available resources that could ensue when the lag between the  $(i - 1)$ -th and  $i$ -th action potentials is smaller than the lag between the  $i$ -th and  $(i + 1)$ -th ones, that stands for the scenario of *recovery from depression* (RFD). The degree of freedom related to  $u_0$  makes possible, for transient time observation, the effect of facilitation even if the inter-spikes interval between consecutive action potentials does not satisfy the above condition. Indeed, the increasing dynamical behaviour of  $u_0$  between two consecutive gliorelease events provides the mechanism of astrocytic-induced facilitation effects. Moreover, it is not out of sense to suppose that this transient time is proportional to the intensity of the neuron-glia connection. One of the parameters that regulates the interaction's strength is the gliotransmitter concentration released at each exocytosis, indeed an increase of  $G_T$  leads to an increase of  $G_A$  and the activation of a greater fraction of presynaptic receptors, therefore the basal release probability is

strongly modulated (top panel in Figure (3.3)). The aforementioned effects can be quantified by considering synaptic release due to pairs of spikes, and computing for each pair the paired-pulse ratio (PPR) of the fraction of neurotransmitter released by the first one

$$\text{PPR} = \frac{r_{S_{i+1}}}{r_{S_i}}. \quad (3.8)$$

When  $\text{PPR} < 1$  the neurotransmitter released by the second action potential is less than the amount released by the first one (depression effect). Conversely, if  $\text{PPR} > 1$  the synaptic release increases with the incoming action potential (facilitation effect)<sup>2</sup>.

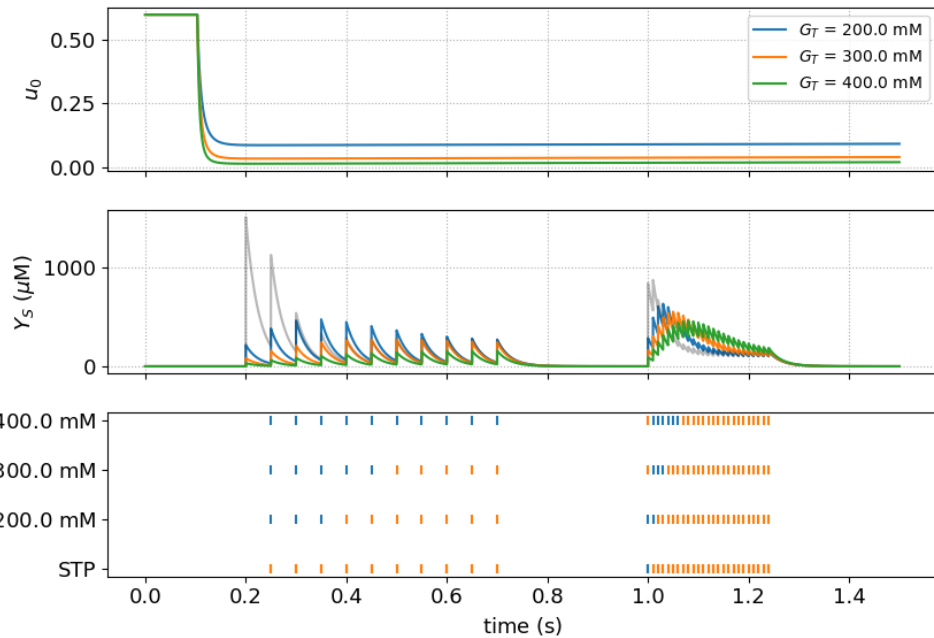


**Figure 3.3: Gliotransmitter-induced facilitation with respect to  $G_T$  in open-loop circuit.** STP and gliotransmitter-induced facilitation effect. Presynaptic firing rate is composed of two distinct regions, the former with 20 spk/s and the latter 100 spk/s. (Top panel) Increasing the gliotransmitter release leads to an increase of  $\Gamma_S$ , as a consequence the basal release probability falls to 0. (Middle panel) Neurotransmitter released by consecutive action potentials shows different behaviour that can be quantified by the PPR factor. (Bottom panel) Every release event is coloured in orange (depression) and blue (facilitation), the transient time of facilitation effect changes across the strength of gliotransmission. Time simulation of 1.5 seconds with integration step of 0.05 ms. Parameters as in table in Appendix C.

The bottom panel in Figure (3.3) summarized the most peculiar results that we can appreciate. In the case of simple STP and with weak gliomodulation, the depletion events dominate the facilitation ones however, in the latter scenario the astrocytic-induced facilitation is present as well as the RFD. The transient time of facilitation is further extended with strong gliomodulation, moreover the RFD event is not more visible. In conclusion, the sequence of depletion and facilitation drives the synaptic transmission that changes in heterosynaptic connection. Without gliotransmission, the extracellular neurotransmitter concentration progressively decreases, whereas this amount tends to increase at every action potential with respect to the preceding one in presence of gliomodulation (middle

<sup>2</sup>We want to stress that, with this expression, we point out the same effect described by analytic equation (3.3) and (3.4). The focus in both scenarios is to understand the behaviour of release probability regarding the presynaptic spike train and the relative switch of transmission modality.

panel in Figure (3.3)).

According to the above results, the strength of astrocytic activity defined by the quantities of released transmitters affects the synaptic transmission. Nevertheless, equations (2.28) and (3.6) suggest that the frequency of gliorelease deeply characterized the dynamics of presynaptic receptors. In these regards, the mean field equations (2.29), (2.31) and (2.32) explain how the temporal scale of gliorelease events involves the modulation of basal release probability. For constant astrocytic firing rate, i.e.  $\nu_A(t) = \nu_A$  is relevant considering the steady state solution of  $\langle \bar{x}_A \rangle$ ,  $\langle \bar{\Gamma}_S \rangle$  and  $\langle \bar{u}_0 \rangle$

$$\begin{aligned}\langle \bar{x}_A \rangle &= \frac{\Omega_A}{\Omega_A + U_A \nu_A} \\ \langle \bar{\Gamma}_S \rangle &= \frac{J_S \Omega_A U_A \nu_A}{\Omega_A \Omega_G + (J_S \Omega_A + \Omega_G) U_A \nu_A} \\ \langle \bar{u}_0 \rangle &= (1 - \langle \bar{\Gamma}_S \rangle) U_0^*\end{aligned}\tag{3.9}$$

For a low astrocytic firing rate,  $\nu_A \rightarrow 0$ , the gliotransmitter resources tends to 1 and the fraction of presynaptic receptors tends to 0, thus the neurotransmitter modulation by astrocyte does not modify the basal release probability. For higher  $\nu_A \rightarrow +\infty$ , instead,  $x_A$  tends to 0 whereas  $\Gamma_S$  approaches to its limit value  $J_S \Omega_A / J_S \Omega_A + \Omega_G$ , in this situation the modulation is stronger than anything else and the basal probability tends to 0. Figure (3.4) shows the behavior of basal release probability for release-decreasing effect, in particular  $\langle \bar{u}_0 \rangle$  decreases with increasing  $\nu_A$ .

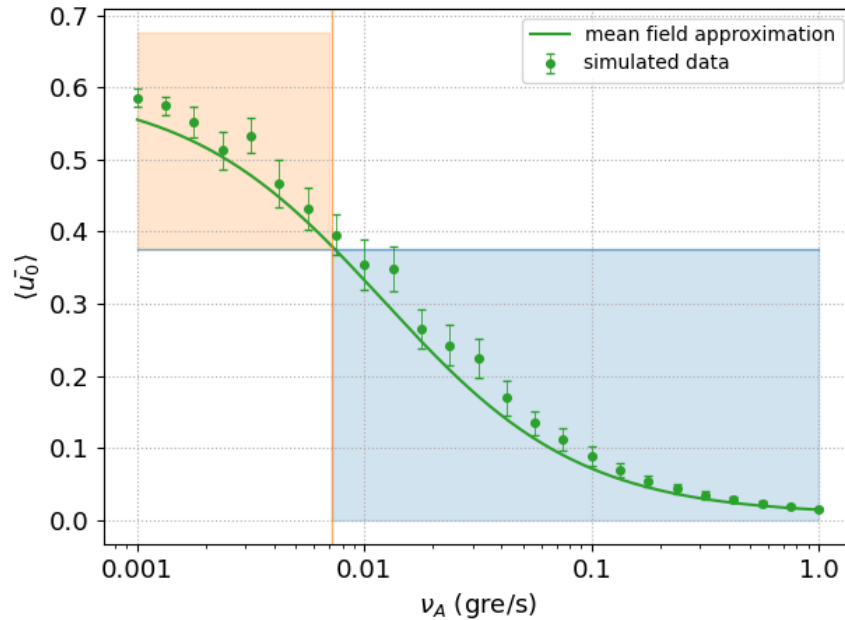


Figure 3.4: **Average basal release probability for heterosynaptic connection and mean field approximation solution.** Basal synaptic release probability is controlled by the rate of gliotransmitter release. For release-decreasing effect  $u_0$  decrease with  $\nu_A$  (green trace and dots) and a threshold  $\nu_\theta$  (orange vertical line) can be identified in correspondence of  $u_\theta$  (horizontal blue line). The astrocytic firing rate drives the shift between depressing (orange-shaded region) and facilitating synapses (blue-shaded region). Mean field approximation (3.9) and simulated data of  $u_0$ . Mean field approximation solution satisfying fit numerical data:  $\chi^2 = 1.80$ . Time simulation cover 1000 s, only data after 300 s are taken to evaluate mean and standard error. Integration steps for synapses and astrocytes are respectively 1 ms and 0.01 s. Parameters as in table in Appendix C except for  $O_G = 0.5 \mu\text{M}^{-1}\text{s}^{-1}$ .

The curve  $\langle \bar{u}_0 \rangle$  versus  $\nu_A$  also shows that for a particular value of the GRE rate, denoted by  $\nu_\theta$  (vertical orange line), basal release probability crosses the threshold release probability  $u_\theta$  (horizontal blue line). Such frequency  $\nu_\theta$  can be regarded as the threshold rate of gliotransmitter exocytosis that triggers the switch between facilitating and depleting synaptic transmission. That is, a depressing synapse, that is originally characterized by  $u_0 > u_\theta$ , could turn facilitating for  $\nu_A > \nu_\theta$  in the presence of release-decreasing gliotransmission whereby  $u_0 < u_\theta$  (Figure (3.4), blue-shaded area). We want to stress again that the novel proprietary induced by the glia is that the synaptic transmission modality is not static, instead it is a dynamical feature regulated by astrocytic activity. Moreover, the further extension toward homosynaptic connection introduces the feedback coupling mechanism synapse-to-astrocyte that make the astrocytic activity dependent on the same synaptic one. Therefore, in this situation, the presynaptic firing rate modulates the process of synaptic transmission to the postsynaptic target. In this sense, the implications of bidirectional coupling are the topic of further analysis.

### 3.2.2 Homosynaptic Connection - closed loop

In the previous discussion, we have only considered one-way interactions between synapse and astrocyte, the modulation of synaptic release by gliotransmission. However, in the general case, the other possible pathway namely the astrocytic activity dependence on synaptic release may coexist with the other in the closed-loop circuit. Indeed, the synaptic exocytosis triggers in astrocytes an additional mechanism of  $\text{IP}_3$  production depending on

extracellular neurotransmitters concentration. The exogenous  $\text{IP}_3$  production profoundly affects the dynamics of its concentration  $I$  and, for the strong nonlinear coupling with  $C$ , also the onset of calcium oscillation and the timing of gliorelease events as reported in Figure (3.5).

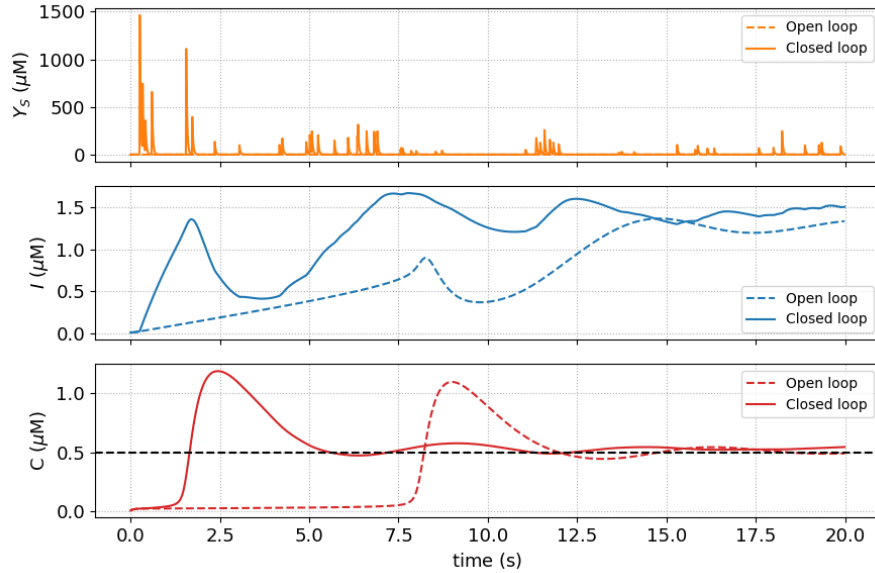


**Figure 3.5: Differences between astrocyte dynamics in open- and close-loop circuit.** Astrocytic variable dynamics in open- (dashed) and closed-loop (solid) circuit. By definition, the neurotransmitter concentration that stimulates the open-loop circuit is equal to 0, for this reason in the top panel the associated dashed line is not visible. Exogenous  $\text{IP}_3$  production deeply changes the  $I$  time evolution and this is reflected in the onset of calcium oscillations. Time simulation is equal to 20.0 seconds. the initial conditions are equals in both open- and closed-loop scenario. Parameters as in table in Appendix C;  $C_\theta = 0.5 \mu\text{M}$  (dashed black line).

The neurotransmitter concentration in the synaptic cleft is the variable that regulates the modulation of astrocyte dynamics due to synaptic activity. As the presynaptic receptors are sensible to gliotransmitters, the astrocytic receptors  $\Gamma_A$  show the activation and inactivation mechanism due to the  $Y_S$  through the first equation in (3.5). In the first stage, we can consider the release from presynaptic button independent to gliorealese event. With this constraint, we can appreciate the variation of the dynamical regime due to synaptic activity. More precisely, from equation (3.6) and the mean value of the release probability (3.2), we can deduce the average quantity in the extracellular space induced by STP synapses:

$$\langle \bar{Y}_S \rangle = \frac{\rho_s Y_T}{\Omega_c} \langle \bar{r}_S \rangle \nu_S \quad (3.10)$$

The typical behaviour of plasticity tends to a fixed value of neurotransmitters for increasing presynaptic firing rate  $\nu_S$  (right panel in Figure (3.6)).

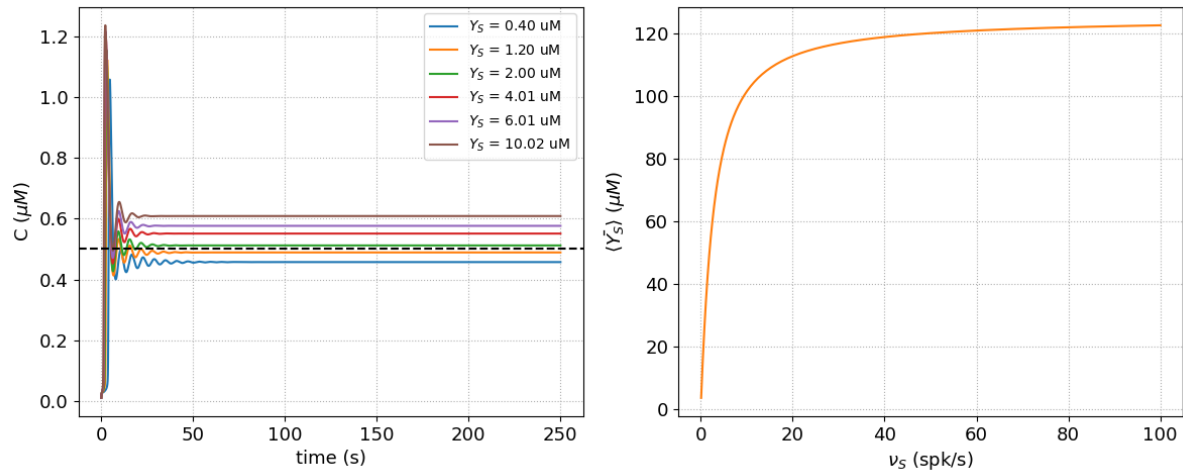


**Figure 3.6: Synaptic modulation of astrocytic dynamics.** (Right panel) The average value of neurotransmitters concentration in the synaptic cleft concerning the presynaptic firing rate. (Left panel) The astrocytic calcium time courses for G-ChI model with 6 constant values of  $Y_S$ . The steady state stands for the average value of calcium in the complete dynamical model, namely when we consider also the dynamics of  $Y_S$ . Time simulation and integration steps are respectively equal to 250 s and 0.01 s. Parameters as in table in Appendix C except for  $O_\beta = 2.0 \mu M s^{-1}$ ,  $O_\delta = 0.6 \mu M s^{-1}$ ;  $C_\theta = 0.5 \mu M$  (dashed black line).

The G-ChI model with control (constant) parameter  $Y_S$  represents the dynamics of the mean astrocytic variables. The left plot in Figure (3.6) elucidates the encoding mechanism of the external stimulus. The mean value of intracellular calcium concentration increase with the intense concentration of neurotransmitters.

Nevertheless, this is a simplistic portrait of the complex dynamics of homosynaptic connection. Indeed, we cannot neglect the time course of  $Y_S$  to take into account all possible dynamical regimes as amplitude or frequency modulation described in section 2.1.3. Therefore, we need to deal with the full G-ChI model coupled with STP synapses to describe the main physiological features of homosynaptic connection. The description of synaptic regulation of astrocytic dynamics highlights an important aspect that drives all the below considerations. In the tripartite synapses, and more specifically in homosynaptic connection, the driving "force" is the presynaptic firing rate. Accordingly, we consider a Poisson process with a rate  $\nu_S$  to simulate the neural variability and make the model closer to the physiological setting.

In this sense, the average across several synaptic release events in the bipartite and tripartite synapses sheds light on the functional implications of gliotransmission. Figure (3.7) shows the time evolution of average neurotransmitter concentration in the synaptic cleft in response to a constant input rate. Gliotrasmission dramatically changes synaptic transmission: after a gliorelease event, the neurotransmitters abruptly decrease both in open- and closed loops, and then increase according to the facilitation effect tenting to reach the concentration in the simple situation. The notable differences are found in GRE distribution shown in the right panel. The astrocytes in heterosynaptic connection are independent of synaptic activity, hence fire at the same time whereas in closed-loop the bidirectional coupling makes the distribution of GREs sparser. Despite the timing of exocytosis events by astrocytes, the inactivation and activation process of presynaptic receptors are the main protagonists in tripartite synapses. More precisely, the rate of the inactivation process can be interpreted as the drift moving the systems toward its baseline

condition, namely without gliomodulation. Hence, an increase in  $\Omega_G$  gets the presence of astrocytic activity less weighty and the synaptic transmission tends to be equal to bipartite synapses one (Figure (3.8) A). Similarly, the activation process regulates the susceptibility of the synapse to the concentration of gliotransmission, thereby increasing  $O_G$  leads to faster release-decreasing effects (Figure (3.8) B).

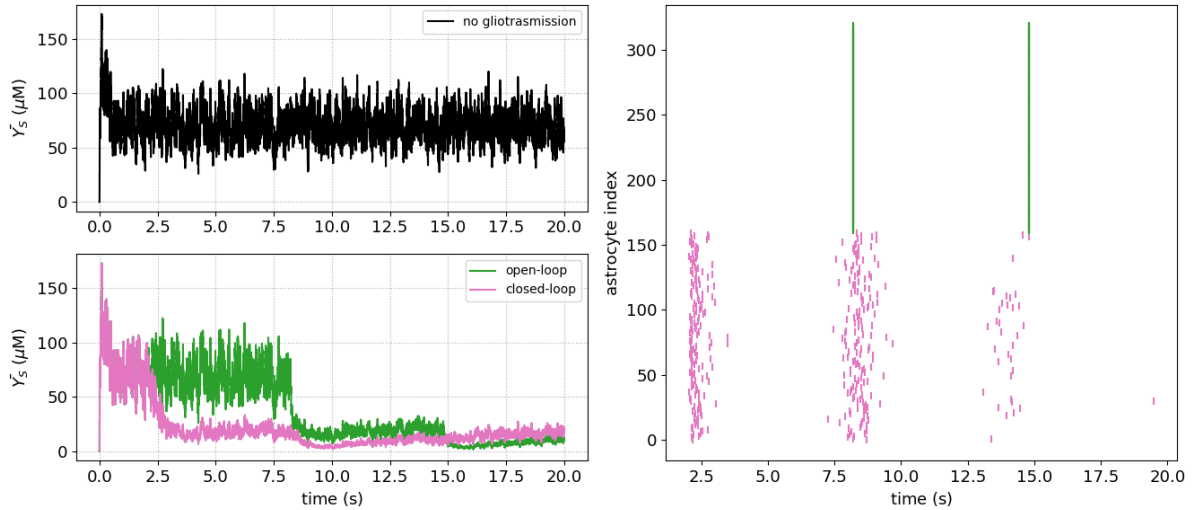


**Figure 3.7: Average neurotransmitter release in case of bipartite and tripartite synapses.**  
 Average neurotransmitter release across 160 independent and identical synapses for 20 second long simulation with identical initial condition. The presynaptic firing rate is generated by the homogeneous Poisson process with  $\nu_S = 3.5$  (spk/s). In simple synapses (black trace)  $\bar{Y}_S$  have a constant mean value of  $70 \pm 15 \mu\text{M}$  over all time simulation, gliotransmission modulation of  $u_0$  deeply changes this dynamical behaviour both in open- (green trace) and closed-loop (pink trace). Raster plot of GRE, astrocytes labeled from 0 to 160 (pink marker) are part of closed-loop, the other one (green) of open-loop. Initial conditions:  $I=C=0.01 \mu\text{M}$ ,  $h=0$ ,  $Y_S=0 \mu\text{M}$ . Time simulation cover 20 second with integration steps of 0.05 ms. Parameters as in table in Appendix C

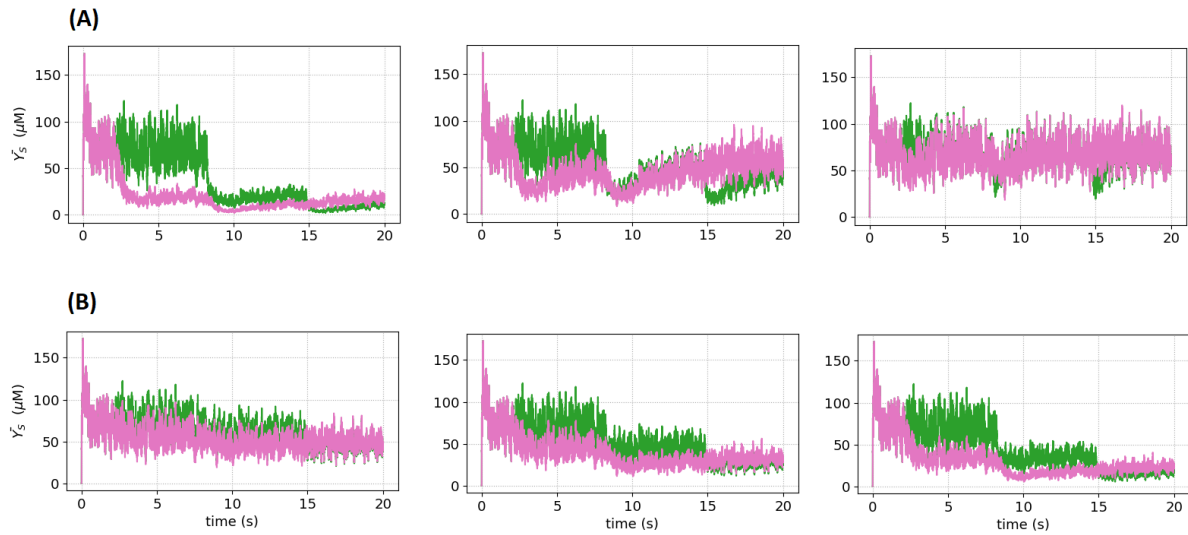


**Figure 3.8: Depressing and Facilitation effects with respect to  $\Omega_G$  and  $O_G$ .** Inactivation and activation of presynaptic receptor drive respectively facilitation (A) and depression (B) effects. Time simulation cover 20 second. Parameters: (A)  $O_G = 1.5 \mu\text{M}^{-1}\text{s}^{-1}$ , from left to right  $\Omega_G = 0.0083 \text{ s}^{-1}$ ,  $\Omega_G = 0.0833 \text{ s}^{-1}$ ,  $\Omega_G = 0.8333 \text{ s}^{-1}$ . (B) (B)  $\Omega_G = 0.0083 \text{ s}^{-1}$ , from left to right  $O_G = 0.3 \mu\text{M}^{-1}\text{s}^{-1}$ ,  $O_G = 0.6 \mu\text{M}^{-1}\text{s}^{-1}$ ,  $O_G = 0.9 \mu\text{M}^{-1}\text{s}^{-1}$

### Filtering characteristic

The differences in terms of signalling transmission between bipartite and tripartite synapses are further elucidated by looking at the average synaptic release for different rates of randomly incoming action potentials. In this way, we may analyse the nature of filtering behaviour in presence of gliotransmitters release.

We have already depicted in Figure (3.1) how short-term plasticity in bipartite synapses affects neurotransmitter release as a low-pass filter. Indeed, for the selected facilitation and depression rate,  $r_S$  exponentially decreases for increasing inputs rate, hence only low frequencies can carry out the signal to the target neurons. Moreover, the gliomodulation induced by heterosynaptic connection allows the synapses to dynamically switch their transmission mode through the value of gliorelease rate. Nevertheless, the astrocytic exocytosis happens when intracellular calcium concentration overreaches a threshold value, furthermore, the neuron-astrocyte interaction became much more intricate in homosynaptic connection. Indeed, the bidirectional coupling makes the inner astrocytic dynamics dependent on the synaptic one, in other words, the modulation of gliorelease by the synapses is beside the modulation of synaptic release by the glia. It is pleonastic to underline that a quantitative description of such complex systems is far more demanding than the previous ones, however, we have enough information, also through the numerical effort, to deduce a qualitative description of synaptic transmission in the closed-loop scenario.

Firstly, the calcium oscillations across the threshold are mandatory to observe the gliomodulation and their temporal scale drives the depletion and facilitation effects. Additionally, in the closed-loop the type of connection makes the dynamics of the whole system totally regulated by the presynaptic spikes train, namely  $\nu_S$  is regarded as control parameter. The bifurcation plots are suitable tools to individuate the range of control parameter for which the gliomodulation is present.

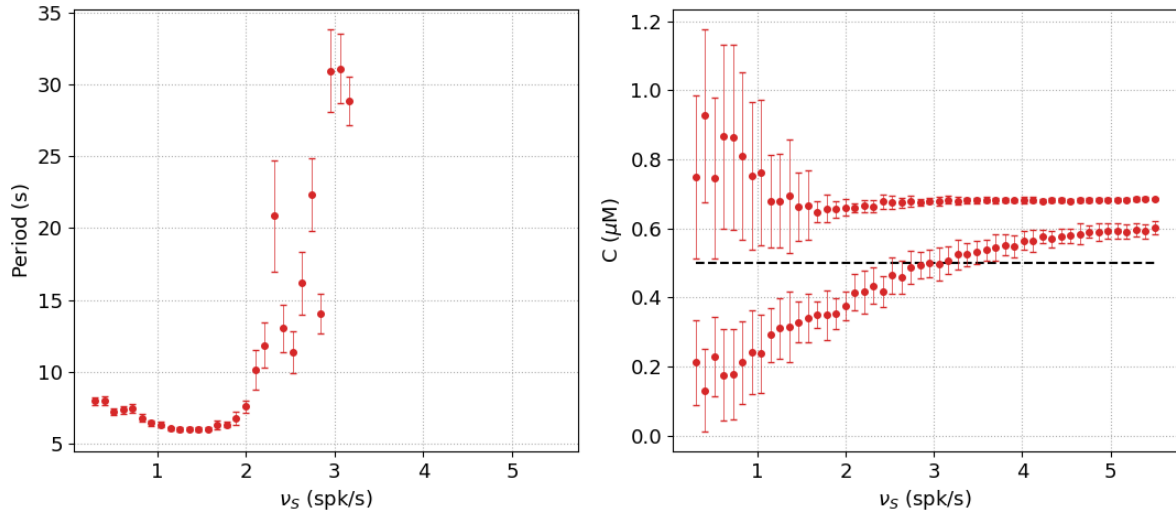


Figure 3.9: **Bifurcation analyses of noisily closed-loop synapses.** (Right panel) calcium oscillations across the threshold arise for low presynaptic firing rate. (Left panel) Periods of such oscillations. Mean and standard error are computed over 30 different runs with the same initial condition for all  $\nu_S$  values. Time simulation cover 500 second, only data after 400 second are taken to compute bifurcation plots. Integration steps for synapses and astrocytes are respectively 1 ms and 0.01 s. Parameters:  $O_\beta = 2.0 \mu\text{M s}^{-1}$ ,  $O_\delta = 0.6 \mu\text{M s}^{-1}$ ,  $O_G = 1.5 \mu\text{M}^{-1}\text{s}^{-1}$ ,  $\Omega_G = 0.0083 \text{s}^{-1}$ ,  $C_\theta = 0.5 \mu\text{M}$  (dashed black line).

As illustrated in the right plot of Figure (3.9), the oscillations across the threshold are visible for low inputs rate whereas they are above the threshold for  $\nu_S$  greater than  $\sim 3$  spk/s. The periods of such oscillations also show an increasing dependence on the presynaptic firing rate. This particular behaviour gives us an important clue about the modulation of basal release probability.

The modulation of astrocytic activity by synaptic release provides a relation between gliotransmitters and neurotransmitters release rate, i.e.  $\nu_A \equiv \nu_A(\nu_S)$  as reported in the left panel of Figure (3.9). More precisely, the inversely proportional relation leads to null astrocytic firing rates in correspondence with high input rates. Thus, we expect the modulation of  $u_0$  and the switch between transmission modes to be regulated by  $\nu_S$ . This is an emergent behaviour not present in naive synapses where the signalling modality depends exclusively on facilitation and depression parameters. Indeed, we can appreciate the switch from facilitating to depressing mode with increasing presynaptic firing rate (Figure(3.10)).

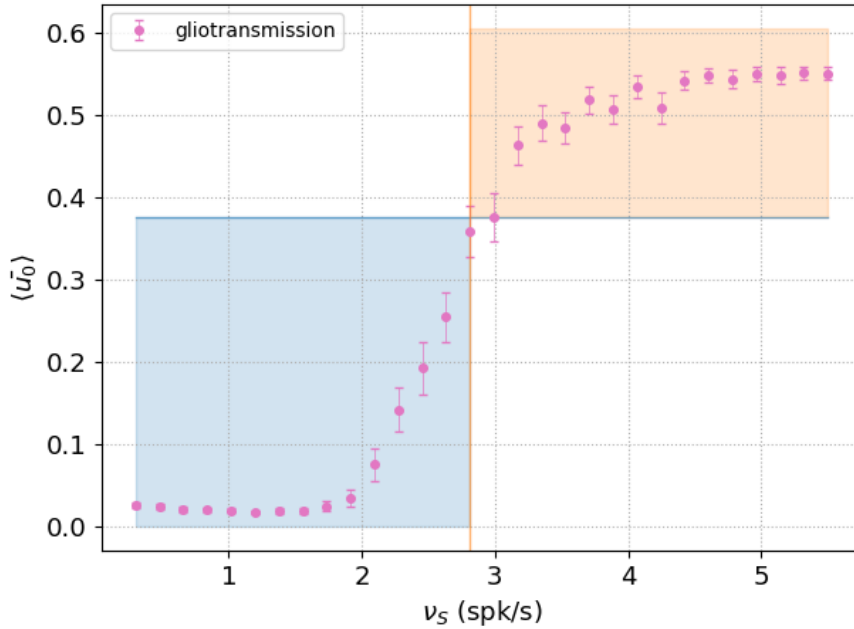


Figure 3.10: **Average basal release probability for homosynaptic connection.** The mean value of  $\bar{u}_0$  in the closed-loop (pink dots) scenario shows a symmetric behaviour with respect to open-loop one. Presynaptic firing rate regulates the transition mode from facilitating (blue-shaded region) for low  $\nu_S$  to depressing synapses (orange-shaded region). Mean and standard error are computed over 20 different runs with the same initial condition for all  $\nu_S$  values. Time simulation cover 200 s, only data after 50 s are taken to evaluate mean and standard error. Integration steps for synapses and astrocytes are respectively 1 ms and 0.01 s. Parameters:  $O_\beta = 2.0 \text{ } \mu\text{M} \text{ s}^{-1}$ ,  $O_\delta = 0.6 \text{ } \mu\text{M} \text{ s}^{-1}$ ,  $O_G = 1.5 \text{ } \mu\text{M}^{-1} \text{ s}^{-1}$ ,  $\Omega_G = 0.0083 \text{ s}^{-1}$

For the selected parameter, the rate of facilitation effect ( $\Omega_G$ ) is greater than the release-decreasing one ( $O_G G_A$ ). This is the crucial point to qualitatively explain the switch of transmission modes.

For low frequencies, the concentration of neurotransmitters allows a persistent astrocytic activity with a specific rate (see the right plot in figure 3.9). Then, due to the time characteristic of  $\Gamma_S$ , the system is not able to reach its baseline condition and, as a consequence, the average value  $\bar{u}_0$  is strongly modulated. Therefore, between two consecutive gliorelease events, the slight increase of basal release probability provides the glial-induced facilitation effect (blue-shaded region). The lower astrocytic activity ensues in the neighbourhood of threshold value  $\nu_\theta$  (orange vertical line) which able the system to tend at its baseline condition that comes only in the total absence of glial activity, namely in the depression region (orange-shaded region). This condition occurs when the concentration of neurotransmitters in the cleft is so elevated that does not allow the deactivation process of the astrocytic membrane receptor needed for the onset of gliorelease.

All the ensuing features from the above qualitative description are condensate in the filtering feature. Only low input rates could modulate neurotransmitter release probability and make the synapse more silent than in the absence of an astrocyte whereas, high input rates cannot further sustain gliotransmitter release and the release probability equals the case of simple synapses. This is elucidated in Figure (3.11) where the filter characteristic of simple bipartite synapse is compared with tripartite synapses in closed-loop one. The low-pass filter characteristic of synapses without gliotransmission (black dots) turns into a bell-shaped, band-pass filter characteristic caused by homosynaptic connection (pink

dots).

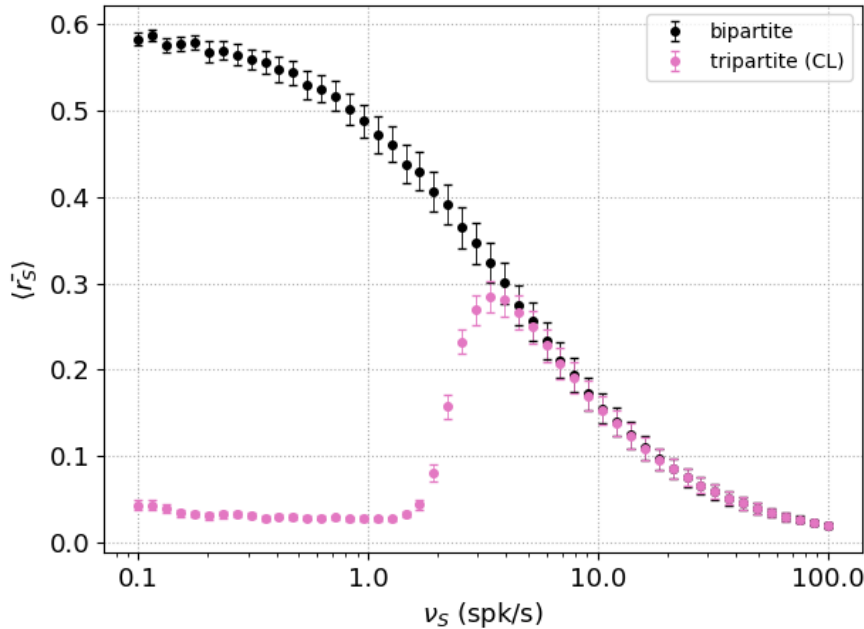


Figure 3.11: **Average release probability for TM model of bipartite synapses and closed-loop tripartite synapse ones.** Filtering characteristic curve passes from low-pass filter for bipartite synapse to a band-pass filter for tripartite one. Mean and standard error are computed over 30 different runs with the same initial condition for all  $\nu_S$  values. Time simulation cover 200 second, only data after 50 second are taken to evaluate mean and standard error. Integration steps for synapses and astrocytes are respectively 1 ms and 0.01 s. Parameters:  $O_\beta = 2.0 \text{ } \mu\text{M} \text{ s}^{-1}$ ,  $O_\delta = 0.6 \text{ } \mu\text{M} \text{ s}^{-1}$ ,  $O_G = 1.5 \text{ } \mu\text{M}^{-1} \text{ s}^{-1}$ ,  $\Omega_G = 0.0083 \text{ s}^{-1}$

According to the above considerations, the emergent aspect induced by glia is the possibility to process the external input in two distinct ways and this occurs in a dynamical fashion depending on the frequency of the input. Indeed, the modulation of synaptic filtering by gliotransmission offers the possibility that the same stimulus could be differently processed and transmitted to the postsynaptic target in the presence or not of surrounding astrocytic processes, ultimately providing synapses with a versatile processing feature with respect to the incoming action potential. Notably, to the extent of the synaptic dynamics critically shape the computations performed by the neural circuitry, such versatility could also be reflected at the network level.

### 3.2.3 Mean field description of homosynaptic connection

The mean field derivations of neurotransmitters release probability in simple short-term plasticity synapses in section 3.1 and of the gliotransmission modulation in section 3.2.2 are the starting points of a possible analytical description of homosynaptic connection. The fundamental assumptions used to deduce the steady states of mean-dynamical variables are the statistical independence and the description by Poisson processes of neurotransmitters and gliotransmitters release. Moreover, by definition, the basal release probability in heterosynaptic connection is independent of synaptic dynamics. Therefore, the sets of relations (3.1) and (3.9) describe the mean quantities of two totally disjointed systems. The great issue induced by homosynaptic connection is the link between these two systems that makes  $u_0$  dependent on the very synaptic dynamics. Following the same

kind of reasoning, we can deduce a mean field derivation of homosynaptic connection with the assumption of statistical independence between  $u_0$  and  $u_S$ , accordingly the mean field dynamics reads as

$$\begin{aligned}\frac{d\langle\bar{u}_S\rangle}{dt} &= \Omega_f(\langle\bar{u}_0\rangle + \langle\bar{u}_S\rangle) + \langle\bar{u}_0\rangle(1 - \langle\bar{u}_S\rangle)\nu_S \\ \frac{d\langle\bar{x}_S\rangle}{dt} &= \Omega_d(1 - \langle\bar{x}_S\rangle) - \langle\bar{u}_S\rangle\langle\bar{x}_S\rangle\nu_S \\ \frac{d\langle\bar{x}_A\rangle}{dt} &= \Omega_A(1 - \langle\bar{x}_A\rangle) - U_A\langle\bar{x}_A\rangle\nu_A \\ \frac{d\langle\bar{\Gamma}_S\rangle}{dt} &= J_S U_A\langle\bar{x}_A\rangle(1 - \langle\bar{\Gamma}_S\rangle)\nu_A - \Omega_G\langle\bar{\Gamma}_S\rangle \\ \langle\bar{u}_0\rangle &= U_0^* + (\alpha - U_0^*)\langle\bar{\Gamma}_S\rangle\end{aligned}\tag{3.11}$$

The information about the bidirectional coupling is embedded into the relation between  $\nu_A$  and  $\nu_S$ . Therefore, assuming the presynaptic firing rate as a control parameter, we need to deduce a cert biological function  $\nu_A \equiv \nu_A(\nu_S)$ , thus the equations (3.11) become

$$\begin{aligned}\frac{d\langle\bar{u}_S\rangle}{dt} &= \Omega_f(\langle\bar{u}_0\rangle + \langle\bar{u}_S\rangle) + \langle\bar{u}_0\rangle(1 - \langle\bar{u}_S\rangle)\nu_S \\ \frac{d\langle\bar{x}_S\rangle}{dt} &= \Omega_d(1 - \langle\bar{x}_S\rangle) - \langle\bar{u}_S\rangle\langle\bar{x}_S\rangle\nu_S \\ \frac{d\langle\bar{x}_A\rangle}{dt} &= \Omega_A(1 - \langle\bar{x}_A\rangle) - U_A\langle\bar{x}_A\rangle\nu_A(\nu_S) \\ \frac{d\langle\bar{\Gamma}_S\rangle}{dt} &= J_S U_A\langle\bar{x}_A\rangle(1 - \langle\bar{\Gamma}_S\rangle)\nu_A(\nu_S) - \Omega_G\langle\bar{\Gamma}_S\rangle \\ \langle\bar{u}_0\rangle &= U_0^* + (\alpha - U_0^*)\langle\bar{\Gamma}_S\rangle\end{aligned}\tag{3.12}$$

Without experimental data, a possible procedure to find a analytic expression of guess function is the qualitative approach, more precisely analysing how the tripartite synapse responds to noiseless input. A constant external input leads to inter-spikes interval having a delta function-like distribution, accordingly we can further elucidate the inner dynamical features of tripartite synapses unrelated to neuronal variability.

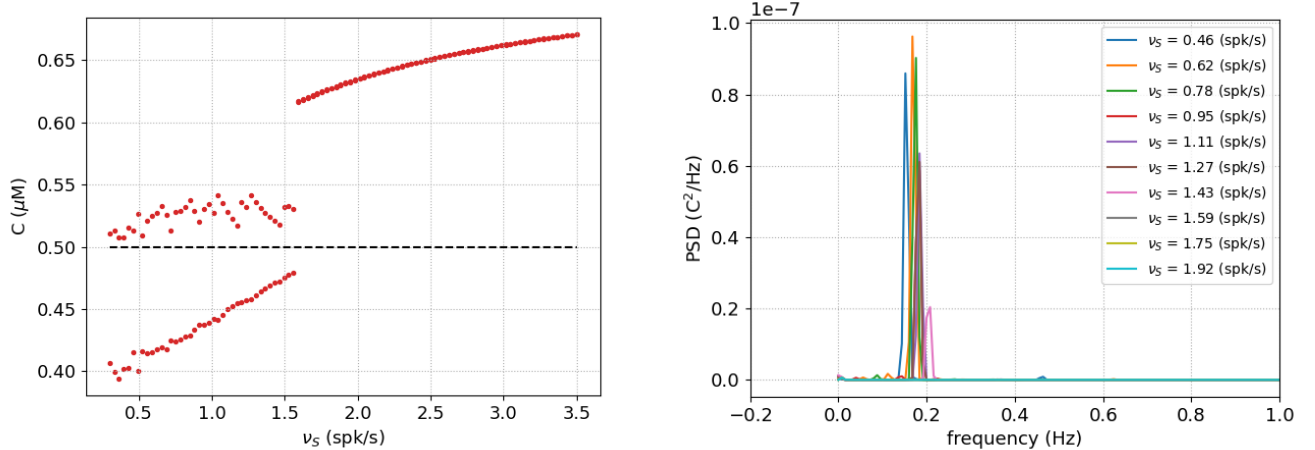


Figure 3.12: **Bifurcation plot and power spectral density of noiseless closed-loop synapses.** Noiseless bifurcation analysis (right plot) shows bifurcation for low frequencies input rate and different amplitude of calcium oscillation, power spectrum densities suggest the amplitude modulation [19]. Parameters:  $O_\beta = 2.0 \mu\text{M s}^{-1}$ ,  $O_\delta = 0.6 \mu\text{M s}^{-1}$ ,  $O_G = 1.5 \mu\text{M}^{-1}\text{s}^{-1}$ ,  $\Omega_G = 0.0083 \text{ s}^{-1}$ ;  $C_\theta = 0.5 \mu\text{M}$  (dashed black line).

With these aims, we can individuate the possible range of input signals for which the gliomodulation occurs. Indeed, as reported in the left panel of Figure (3.12), the oscillations across the threshold with varied amplitudes turn into suprathreshold steady states for  $\nu_S = \nu_S^{bif}$ . This qualitative change in dynamical features can be regarded as a bifurcation and used as a guide to deduce a guess function for  $\nu_A(\nu_S)$ . The power spectrum in the right panel of Figure (3.12) indicates the oscillations arise at constant frequencies  $\nu_{A_0}$ , otherwise the steady states do not sustain any kind of gliomodulation. These evidences suggest for a guess function a step-like one with constant gliorelease rate  $\nu_{A_0}$  for input frequencies less than  $\nu_S^{bif}$ . However, to consider a continuous relation between  $\nu_A$  and  $\nu_S$  we select an exponential decay with characteristic time  $\tau_A$  to link the two regions. Finally, for  $\nu_A(\nu_S)$  is proposed the following expression:

$$\nu_A = \begin{cases} \nu_{A_0} & \text{with } \nu_S \leq \nu_S^{bif} \\ \nu_{A_0} e^{-\tau_A(\nu_S - \nu_S^{bif})} & \text{with } \nu_S > \nu_S^{bif} \end{cases} \quad (3.13)$$

In principle, the rate of exponential decay might be any combination of astrocytic parameters. Moreover, the bifurcation analysis shows that the qualitative change of dynamical behaviour arises in a discontinuous fashion. Then, the parameters  $\tau_A$  strongly limps biophysical information about the systems. The steady states of these mean field approximation reads as:

$$\begin{aligned} \langle \bar{u}_S \rangle &= \frac{\langle \bar{u}_0 \rangle (\Omega_f + \nu_S)}{\Omega_f + \nu_S \langle \bar{u}_0 \rangle} \\ \langle \bar{x}_S \rangle &= \frac{\Omega_d}{\Omega_d + \langle \bar{u}_S \rangle \nu_S} \\ \langle \bar{x}_A \rangle &= \frac{\Omega_A}{\Omega_A + U_A \nu_A(\nu_S)} \\ \langle \bar{\Gamma}_S \rangle &= \frac{J_S \Omega_A U_A \nu_A(\nu_S)}{\Omega_A \Omega_G + (J_S \Omega_A + \Omega_G) U_A \nu_A(\nu_S)} \\ \langle \bar{u}_0 \rangle &= U_0^* + (\alpha - U_0^*) \langle \bar{\Gamma}_S \rangle \end{aligned} \quad (3.14)$$

where  $\nu_A(\nu_S)$  is given by equation (3.13).

The bifurcation analysis allow us to deduce the gliorelease rate  $\nu_{A_0}$  and the bifurcation point  $\nu_S^{bif}$  starting from the results presented in Figure (3.12). Nevertheless, it is anything but trivial to find a relation between  $\tau_A$  and the time scale parameters that regulate the synapse-to-astrocyte interplay. Thus, we have to estimate its value from simulated data. More specifically, we present to the system different realizations of input  $\nu_S$  for all investigated values. Then, we evaluate the frequency of gliorealese events, namely the biological guess function  $\nu_A(\nu_S)$ . From this numerical data, we can compute a linear fit (in logarithmic scale) of the equation (3.13) to estimate the parameters  $\tau_A$  as reported in Figure (3.13).

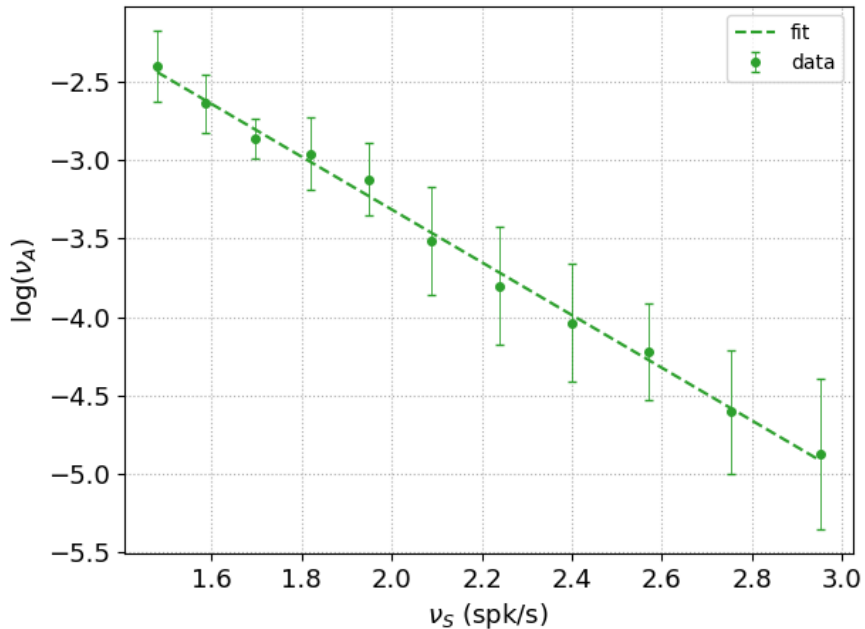


Figure 3.13: **Linear fit used to estimate  $\tau_A$ .** Numerical data of guess function (dots) and linear fit (dashed line). The data are computed over 30 different trials. We evaluate the fit only for  $\nu_S > \nu_S^{bif}$ , the region of interest of exponential decay. The equation used for the fit reads as:  $\log(\nu_A) = \log(\nu_{A_0}) - \tau_A (\nu_S - \nu_S^{bif})$ . we estimate the other two parameters keeping fix  $\nu_S^{bif}$ :  $\nu_{A_0} = 0.084 \pm 0.003$  gre/s,  $\tau_A = 1.68 \pm 0.04$  s. The intersection estimation does not provide a good method (at least for this set of parameters) to evaluate the astrocytic firing rate because we do not take into account the low frequencies, i.e.  $\nu_S < \nu_S^{bif}$ . Parameters for numerical data:  $O_\beta = 2.0 \mu\text{M s}^{-1}$ ,  $O_\delta = 0.6 \mu\text{M s}^{-1}$ ,  $O_G = 1.5 \mu\text{M}^{-1}\text{s}^{-1}$ ,  $\Omega_G = 0.0083 \text{ s}^{-1}$

The mean field approximation and simulated data of average release probability are reported in Figure (3.14). The approximation solution (solid line) can reproduce the bandpass filter characteristic described by numerical data (dots). Nevertheless, it is quite clear looking at the data that the goodness of the prediction changes with respect to the control parameters. In particular, the analytical solution fits numerical data more adequately for high values of input frequencies.

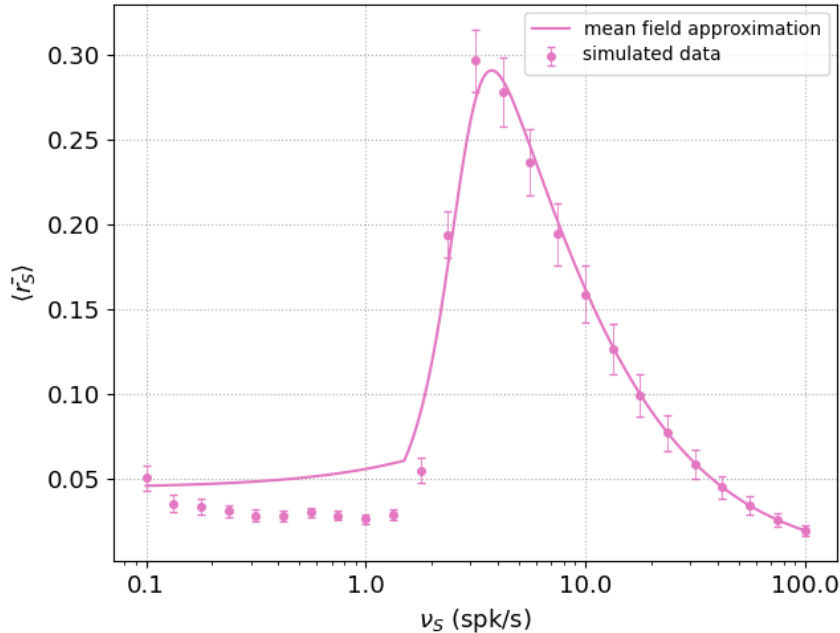


Figure 3.14: **Average release probability for closed-loop tripartite synapses and mean field approximation solution.** Mean field approximation (3.14) and simulated data of  $r_S$ . Mean and standard error are computed over 30 different runs with the same initial condition for all  $\nu_S$  values. Time simulation cover 200 s, only data after 50 s are taken to evaluate mean and standard error. Integration steps for synapses and astrocytes are respectively 1 ms and 0.01 s. Parameters for mean field:  $\nu_{A_0} = 1.80 \pm 0.07$  gre/s,  $\nu_S^{bif} = 1.55 \pm 0.05$  spk/S,  $\tau_A = 1.68 \pm 0.04$  s. Parameters for numerical data:  $O_\beta = 2.0 \mu\text{M s}^{-1}$ ,  $O_\delta = 0.6 \mu\text{M s}^{-1}$ ,  $O_G = 1.5 \mu\text{M}^{-1}\text{s}^{-1}$ ,  $\Omega_G = 0.0083 \text{ s}^{-1}$

A closer inspection of the mean field description highlights the weakness to predict the behaviour for the low-frequency range. Therefore, further considerations are necessary to understand all the underpinning mechanisms that drive the tripartite synapses in this range of input stimuli.

The plots in figure (3.12) are related to a dynamical response of the system to noiseless external input. Instead, we consider several trials with different noise realization in the filter characteristic dotted curve for each presynaptic firing rate. In the general case, it might be possible that the oscillations above the threshold are induced by neuron variability for some astrocytic parameters range. Therefore, the information coming from noiseless systems might lead to incomparably clues with the real physiological setting.

To elucidate this scenario, we consider other combinations of astrocytic parameters that determine the time scale of IP<sub>3</sub> production, i.e.  $O_\beta = 0.5 \mu\text{Ms}^{-1}$ ,  $O_\delta = 1.2 \mu\text{Ms}^{-1}$ . The left panel in Figure (3.15) elucidates the noiseless behaviour of the system. For all investigated presynaptic firing rates, suprathreshold dynamical regimes are always present. In other words, the total absence of gliorelease events does not trigger gliomodulation. This evidence leads us to a null estimation of parameters  $\nu_{A_0}$  and  $\nu_S^{bif}$ . Accordingly, the mean field description (solid line in the right panel) reproduces the filter characteristic curve of simple bipartite synapses with STP. Interesting, the simulated data about the system with neural variability (dots in the right panel), show a completely different situation. Instead, for low inputs, the gliomodulation is clearly visible and the band-pass filter is restored. Therefore, this conclusion suggests that the inner dynamic of astrocytic does not provide alone the mechanism of gliomodulation.

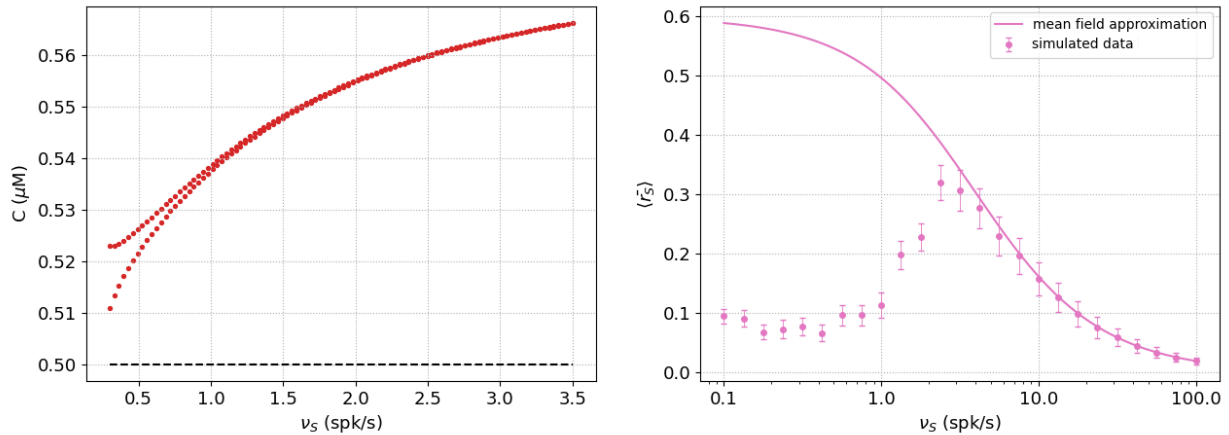


Figure 3.15: **Limits of mean field description to capture low frequency behavior.** Mean field approximation (3.14) and simulated data of  $r_S$ . (Left panel) Bifurcation plot of noiseless system, suprathreshold dynamical regimes are present for all presynaptic firing rates. (Right panel) Mean field (solid line) and simulated data (dots) follow completely different behaviour. Mean and standard error are computed over 10 different runs with the same initial condition for all  $\nu_S$  values. Time simulation cover 200 s, only data after 50 s are taken to evaluate mean and standard error. Integration steps for synapses and astrocytes are respectively 1 ms and 0.01 s. Parameters for mean field:  $\nu_{A_0} = 0$  gre/s,  $\nu_S^{bif} = 0$  spk/s. Parameters for numerical data:  $O_\beta = 0.5 \mu\text{M s}^{-1}$ ,  $O_\delta = 1.2 \mu\text{M s}^{-1}$ ,  $O_G = 1.5 \mu\text{M}^{-1}s^{-1}$ ,  $\Omega_G = 0.0083 \text{ s}^{-1}$ ;  $C_\theta = 0.5 \mu\text{M}$  (dashed black line).

Possible evidence that the neuronal variability generates the gliomodulation effect emerges from the most significant signals of astrocytic dynamics plotted in Figure (3.16). As we have already seen, an increase in synaptic activity leads to an astrocytic calcium steady state further away from the threshold value. The neural variability of synaptic response provides a degree of variability also in the calcium dynamics. Thus, if its steady state is close to the threshold, the variability allows the train of gliorelease events (left and middle columns). Instead, for intense presynaptic firing rates, the steady state is far enough from the threshold and, the gliomodulation is not further sustained (right column).

In other words, the astrocytic firing rate  $\nu_{A_0}$  strongly depends on the neural variability. Therefore, the estimation from the data of noiseless systems guides us to inconsistent results for this set of parameters. It is important to underline that also for the first combination of parameters, the neural variability affects the dynamical behaviour of tripartite synapses. However, as we have already depicted, the oscillations across the threshold are dominated by the proper dynamical behaviour of astrocytes. Therefore, with the aforementioned procedure we can reproduce the shape of the functional relationship between the release of neurotransmitters and the presynaptic firing rate.

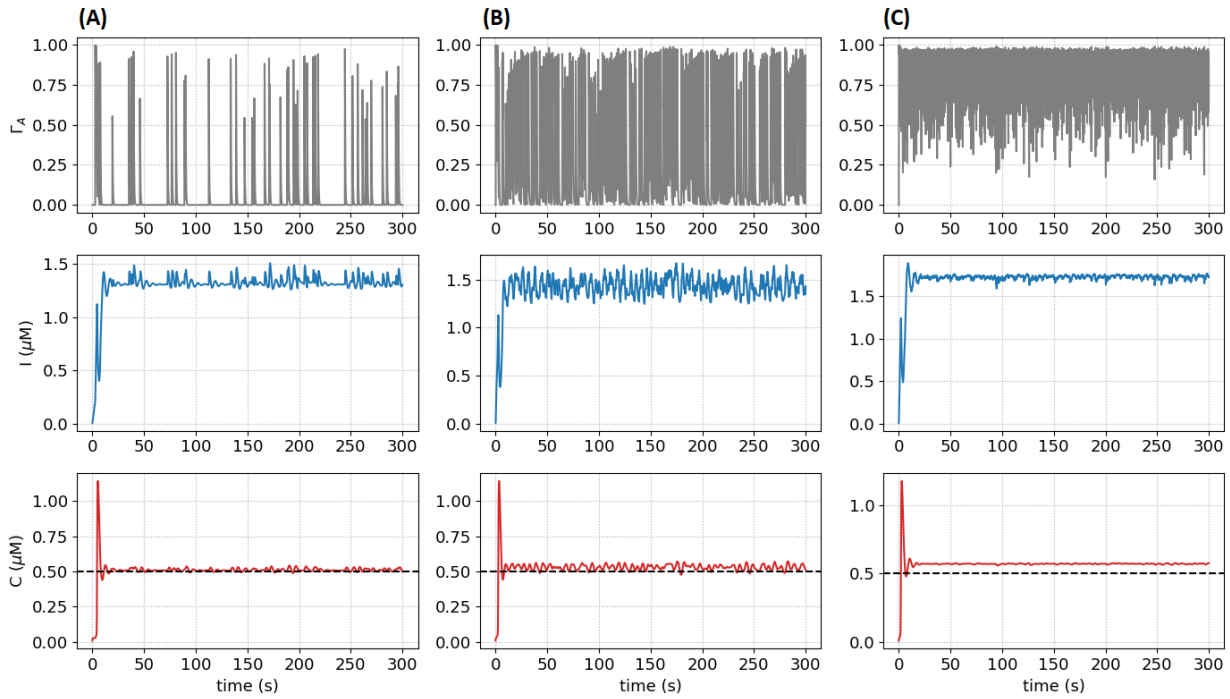


Figure 3.16: **Oscillations across threshold induced by neural variability.** Astrocytic variables time courses:  $\Gamma_A$  (grey),  $I$  (blue),  $C$  (red). The oscillations across the threshold are present only for low firing rates (left and middle column). An increase in presynaptic firing rate leads to an increase in calcium steady and the variability induced by noise does not provide any further gliorelease event (right column). Time simulation cover 300 s. Presynaptic firing rate: (A)  $\nu_S = 0.15 \text{ spk/s}$ , (B)  $\nu_S = 1.12 \text{ spk/s}$ , (C)  $\nu_S = 12.6 \text{ spk/s}$ . Parameters:  $O_\beta = 0.5 \mu\text{M s}^{-1}$ ,  $O_\delta = 1.2 \mu\text{M s}^{-1}$ ,  $O_G = 1.5 \mu\text{M}^{-1}s^{-1}$ ,  $\Omega_G = 0.0083 \text{ s}^{-1}$

However, also in the case of neuron-variability-induced gliomodulation, the bifurcation analysis and the biological guess function could be used to spot (at least) the typical bell-shaped curve of filtering behaviour. Indeed, with the parameters in Figure (3.15),  $\nu_S^{bif}$  equals to 0, thereby the guess function becomes:

$$\nu_A = \nu_{A_0} e^{-\nu_S \tau_A} \quad (3.15)$$

This equation describes our biological guess function as a simple exponential decay starting from an initial value of the astrocytic activity. Therefore, it is possible to estimate both the characteristic time decay  $\tau_A$  and the initial value  $\nu_{A_0}$  through the linear form of the equation (3.15). In Figure (3.17) the mean field approximation solution is plotted besides numerical data. Finally, we can obtain a mean field solution closer than the one shown in Figure (3.15). More specifically, we can reproduce the bell-shaped curve by taking to account also the neuron variability.

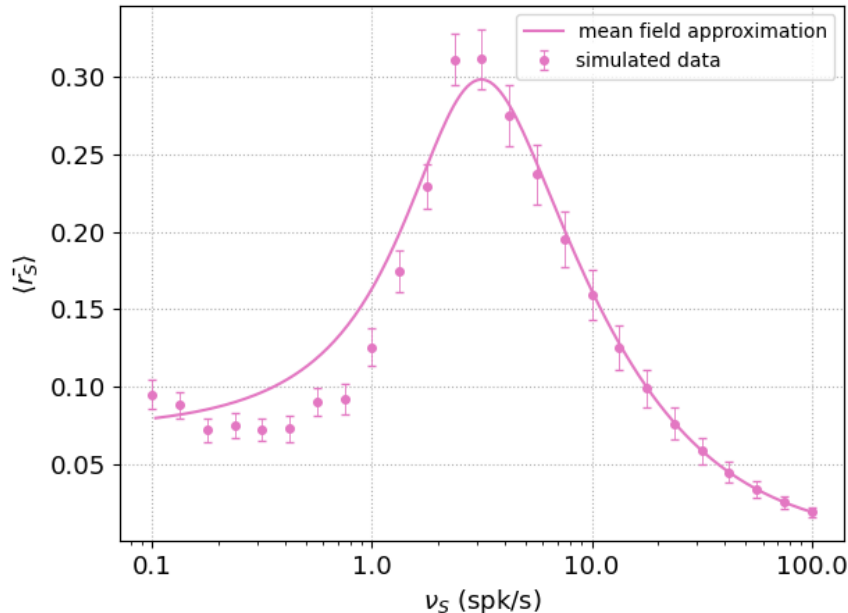


Figure 3.17: **Average release probability for closed-loop tripartite synapses and mean field approximation solution.** Mean field approximation (3.14) and simulated data of  $r_S$ . Mean and standard error are computed over 30 different runs with the same initial condition for all  $\nu_S$  values. Time simulation cover 200 s, only data after 50 s are taken to evaluate mean and standard error. Integration steps for synapses and astrocytes are respectively 1 ms and 0.01 s. Parameters for mean field:  $\nu_{A_0} = 0.097 \pm 0.003$  gre/s,  $\nu_S^{bif} = 0$  spk/S,  $\tau_A = 0.87 \pm 0.03$  s. Parameters for numerical data:  $O_\beta = 0.5$   $\mu\text{Ms}^{-1}$ ,  $O_\delta = 1.2 \mu\text{Ms}^{-1}$ ,  $O_G = 1.5 \mu\text{M}^{-1}\text{s}^{-1}$ ,  $\Omega_G = 0.0083 \text{ s}^{-1}$

The attempt to derive an analytic approximation solution of the closed-loop tripartite synapse brought all the issues out of the nonlinear dynamical system. Indeed, taking to account the functional coupling between two variables makes demanding quantitative analysis.

The first limitation lies in the range of validity of statistical independence between  $u_0$  and  $u_S$ . The estimation of the error due to this approximation is mandatory to control the goodness of adopted mean field derivation (see Appendix A.1). Despite the possibility to take under control the error due to this assumption, the functional coupling between astrocyte and synapse is the most peculiar characteristic of homosynaptic connection. Therefore, taking to account the statistical independence of these two systems is a strong limitation for physiological points of view. The second issue concerns the biological function bridging the neurotransmitters and gliotransmitters releases. As we have depicted above, the relation strongly depends on both astrocytic dynamics and the features that determine neural responses. Neglecting just one of them, for instance neuronal variability, might lead to a completely wrong interpretation of the entire phenomenon.

The assumptions that simplify the system to deduce information as close as possible to the real scenario are anything but straightforward. In this sense, the computational effort arises as a useful tools to investigate the dynamics of such complex physical systems. In the framework of the neuron and neuron-glia networks, computational simulations are even more essential.

# Chapter 4

## RESULTS: NEURON-GLIA NETWORKS

Once obtained the information about the gliomodulation on the microscopic level, the forward step is describing how the presence of glial cells affects mesoscopic dynamics, namely the neuron-glia network dynamics. The original results concern the variation of network balance and the modulation of the power spectrum induced by astrocytic activity. To obtain these goals, it is necessary to understand how the network organization and the coupling between elements drive the network dynamics. Therefore, we describe the structural organization of the model of the spiking excitatory/inhibitory network and the neuron-glia one. Following a step-by-step procedure, we emphasize the main alteration induced by the mechanisms that drive the network dynamics, namely synaptic plasticity and gliomodulation. Accordingly, the effects due to the presence of STP are investigated concerning the structural feature of the neural network. Then, we investigate how gliomodulation affects the mesoscopic quantities coming from the above results. Finally, the long-term effects of astrocytic activity are quantified by looking at the average value of mesoscopic measurements and the network oscillations.

### 4.1 Network Model

For the core of our neuron-glia network, we chose an excitatory/inhibitory spiking neural network with inter- and intrapopulation connections. This network is composed of  $N = N_e + N_i = 4000$  neurons,  $N_e = 3200$  excitatory and  $N_i = 800$  inhibitory ones. The network connectivity among neurons is described by a random and sparse matrix  $C_{l,m}$  with  $l, m = 1, \dots, N$ , in particular, the connecting probability with an excitatory neuron is  $p_e = 0.05$  whereas it is  $p_i = 0.2$  with an inhibitory one. With this choice of parameters, each cell receives on average the same amount of recurrent input equal to  $N_e p_e = N_i p_i = 160$ . Because the inhibitory synaptic strength is 20 times greater than the excitatory one (see parameters values in Appendix C), the entire network has a strong inhibitory recurrent connection. Nevertheless, we introduce the structural variable  $g$  (degrees of balance) to treat networks with different ratios between recurrent excitation and inhibition. The excitatory/inhibitory balance implies the total excitatory synaptic strength ingoing each neuron is equal to the inhibitory ones:

$$w_e N_e p_e = w_i N_i p_i \quad (4.1)$$

thus, fixed the number of neurons  $N_x$  and the synaptic strength  $w_x$  ( $x = e, i$ ), the degrees of balance is defined as

$$g = \frac{p_e}{p_i} = \frac{w_i N_i}{w_e N_e} \quad (4.2)$$

the value  $g = 5$  satisfies the balance condition (4.1), if  $g < 5$  the network presents strong inhibitory recurrent connections, complementary  $g > 5$  represents the case where the recurrent excitation prevails.

The inner connections are provided by short-term plasticity synapses, hence the synaptic strengths  $w_e$  and  $w_i$  are modulated by the factor  $r_S$  described in equation (2.7). All neurons are described by conductance-based leaky integrate and fire (see equations (2.4) where the external input comes from a pool of excitatory neurons thereby the frequency  $\nu_{ext}(t)$  characterizes the input stimuli. Moreover, to describe the neural variability, each spikes train of external input is a different realization of Poisson process (see section 4.1.1). To deal with the heterogeneous input connections, the external conductance  $\tilde{w}_e$  is equal to  $w_e$  on excitatory and  $s w_e$  on inhibitory neurons, where  $s$  is the parameter that measures how much the external input on the inhibitory population is stronger than on excitatory one. In particular, for  $s = 1$  the homogeneous scenario is restored.

The membrane potential of neuron  $l$  in the excitatory/inhibitory network ( $V^{(l)}$ ) evolves according to:

$$\begin{aligned} C_m \frac{dV^{(l)}}{dt} &= g_l(E_l - V^{(l)}) + g_e^{(l)}(E_e - V^{(l)}) + g_i^{(l)}(E_i - V^{(l)}) + g_{ext}^{(l)}(E_e - V^{(l)}) \\ \frac{dg_e^{(l)}}{dt} &= -\frac{g_e^{(l)}}{\tau_e} + \sum_{m=1}^{N_e} C_{l,m} w_e \sum_k r_S(t_{m_k}) \delta(t - t_{m_k}) \\ \frac{dg_i^{(l)}}{dt} &= -\frac{g_i^{(l)}}{\tau_i} + \sum_{n=1}^{N_i} C_{l,n} w_i \sum_k r_S(t_{n_k}) \delta(t - t_{n_k}) \\ \frac{dg_{ext}^{(l)}}{dt} &= -\frac{g_{ext}^{(l)}}{\tau_e} + \sum_{p=1}^{N_{ext}} \tilde{w}_e \sum_k \delta(t - t_{p_k}) \end{aligned} \quad (4.3)$$

As described in section 2.1.3, the neuron-glia interaction appears at the synaptic level and it is quite noticeable that the situation is further complicated when we have to treat gliomodulation at the network level. Precisely, experimental evidence suggests that an hippocampal astrocyte contacts about 100.000 synapses [65] moreover, astrocytes are organized in complex networks through connections by gap junction channels that are regulated by extra- and intracellular signals [14]. Theoretical and computational efforts to understand the dynamical properties of such complex system go beyond the purpose of the present thesis. Nevertheless, we consider a network which can contain information as close to the current physiological knowledge as possible: each astrocyte is available to take part in several tripartite synapses whereas we only neglect the connectivity among non-neural cells.

Starting from the model described in [16], we consider  $N_a = N = 4000$  astrocytes whereby each of them is coupled with all the excitatory synapses ingoing into a post-synaptic neurons, thus neurons-astrocytes connectivity is described by a matrix  $A_{l,m_l}$ , where  $l = 1, \dots, N_a$  and  $m_l = 1, \dots, N_e^{syn}$ , the total number of excitatory synapses. More precisely, an astrocyte is coupled on average with  $N_e p_e$  excitatory synapses each of them

is a recurrent input of a single neuron. Therefore we deal with a uniform distribution of neurons-astrocytes connection. However, the latter affects all the excitatory recurrent inputs ingoing neuronal cells and, moreover, its dynamic is driven by the average activity across each synapse <sup>1</sup>.

Finally, the system of the ODEs describing the time evolution of single neuron in neuron-glia network reads as:

$$\begin{aligned} C_m \frac{dV^{(l)}}{dt} &= g_l(E_l - V^{(l)}) + g_e^{(l)}(E_e - V^{(l)}) + g_i^{(l)}(E_i - V^{(l)}) + g_{ext}^{(l)}(E_e - V^{(l)}) \\ \frac{dg_e^{(l)}}{dt} &= -\frac{g_e^{(l)}}{\tau_e} + \sum_{m=1}^{N_e} C_{l,m} w_e \sum_k A_{l,m_l} r_S(t_{m_k}) \delta(t - t_{m_k}) \\ \frac{dg_i^{(l)}}{dt} &= -\frac{g_i^{(l)}}{\tau_i} + \sum_{n=1}^{N_i} C_{l,n} w_i \sum_k r_S(t_{n_k}) \delta(t - t_{n_k}) \\ \frac{dg_{ext}^{(l)}}{dt} &= -\frac{g_{ext}^{(l)}}{\tau_e} + \sum_{p=1}^{N_{ext}} \tilde{w}_e \sum_k \delta(t - t_{p_k}) \end{aligned} \quad (4.4)$$

the term  $r_S(t_{m_k})$  lumps all the information about astrocytic regulation through equations (2.27) and (2.28). Once the time evolution of a single neuron in the interacting populations is known, it is natural finding some measurements to quantify the global activity. One common measurement of network activity is the *instantaneous firing rate* defined as:

$$\nu(t) = \lim_{\Delta t \rightarrow 0} \frac{1}{\Delta t} \frac{n_{act}(t; t + \Delta t)}{N} = \frac{1}{N} \sum_{i=1}^N \sum_k \delta(t - t_{i_k}) \quad (4.5)$$

where  $n_{act}(t; t + \Delta t)$  is the number of active neurons in a small time interval  $\Delta t$ . Looking at equation (4.5), global activity is defined by a population average. More delicate is monitoring the LFP in a spiking model. Following the computational effort of the morphological [33] and dimensionless model [32], in this project, we approximate the LFP as the sum of absolute values of recurrent excitatory and inhibitory currents and external excitatory stimulus on the pyramidal cells:

$$\text{LFP} = \sum_{l=1}^{N_e} |I_{exc_l}| + |I_{inh_l}| \quad (4.6)$$

#### 4.1.1 Poisson Heterogeneity

In the model presented in [16], the external signal is a constant current  $I_{ext}$  injected to each neuron. We consider a more realistic scenario where the stimulus comes from external neurons coupled to the network ones with excitatory synapses. These synapses have constant strength  $\tilde{w}_e$  without any kind of plasticity dynamics. We have used the following procedure to obtain the same neural activity between the two above types of connection:

---

<sup>1</sup>The connection between synapses and astrocytes in the network is slightly but significantly different to the simple situation in chapter 3. To describe the behaviour of tripartite synapses we consider a 1-to-1 link between single elements. In our network with uniform distribution, on average, we deal with 160-to-1 like tripartite synapses. This feature particularly emerges in long-time effects.

1. evaluate the neural activity  $\nu_{out}$  due to constant external current  $I_{ext}$ ;
2. evaluate the same activity in the case of synaptic connection with  $\nu_{ext}$ ;
3. plot the input/output curve for different values of  $\nu_{ext}$ ;
4. set  $\nu_{ext}$  such that the activity in 1. is equal to activity in 2.

The input/output curve described in 3 is reported in figure (4.1). For instance, we have to set a rate  $\nu_{ext} = 7.63$  kHz to obtain the same neural activity of  $I_{ext} = 100$  pA. The synaptic connection provides that each neuron receives, on average, the same amount of injected current with different noise realization.

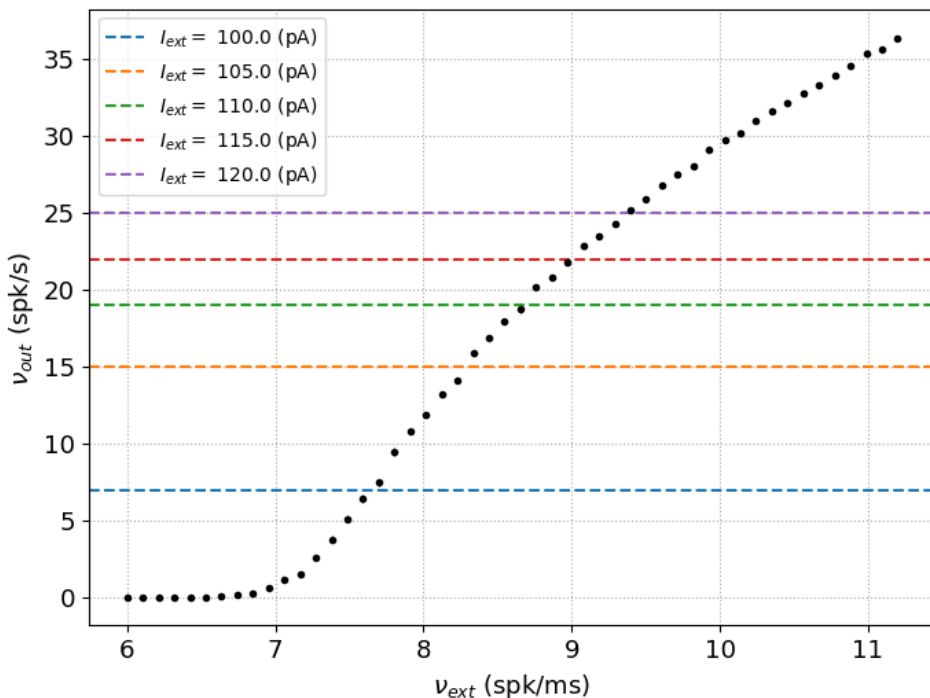


Figure 4.1: **Input/output characteristic curve for the network's neuron.** The input/output characteristic curve (black dot) and the neural activity with a constant external input for 5 different  $I_{ext}$  values (horizontal coloured dashed lines). Each point of the curve is the mean across 50 different realizations of the same Poisson process. The time simulation is 1 second with an integration step of 0.05 ms. Neuron dynamics is described by equations (B.2) without synaptic currents. Parameters:  $N_{ext} = 160$ .

## 4.2 STP influence on E/I Network

The physiological and dynamical features of a single unit are not sufficient to understand the behaviour of the interacting complex system. A neural network of interacting inhibitory and excitatory populations can generate a wide range of dynamical regimes. We can appreciate this variegated dynamical portrait because of the strong nonlinearity of the neural dynamics and the type of connection, even in the absence of plasticity [66]. It is straightforward to stress that the situation is further complicated if we introduce the dynamical properties of synaptic connections, such as short-term plasticity and, of course, gliomodulation. Accordingly, the first step is to analyse how the presence of synaptic

plasticity drives the global activity of neural networks concerning the architecture parameters. More precisely, different external inputs are presented to two networks with and without STP to investigate the variation of their responses in terms of the mean firing rate of excitatory and inhibitory populations and LFP.

We have illustrated in section 3.1 that plasticity involves depletion of neurotransmitter release. A less intense recurrent synaptic connection, though, does not lead necessarily to a drop in network activity.

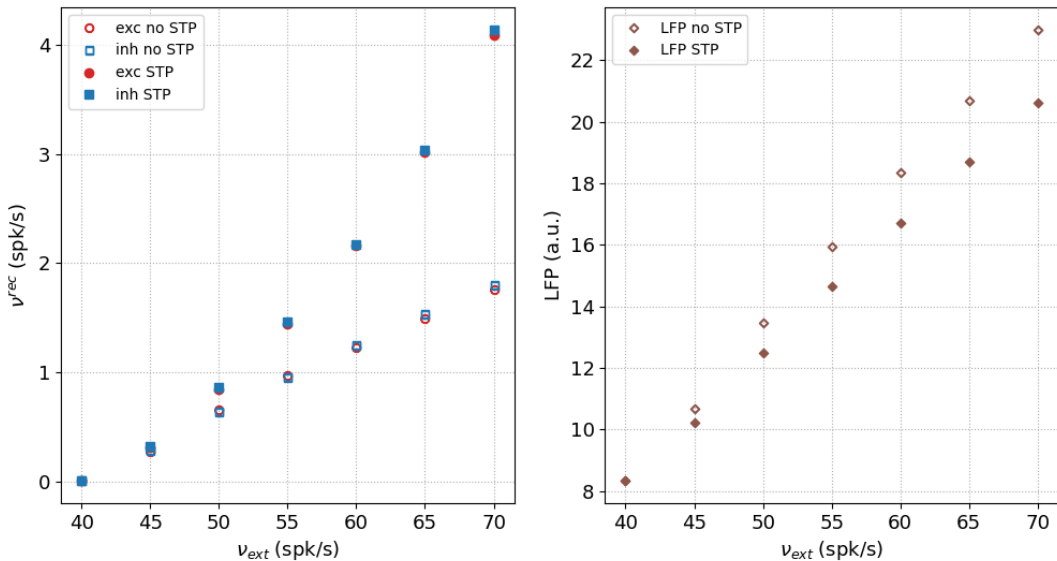


**Figure 4.2: Average Population Activities with respect to different inputs.** Population activity is monitored by average values of population firing rate (left panel) and LFP (right panel). The behaviour with increasing external input shows that the SPT have a different influence on firing rate and LFP. In the former case, the activity of the network is higher for STP (fully coloured symbols) than in absence of STP (edges coloured symbols). The latter case shows conversely situations. Neurons receives an input of  $\nu_{ext}$  coming from  $N_{ext} = 160$  external neurons. Each simulation run for 3.5 second long time simulation with integration steps of 0.05 ms. The data are monitored after a transient of 500 ms. Parameters:  $g = 0.25$ ,  $s = 1.0$

Indeed, the plots in Figure (4.2) reveal that STP leads to an increase in average firing rate in both populations (left panel), whereas it induces a drop in average LFP (right panel). The motivation of such effects must be found in the time evolution of synaptic conductance in equation (4.3).

All information about synaptic modulation is embedded in  $r_S$ . In absence of plasticity the releases are independent of previous action potential arrivals, thus  $r_S = 1$  such that the conductance's jumps are always equal to  $w_x$  ( $x = (e, i)$ ). In presence of STP, instead, the amplitude of jumps changes across the spikes train. For instance, the arrival of inhibitory presynaptic action potential determines an increase of  $w_i r_S(t_{J_j})$  in  $g_i$  variable, where  $t_{J_j}$  is the  $j$ -th spike timing of inhibitory presynaptic neuron  $J$ . The mean value of total inhibitory jumps is given by the sum of all presynaptic neurons and overall their spikes:

$$\overline{\Delta g_i} = \frac{1}{N_{tot}} \sum_{J,j} w_i r_S(t_{J_j}) \quad (4.7)$$

accordingly, the mean values of  $r_S$  computed over inhibitory synaptic variables  $\overline{r_{Sinh}}$  reads as:

$$\overline{r_{Sinh}} = \frac{\overline{\Delta g_i}}{w_i} \quad (4.8)$$

It may be possible to compute in the same way the mean value of  $r_S$  from the excitatory synaptic variable related to the same neuron:

$$\begin{aligned} \overline{\Delta g_e} &= \frac{1}{N_{tot}} \sum_{K,k} w_e r_S(t_{K_k}) \\ \overline{r_{Sexc}} &= \frac{\overline{\Delta g_e}}{w_e} \end{aligned} \quad (4.9)$$

where  $t_{K_k}$  is the  $k$ -th spike timing of excitatory presynaptic neuron  $K$ . The quantities in (4.8) and (4.9) are computed in the presence and absence of STP and reported in Table (4.1). In the former case, the values lie beyond the unit according to the depletion effects, in the latter instead the release probability equals 1.

	STP	without STP
$\overline{r_{Sexc}}$	$0.506 \pm 0.006$	$1.002 \pm 0.008$
$\overline{r_{Sinh}}$	$0.517 \pm 0.007$	$0.998 \pm 0.006$

Table 4.1: Average values of  $r_S$  computed on excitatory and inhibitory conductances of a single postsynaptic neuron. Parameters:  $\nu_{ext} = 50.0$  spk/s,  $g = 0.25$ ,  $s = 1.0$ .

Remarkably, the data suggest that the depletion induced by the plasticity equally affects inhibitory and excitatory neurons. This arises from the particular choice of connectivity parameters  $g$  and  $s$ . The type of network connectivity, indeed, provides two population holds the same firing rate (as shown in Figure (4.2)), i.e.  $\nu_I^{rec} = \nu_E^{rec}$ . Moreover, the balance degrees  $g = 0.25$  leads to the same number of inhibitory and excitatory recurrent input, namely  $N_e p_e = N_i p_i = 160$ . Considering the total observation time  $t_{sim}$ , this evidence involves that the sum over  $J$  runs over the same values of the sum  $K$  (160), and the sum over  $j$  runs over the same values of  $k$  ( $\nu^{rec} \cdot t_{sim}$ ). However, in principle, inhibitory and excitatory synaptic variables could have different dynamics whereby the time course of  $r_{Sinh}$  could be different to  $r_{Sexc}$ . Nevertheless, the synaptic variables, regardless the nature of synapses, follow the same dynamics as described in 2.1.2. All this evidences suggest that  $\overline{r_{Sexc}} = \overline{r_{Sinh}}$ .

In this regard, the percentage modulation is equivalent to synaptic conductances  $g_i$  and  $g_e$ . Although, the strength of inhibitory synapses is greater than excitatory ones, the dynamical effects due to plasticity modulation result in a consistent decrease in inhibitory activity. The network with STP is characterized by a strong excitation that provides an intense spiking activity. Otherwise, the LFP is defined as the sum of synaptic current, i.e.  $I_x = g_x(E_x - v)$  with  $x = (e, i)$ , therefore the STP produces a decrease in its value.

#### 4.2.1 Heterogeneity of the external connectivity $s$ and degrees of balance $g$

The previous results highlight the significant role of both recurrent and external connections in network activity. It is natural to investigate how this global behaviour changes

with respect to the heterogeneity links with external environment  $s$  and the inner degrees of balance  $g$ .

In literature, some cortical neuronal networks present heterogeneous external connections simulated thalamic signal: both populations receive external excitatory input with inhibitory neurons receiving stronger inputs than excitatory ones [31, 32].

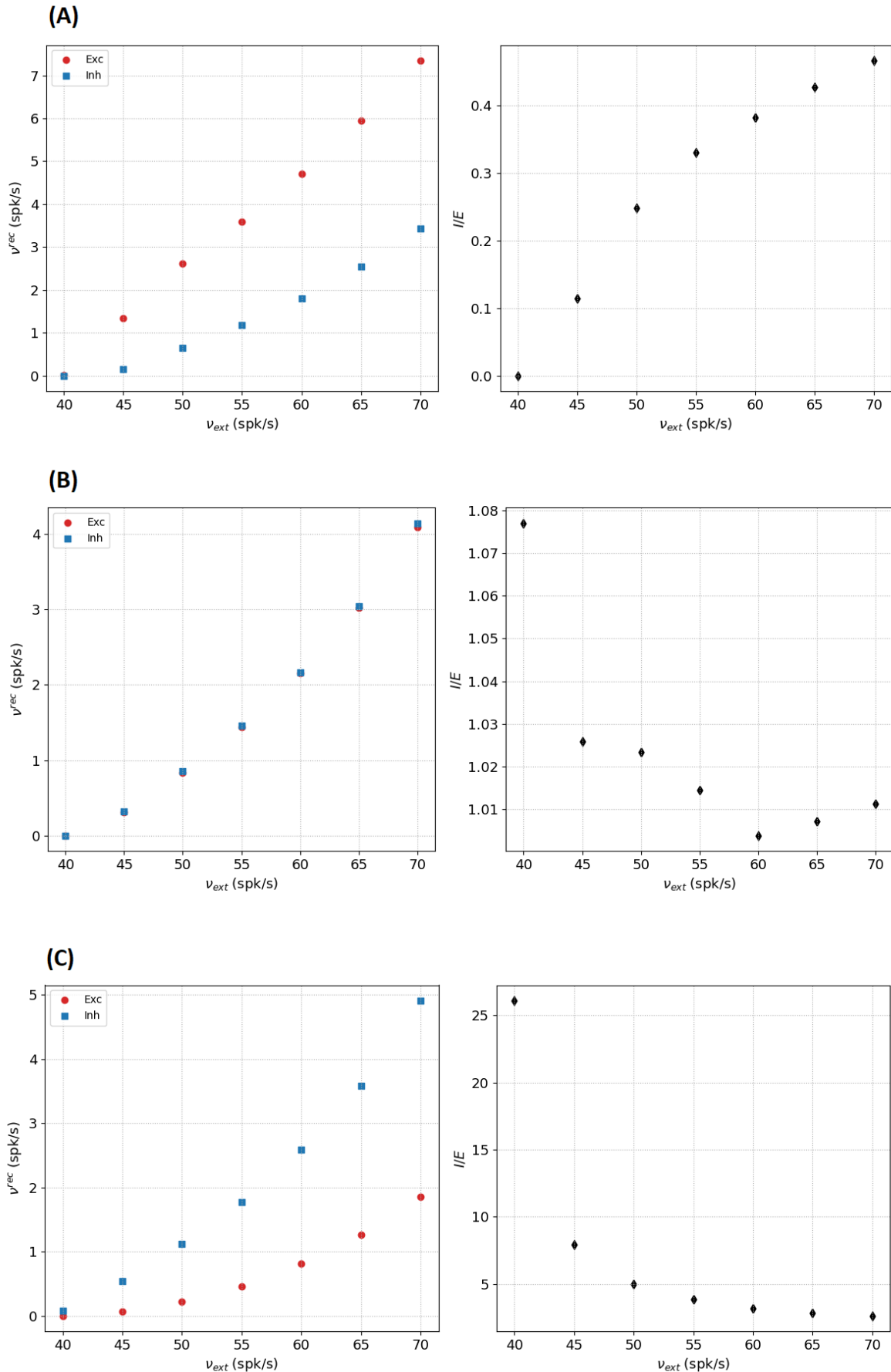


Figure 4.3: **Average Population Activities with respect to heterogeneity external connection  $s$ .** Neurons receives an input of  $\nu_{ext}$  coming from  $N_{ext} = 160$  external neurons. Each simulation run for 3.5 second long tiem simulation with integration steps of 0.05 ms. The data are monitored after a transient of 500 ms. Parameters:  $g = 0.25$ , (A)  $s = 0.95$ , (B)  $s = 1.00$ , (C)  $s = 1.05$ .

Keeping fixed the type of network connectivity, we compute the average firing rate for different values of  $s$  concerning the intensity of the constant input signal. Moreover, the ratio between inhibition and excitation  $I/E$  is computed to have a clear representation of effects induced by these type of heterogeneity. The results are collected in the plots in Figure (4.3). In the case of homogeneity connections  $s = 1$ , as we already depicted in the above section, the two populations share the same firing pattern over the range of investigated signals (B). Instead, with  $s < 1$  the signals have a greater impact on the excitatory population, accordingly the  $I/E$  is less than the unit (A). On the other side, with  $s > 1$ , the ratio is always above the unit (C). In particular, the results of the last scenario are in agreement with experimental data for which the fast-spiking inhibitory interneurons fire with higher frequencies than glutamatergic pyramidal neurons [67].

Finally, we just have to explain the behaviour concerning the inner connectivity. The parameter  $g$  settles the mean value of excitatory and inhibitory recurrent inputs ingoing to each neuron. According to the definition in (4.2),  $g > 5$  sets the dominance of the excitation on the inhibition, the opposite relation occurs for  $g < 5$ . Therefore, keeping fixed the parameters  $s$  the mean firing rate depends exclusively on the degrees of balance. In general, the spiking activity of single neurons raises with excitatory inputs. This reflects on the network level too, as reported in Figure (4.4). With heterogeneous external connections, the firing activity of excitatory and inhibitory populations increases with  $g$  (right panel). Moreover, this effect is clearly visible for homogeneous scenario (left panel).

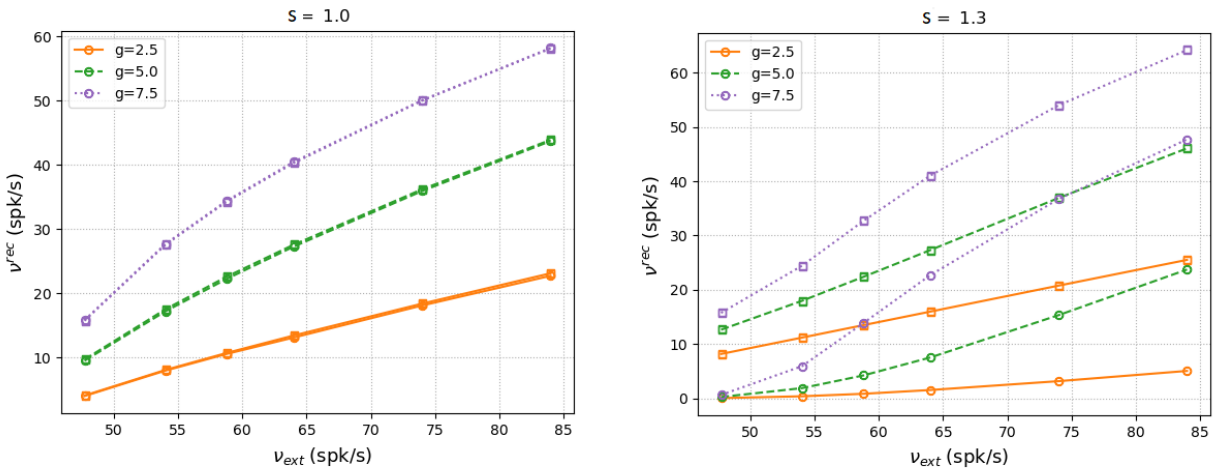


Figure 4.4: **Average Population Activities with respect to degrees of balance  $g$ .** Average firing rate of excitatory (circle dots) and inhibitory (squared dots) are plotted with three degrees of balance. According to the susceptibility induced by excitatory input, with the lower value (orange solid line), the network activity is less intense than the balanced network (green dashed line) and strong excitatory one (purple dotted line). The modulation effects on  $g$  are clearly visible for heterogeneous (right panel) and homogeneous (left panel) external connections. Neurons receives an input of  $\nu_{ext}$  coming from  $N_{ext} = 160$  external neurons. Each simulation run for 3.5 second long time simulation with integration steps of 0.05 ms. The data are monitored after a transient of 500 ms. Parameters: (left panel)  $s = 1.0$   $g = 2.5, g = 5.0, g = 7.5$ ; (right panel)  $s = 1.3$   $g = 2.5, g = 5.0, g = 7.5$

### 4.3 Activation of Gliorelease events

Once understood the dynamics at baseline condition, the purpose is to see how the gliomodulation occurs at the network level. In the previous chapter, we have detailed investigated the combination of the release-decreasing effect of glutamate and the astrocytic-

induced facilitation effect in the transmission mode of tripartite synapses. The straightforward question is how these two mechanisms could affect the mesoscopic quantities of the neuron-glial network. In this sense, the time scales of astrocytic dynamics are essential to underline the time observation of network activity to properly appreciate the gliomodulation effects. As reported in Figure (3.8), the parameters  $\Omega_G$  and  $O_G$  respectively set the time scale of depression and facilitation. In particular, with  $\Omega_G = 0.0083 \text{ s}^{-1}$  and  $O_G = 1.5 \mu\text{M}^{-1}\text{s}^{-1}$  the former mechanism is much faster than the latter. Indeed, with this choice, the depletion occurs much faster than one second whereas the facilitation occurs in the order of tens of seconds (Figure (3.5)). Therefore, long time simulations (in the order of minutes) are required for an overall visualization of these effects.

In the first stage, we want to analyse the plausible effect of depletion induced by a single gliorelease event. Accordingly, we stimulate the neuron-glia network with a constant external input for a 10 seconds long time observation when the astrocytes are activated after the first 5 seconds. This procedure allows us to divide the baseline and the signal of interest, thus the dynamical changes induced by gliomodulation are clearly visible over time. Precisely, the baseline covers the time windows from 0.5 s to 5.0 s and the signal of interest covers the window from 7.0 s to 10.0 s.

The gliomodulation profoundly alters the global activity of balanced network ( $g = 5.0$ ) with fast-spiking inhibitory neurons ( $s = 1.15$ ). The top panel in Figure (4.5) well represents the heterogeneity of external connections. In this scenario, the gliorelease event triggers the release-decreasing effect on excitatory synapses. The middle panel in Figure (4.5) shows how the release of gliotransmitters drops the excitatory recurrent current. Notably, the observation time does not allow to appreciate the facilitation effect therefore, the recurrent current does not reach its baseline value. The decrease of excitatory current leads also to a statistical change in the mean value of LFP, as reported in Table (4.2).

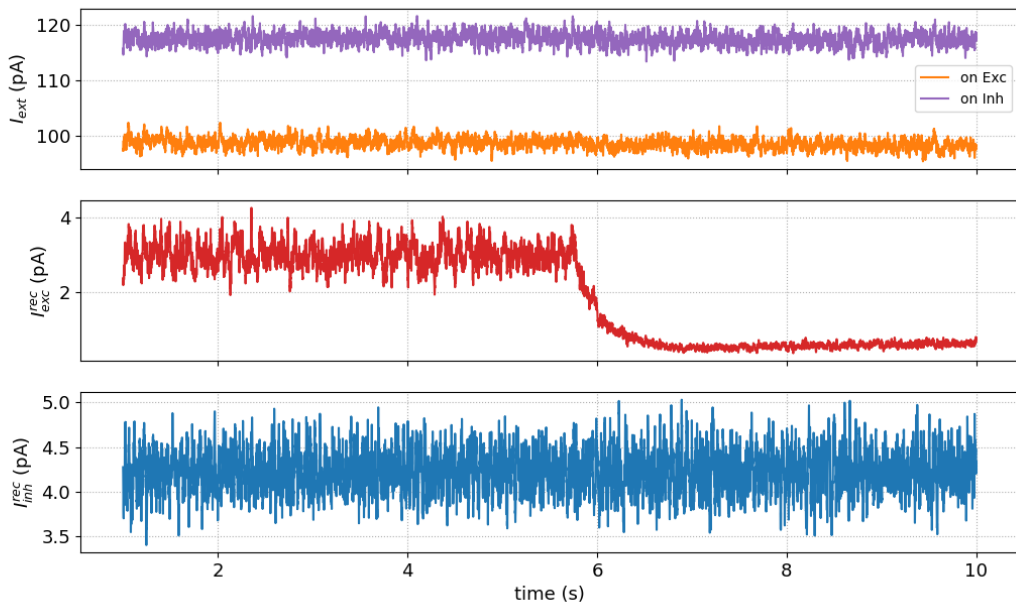
	$I_{exc}^{rec}$ (pA)	$I_{inh}^{rec}$ (pA)	LFP (a.u.)
baseline	$3.0 \pm 0.3$	$4.23 \pm 0.23$	$10.67 \pm 0.07$
gliomodulation	$0.58 \pm 0.08$	$4.23 \pm 0.23$	$10.34 \pm 0.06$

Table 4.2: Average values of recurrent current and LFP for balanced neuron-glia network. The data are presented as (mean  $\pm$  s.t.d.) computed over the proper time observation of baseline (0.5 – 5.0 s) and signal of interest (7.0 – 10.0 s). Parameters:  $g = 5.0$ ,  $s = 1.15$ ;  $O_\beta = 3.2 \mu\text{Ms}^{-1}$ ,  $O_\delta = 0.6 \mu\text{Ms}^{-1}$ .

Instead, the bottom panel in Figure (4.5) illustrates that the inhibitory current does not undergo any changes. Its mean value does not show statistical changes from baseline to signal of interest. The firing rates share similar behaviour. Indeed, the excitatory population drops its activity in correspondence to gliorelease event as reported in Figure (4.6), whereas the inhibitory one is not susceptible to the activation of astrocytic activity (data in Table (4.3)).

	$\nu_{exc}^{rec}$ (spk/s)	$\nu_{inh}^{rec}$ (spk/s)	$\nu$ (spk/s)
baseline	$5.8 \pm 1.2$	$19 \pm 4$	$8.5 \pm 0.6$
gliomodulation	$3.8 \pm 0.9$	$18 \pm 4$	$6.6 \pm 0.5$

Table 4.3: Average values of firing rates for balanced neuron-glia network. A Gaussian smoothing procedure with a bandwidth of 5 ms is applied to the raw signals coming from the equation 4.5 with  $\Delta t = 0.05$  ms. The data are presented as (mean  $\pm$  s.t.d.) computed over the proper time observation of baseline (0.5 – 5.0 s) and signal of interest (7.0 – 10.0 s). Parameters as in Table 4.2



**Figure 4.5: External ad recurrent currents in balanced neuron-glia network.** (Top panel) The mean value over 200 excitatory (orange line) and inhibitory (purple line) neurons of heterogeneity external connections: on excitatory population  $I_{ext} = 98.6 \pm 1.9$  pA, on inhibitory population  $I_{ext} = 117.4 \pm 2.3$  pA. The gliorelease event occur at time  $5.9 \pm 0.1$  s. The release-decreasing effect drop the excitatory recurrent current (red line in middle panel), whereas the inhibitory one is weekly modulated (blue lime in bottom panel). Neurons receives an input of  $\nu_{ext} = 47.7$  spk/s coming from  $N_{ext} = 160$  external neurons. Time simulation is 10 second with integration step of 0.05 ms. Parameters:  $g = 5.0$ ,  $s = 1.15$ ;  $O_\beta = 3.2 \mu\text{Ms}^{-1}$ ,  $O_\delta = 0.6 \mu\text{Ms}^{-1}$ .

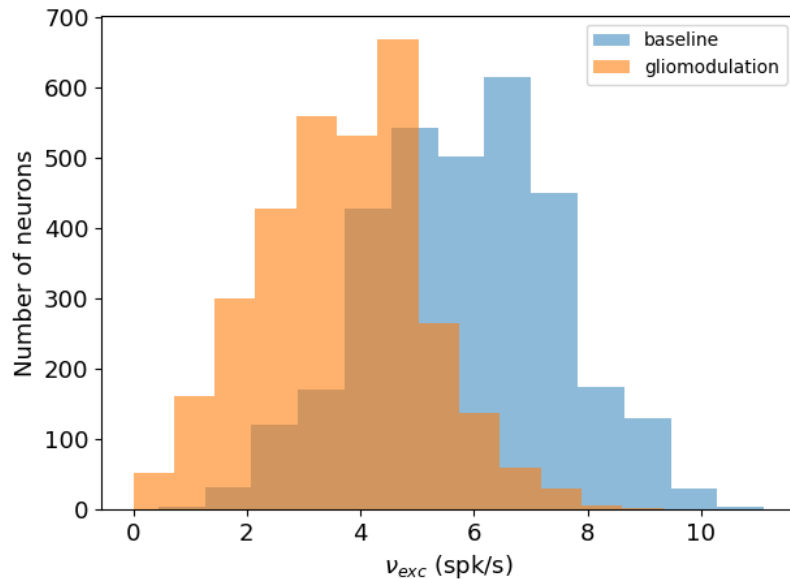


**Figure 4.6: Firing rates distribution of excitatory population in balanced neuron-glia network.** Firing rates distribution in baseline (blue) and signal of interest (orange). Neurons receives an input of  $\nu_{ext} = 47.7$  spk/s coming from  $N_{ext} = 160$  external neurons. Time simulation is 10 second with integration step of 0.05 ms. Parameters:  $g = 5.0$ ,  $s = 1.15$ ;  $O_\beta = 3.2 \mu\text{Ms}^{-1}$ ,  $O_\delta = 0.6 \mu\text{Ms}^{-1}$ .

Overall, these results are in agreement with the discussion about the network's behaviour concerning the architecture parameters. Indeed, in the baseline condition, the recurrent currents share the same intensity. Moreover, the fast-spiking activity of interneurons is induced by a stronger external input. Now, we want to understand if the gliotransmitters modulation could be dependent on the inner degrees of balance and external connections.

The same input is presented to a network with intense recurrent inhibition ( $g = 0.25$ ) and homogeneous external connections ( $s = 1.00$ ). The network dynamics in terms of external and recurrent currents are presented in Figure (4.7). Like the previous scenario, the activation of astrocytes determines the decrease of excitatory recurrent input (middle panel).

	$I_{exc}^{rec}$ (pA)	$I_{inh}^{rec}$ (pA)	LFP (a.u.)
baseline	$0.67 \pm 0.23$	$14 \pm 3$	$11.4 \pm 0.3$
gliomodulation	$0.066 \pm 0.023$	$14 \pm 3$	$11.3 \pm 0.3$

Table 4.4: Average values of recurrent current and LFP for strong inhibitory neuron-glia network. The data are presented as (mean  $\pm$  s.t.d.) computed over the proper time observation of baseline (0.5 – 5.0 s) and signal of interest (7.0 – 10.0 s). Parameters:  $g = 0.25$ ,  $s = 1.00$ ;  $O_\beta = 3.2 \mu\text{Ms}^{-1}$ ,  $O_\delta = 0.6 \mu\text{Ms}^{-1}$ .

Despite the presence of changes in excitatory input, both LFP and population firing rate are not affected by the gliomodulation as reported in Table (4.4) and (4.5).

	$\nu_{exc}^{rec}$ (spk/s)	$\nu_{inh}^{rec}$ (spk/s)	$\nu$ (spk/s)
baseline	$0.6 \pm 0.3$	$0.6 \pm 0.4$	$0.60 \pm 0.19$
gliomodulation	$0.6 \pm 0.3$	$0.6 \pm 0.4$	$0.57 \pm 0.19$

Table 4.5: Average values of firing rates for strong inhibitory neuron-glia network. A Gaussian smoothing procedure with a bandwidth of 5 ms is applied to the raw signals coming from the equation 4.5 with  $\Delta t = 0.05$  ms. The data are presented as (mean  $\pm$  s.t.d.) computed over the proper time observation of baseline (0.5 – 5.0 s) and signal of interest (7.0 – 10.0 s). Parameters as in Table 4.4

A plausible explanation must be found in the magnitude of currents that drive the network dynamics. Despite the balanced case, the inner inputs are considerably different from each other. Indeed, the recurrent excitatory current is circa 20 times less intense than the inhibitory one. Therefore, even if the modification of excitatory inner inputs is statistically significant, the network dynamic is almost completely driven by inhibition. Accordingly, we do not appreciate any changes in the average value in population firing rate and LFP.

Nevertheless, this is not the end of the story. The changes in the inner balance between excitation and inhibition might alter other aspects as the network oscillations. This specific topic is investigated in the following section.

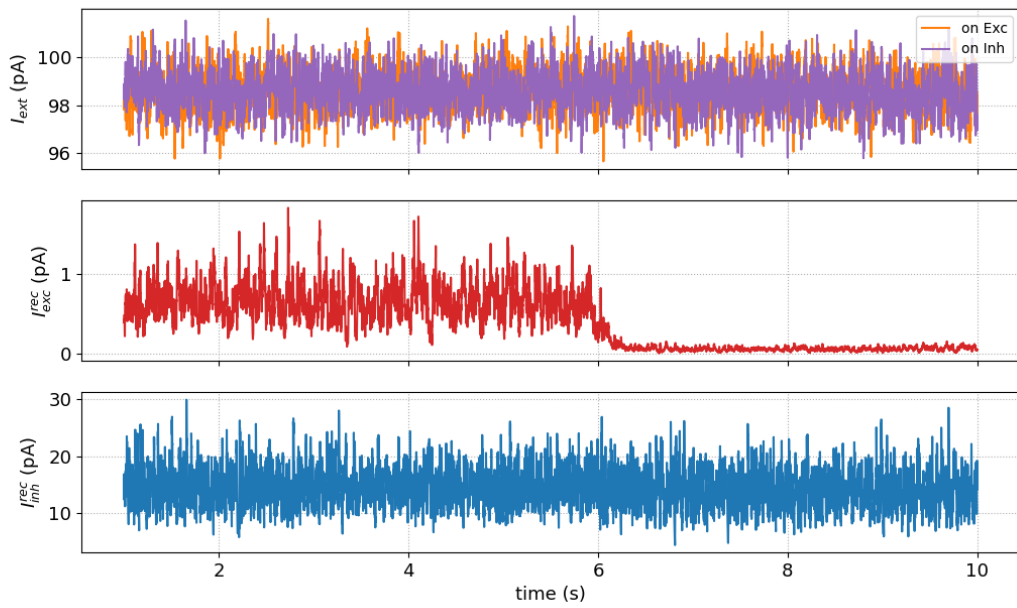


**Figure 4.7: External ad recurrent currents in strong inhibitory neuron-glia network.** (Top panel) The mean value over 200 excitatory (orange line) and inhibitory (purple line) neurons of homogeneity external connections: on excitatory population  $I_{ext} = 98.6 \pm 1.8$  pA, on inhibitory population  $I_{ext} = 98.5 \pm 1.8$  pA. The gliorelease event occur at time  $6.0 \pm 0.1$  s. The release-decreasing effect drop the excitatory recurrent current (red line in middle panel), whereas the inhibitory one is weekly modulated (blue lime in bottom panel). Neurons receives an input of  $\nu_{ext} = 47.7$  spk/s coming from  $N_{ext} = 160$  external neurons. Time simulation is 10 second with integration step of 0.05 ms. Parameters:  $g = 0.25$ ,  $s = 1.00$ ;  $O_\beta = 3.2 \mu\text{Ms}^{-1}$ ,  $O_\delta = 0.6 \mu\text{Ms}^{-1}$ .

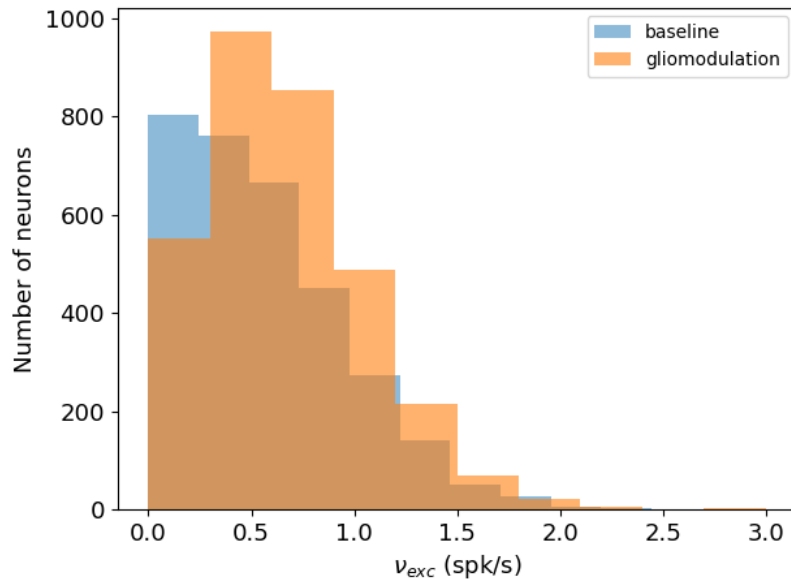


**Figure 4.8: Firing rates distribution of excitatory population in strong inhibitory neuron-glia network.** Firing rates distribution in baseline (blue) and signal of interest (orange). Neurons receives an input of  $\nu_{ext} = 47.7$  spk/s coming from  $N_{ext} = 160$  external neurons. Time simulation is 10 second with integration step of 0.05 ms. Parameters:  $g = 0.25$ ,  $s = 1.00$ ;  $O_\beta = 3.2 \mu\text{Ms}^{-1}$ ,  $O_\delta = 0.6 \mu\text{Ms}^{-1}$ .

## 4.4 Long-Term effect of gliomodulation

When discussing the dynamics of tripartite synapses, both at the microscopic and mesoscopic level, the long time scales arise as one of the main dynamical features driving the systems. Therefore, to obtain a general and complete picture of long-term effects due to gliomodulation, we have to consider an observation time of the order of the minutes. As we have introduced in the previous section, a long observation time allow us to appreciate the facilitation effects besides the release-decreasing ones. In this sense, the meaningful result presented in chapter 3 could be an insightful guide to anticipating some network behaviour.

Nevertheless, in the neuron-glia network, the coupling between astrocyte and synapses are slightly but significantly different from the connection of tripartite synapses used in the previous chapter. Indeed, at the mesoscopic level, each astrocytic dynamics is driven by the average activity of several glutamatergic synapses (on average  $N_e p_e$ ). Accordingly in the network we have a 160-to-1 fashion like tripartite synapse. At the microscopic level, instead, we have considered a 1-to-1 connection between single elements. Therefore, the filtering characteristic presented in section 3.2.2 might suggest only partial clues about network dynamics.

To elucidate this aspect, we set the inner architecture parameters in such a way to achieve a low firing activity of excitatory synapses, namely a mean firing rate lower than 1.5 spk/s. In this range, the filter characteristic curves suggest a change due to astrocytic activity. Precisely, the choice falls on  $g = 0.25$  and  $s = 1.0$  thereby, as illustrated in Figure (4.8), the above requirement is satisfied. With this type of network structure, we want to investigate the changes in time of the excitatory and inhibitory balance. Moreover, it is interesting to see how the combination of facilitation and release-decreasing effects could lead to a totally different behaviour concerning astrocytic parameters. In particular, the exogenous and endogenous IP<sub>3</sub> production are the mechanisms that directly connect synapse and astrocyte release events. Therefore, we select two combinations of  $O_\beta$  and  $O_\delta$ , parameters that regulate the time scale of the aforementioned mechanisms. A constant external input  $\nu_{ext}(t) = \nu_0$  is presented to the network with the same intensity of above simulation.

At the beginning, we select  $O_\beta = 0.5 \mu\text{Ms}^{-1}$  and  $O_\delta = 1.2 \mu\text{Ms}^{-1}$ . The respective characteristic curve of tripartite synapses shows a modulation in the low presynaptic firing rate region (3.15). We expect to find this filtering behaviour also in the network dynamics. Notably, the bottom panel in Figure (4.9) illustrates that the astrocytic calcium reaches a suprathreshold dynamical regime. The only gliorelease events are induced by the relaxation time course after glial activation, i.e. after 5 s. After the relaxation time, the facilitation tends to lead the system to its baseline condition, namely without any kind of gliomodulation. Accordingly, the excitatory recurrent current (middle panel), as well as E/I balance (top panel), increases until reach its baseline value (data not shown).

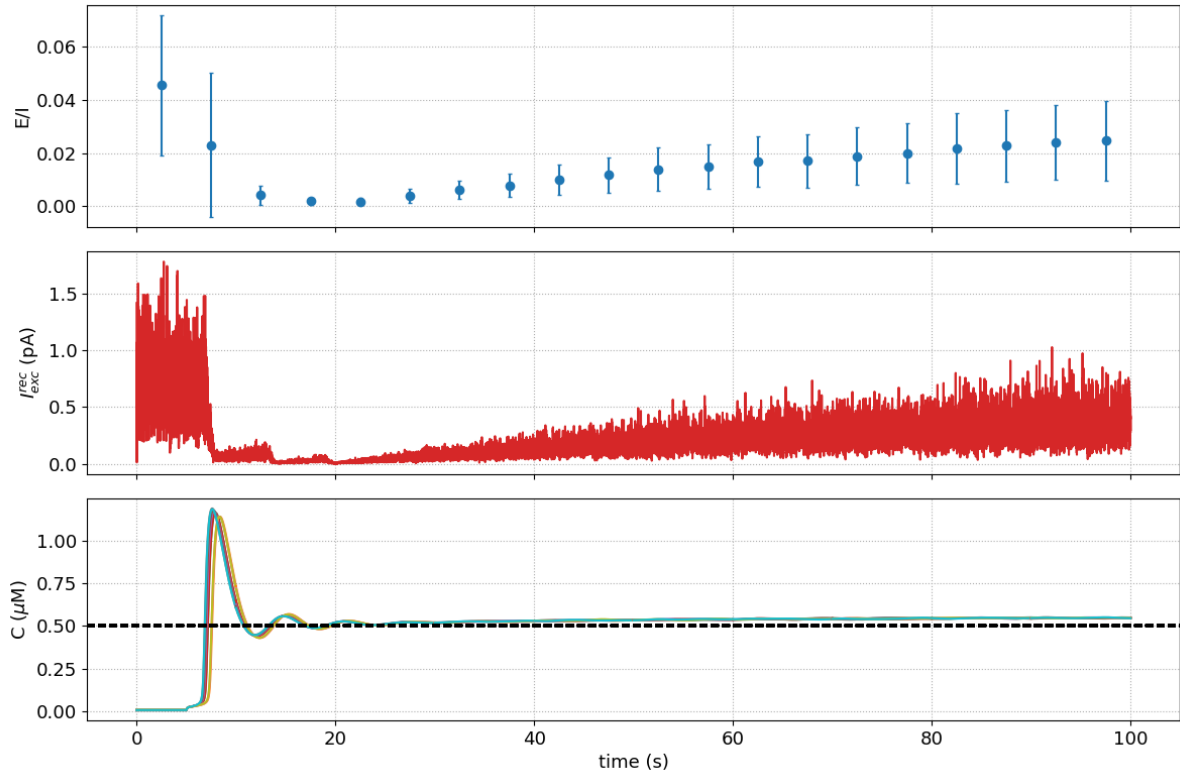


**Figure 4.9: Long-term effect of gliomodulation, return to baseline condition.** (Bottom panel) Calcium time course of 10 astrocytes, the oscillations cross threshold are present over total time simulation. (Middle panel) The excitatory recurrent current decreases and, as a consequence, the balance is strongly modulated (top panel). Neurons receives an input of  $\nu_{\text{ext}} = 47.7 \text{ spk/s}$  coming from  $N_{\text{ext}} = 160$  external neurons. Time simulation is 100 second with integration step of 0.05 ms for neurons and 0.01 s for astrocytes. Parameters:  $g = 0.25$ ,  $s = 1.00$ ;  $O_\beta = 0.5 \mu\text{Ms}^{-1}$ ,  $O_\delta = 1.2 \mu\text{Ms}^{-1}$ .

The situation is different with  $O_\beta = 3.2 \mu\text{Ms}^{-1}$  and  $O_\delta = 0.6 \mu\text{Ms}^{-1}$ . Also, in this case, the filter characteristic curve describes a band-pass filter. However, the calcium oscillations across the threshold value occur also in the absence of noise. Accordingly, when the astrocytic activity is affected by the average of the neurotransmitters released from several presynaptic buttons, we can appreciate a persistent gliomodulation over total observation time.

As shown in Figure (4.10), the result coming from the long-time simulation are in agreement with the above consideration. The astrocytic activity, with this choice of parameters, exhibits oscillation across the threshold value during all observation time (bottom panel). This activity induces a persistent and periodic release of gliotransmitters that modulate all the glutamatergic synapses. Moreover, the frequency of gliorelease event (0.2 gre/s) is much lower of time scale of facilitation effect ( $\Omega_G = 0.008 \text{ Hz}$ ). During two consecutive gliorelease events, the facilitation does not lead the system to its baseline condition. The middle panel in Figure (4.10) elucidates the decrease of excitatory recurrent inputs. The main consequence is that the excitatory/inhibitory balance suffers a significant and persistent decrease as reported in the top panel.

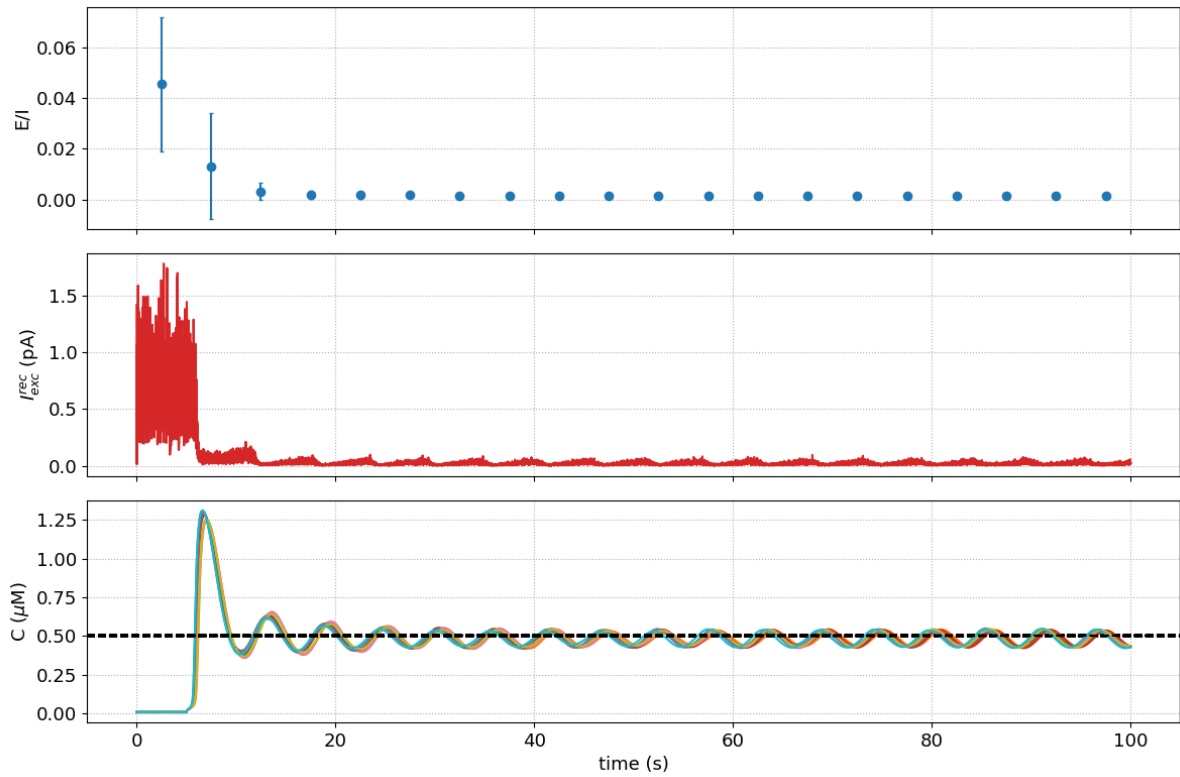


Figure 4.10: **Long-term effect of gliomodulation with persistent astrocytic activity.** Persistent astrocytic activity drives network dynamics. (Bottom panel) Calcium time course of 10 astrocytes, the oscillations cross threshold are present over total time simulation. (Middle panel) The excitatory recurrent current decreases and, as a consequence, the balance is strongly modulated (top panel). Neurons receives an input of  $\nu_{ext} = 47.7$  spk/s coming from  $N_{ext} = 160$  external neurons. Time simulation is 100 second with integration step of 0.05 ms for neurons and 0.01 s for astrocytes. Parameters:  $g = 0.25$ ,  $s = 1.00$ ;  $O_\beta = 3.2 \mu\text{Ms}^{-1}$ ,  $O_\delta = 0.6 \mu\text{Ms}^{-1}$ .

In general, we want to point out the role of the sequence activation and inactivation mechanism of presynaptic receptors on network dynamics. More specifically, the rates of the above mechanisms drive the network dynamics and in particular the regulation of excitatory/inhibitory balance. Indeed, for the parameters in Figure (4.10), the activation rate is two orders greater than the inactivation one and, for this reason, the sequence of depletion and facilitation effects induced by glia leads to an abrupt decrease in excitatory current. However, as reported in (3.8), different time scales settled by  $\Omega_G$  and  $O_G$  provide variegated neurotransmitter time evolution in the synaptic cleft. Therefore, we might speculate that modulation of network balance also depends on  $\Gamma_S$  time scale dynamics.

## 4.5 Network Oscillations

The characterization of network dynamics is not complete by the average value of the population firing rate and LFP. As we have already stressed, one of the most fascinating aspects of complex systems is the presence of emerging dynamical behaviour. In the content of the neuronal population, the network oscillations are a basic example of such collective dynamical behaviour. In this regard, the changes induced by gliomodulation in the excitatory/inhibitory balance might be a clue to the effect on network oscillation due to persistent astrocytic activity. The results of the previous paragraph indicate that the

absence of astrocytic oscillation across the threshold carries the E/I balance to their baseline condition values. Therefore, the gliomodulation effects on network oscillations are appreciable with persistent astrocytic activity. At this early stage, we want to underline the presence of continuous gliorelease is the mandatory requirement for the modulation, regardless of the feature of the input stimulus.

Network oscillations in presence of constant external input  $\nu_{ext}(t) = \nu_0$  are investigated through CWT spectrum analysis (see section 2.4). In particular, with the same network architecture described in Figure (4.10), we known the presence of long-term continuous gliomodulation. The left panel in Figure (4.11) reports the spectrum analysis of baseline (blue) and signal of interest (orange). Both the baseline and the signal of interest show a pronounced oscillation in the proximity of 20 Hz. However, the modulation (right panel) does not highlight significant changes induced by astrocytic activity over the all frequencies range.

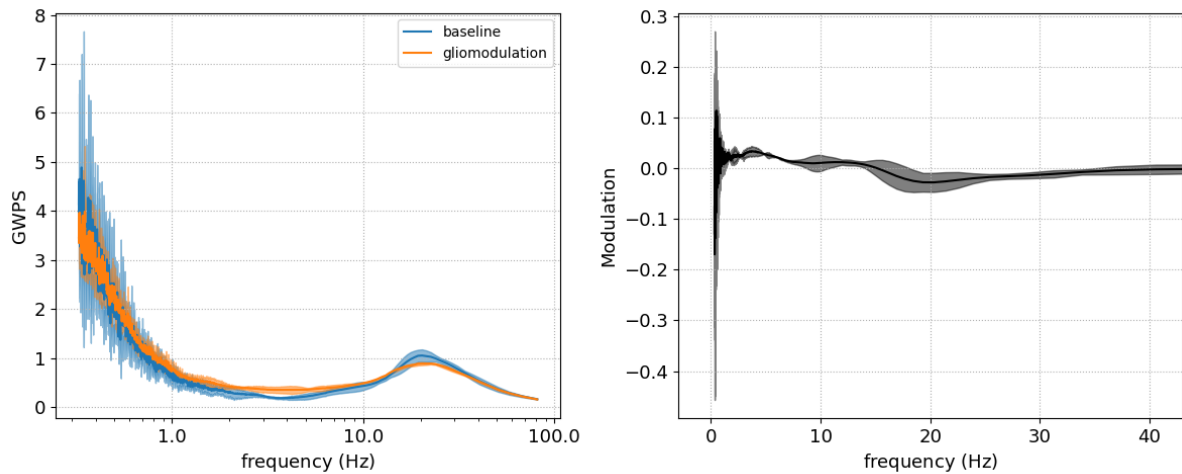


**Figure 4.11: Spectrum analysis for constant external input.** (left panel) Spectrum analysis for baseline (blue) and gliomodulation (orange) signal. Network oscillation arises at 20 Hz, however the modulation (right panel) does not show statistical changes, GWPS For 20 Hz, GWPS at baseline and signal of interest is respectively  $1.05 \pm 0.12$  and  $0.89 \pm 0.03$ . 5 different realizations of the same input are presented to the network. Neurons receives an input of  $\nu_{ext} = 47.7$  spk/s coming from  $N_{ext} = 160$  external neurons. Time simulation is 100 second with integration step of 0.05 ms for neurons and 0.01 s for astrocytes. Signal window: baseline 5–15 s; gliomodulation 50–90 s. Parameters:  $g = 0.25$ ,  $s = 1.00$ ;  $O_\beta = 3.2 \mu\text{M s}^{-1}$ ,  $O_\delta = 0.6 \mu\text{M s}^{-1}$ .

However, the network response to constant external stimuli gives only a partial portrait of the encoding mechanism. Indeed, naturalistic stimuli are not static but vary on time scales with widespread  $1/f$  scaling propriety [72]. As a preliminary study, we examine the network dynamics in response to periodic input signals that oscillate at frequency  $\omega$  with amplitude  $A$ :

$$\nu_{ext}(t) = \nu_0 + A \sin(2\pi\omega t) \quad (4.10)$$

where  $\nu_0$  stands for the constant value like the previous scenario.

From the point of view of dynamical behaviour, with time-dependent external stimulation, the neurons are driven by a non-autonomous vector field. Strictly speaking, the result presented in Chapter 3 is not valid in this condition. However, from the point of view of network dynamics, the presence of persistent astrocytic activity is the main protagonist of gliomodulation. This condition could arise also in the case of periodic external

stimulus. The plots in Figure (4.12) highlight how the presence of astrocytic activity depends on the amplitude of the external signal. In agreement with the above considerations, astrocytic calcium oscillations across the threshold modulates the excitatory recurrent current during all-time simulation (A), whereas the suprathreshold steady state drives the system to its baseline condition (B). Therefore, we want to validate the hypothesis that the modulation of the periodic stimulus (if any) is more intense for amplitude values and vanishes for the higher ones <sup>2</sup>.

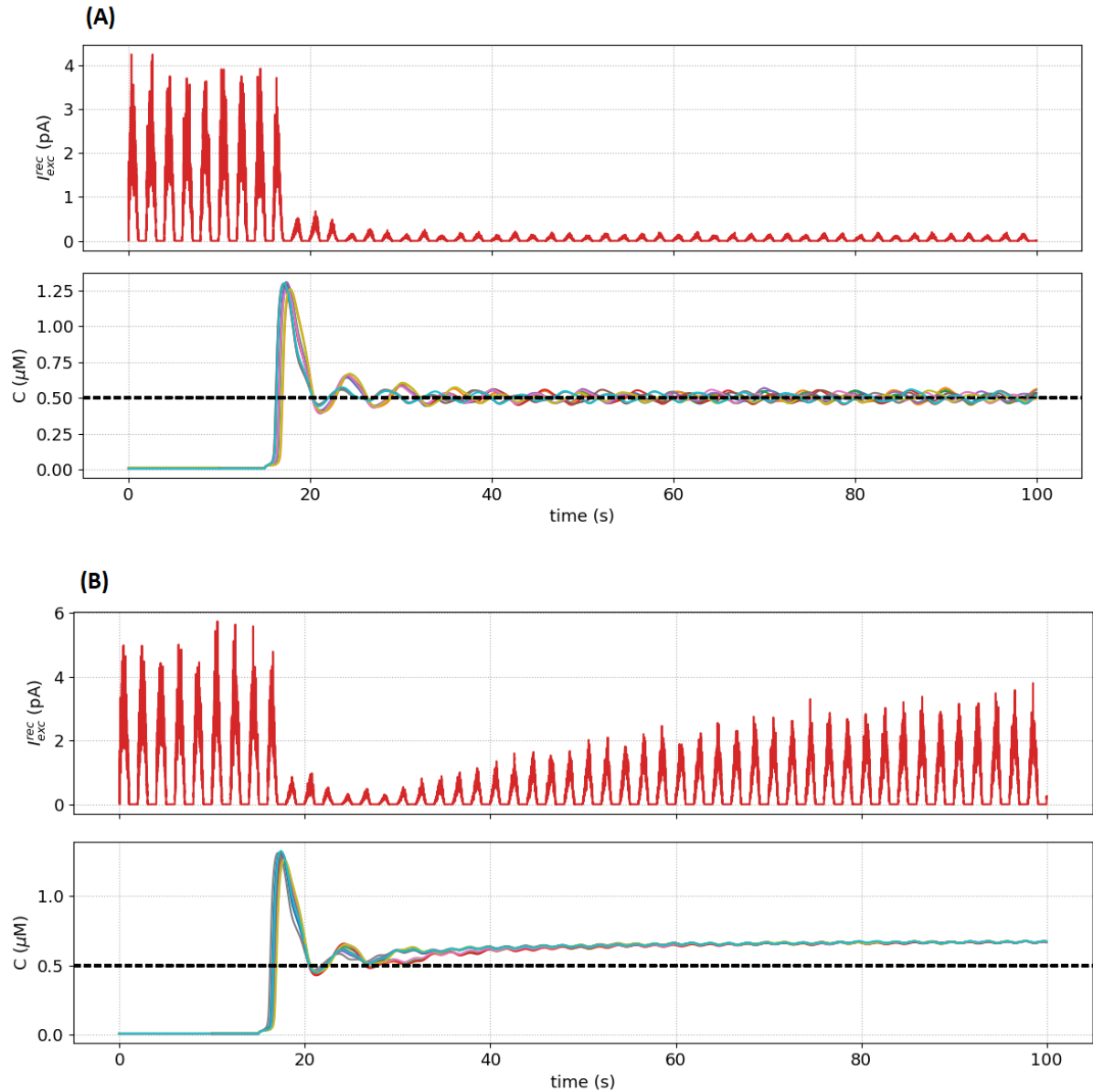


Figure 4.12: **Neuron-glia network dynamics concerning the amplitude of periodic input stimulus.** (A) Persistent astrocytic activity regulates the excitatory recurrent input for long-time simulation. (B) Astrocytic calcium steady state above the threshold guides the system to its baseline condition. Parameters:  $g = 0.25$ ,  $s = 1.00$ ;  $O_\beta = 3.2 \mu\text{M s}^{-1}$ ,  $O_\delta = 0.6 \mu\text{M s}^{-1}$ ,  $\omega = 0.5 \text{ Hz}$ ; amplitude: (A)  $A = 3052.8 \text{ spk/s}$  (B)  $A = 4579.2 \text{ spk/s}$ .

<sup>2</sup>The amplitude of signal in equation 4.10 is a fraction of the constant value  $\nu_0$ :  $A = a \nu_0$ . We investigate the modulation effect for  $a \in [0.05, 1.0]$ .

The plots in Figure (4.13) elucidate the modulation of  $\omega = 0.5$  Hz due to the astrocytic activity with  $A = 763.2$  spk/s. The GWPS for this frequency passes from  $65.24 \pm 0.24 \cdot 10^2$  to  $58.94 \pm 0.19 \cdot 10^2$ , namely a percentage decrease of  $9.6 \pm 0.6\%$ . The decrease of the power spectrum is in agreement with the evidence that the amplitude of excitatory recurrent current drops in the time window of persistent astrocytic activity, as reported in panel (A) of Figure (4.12).

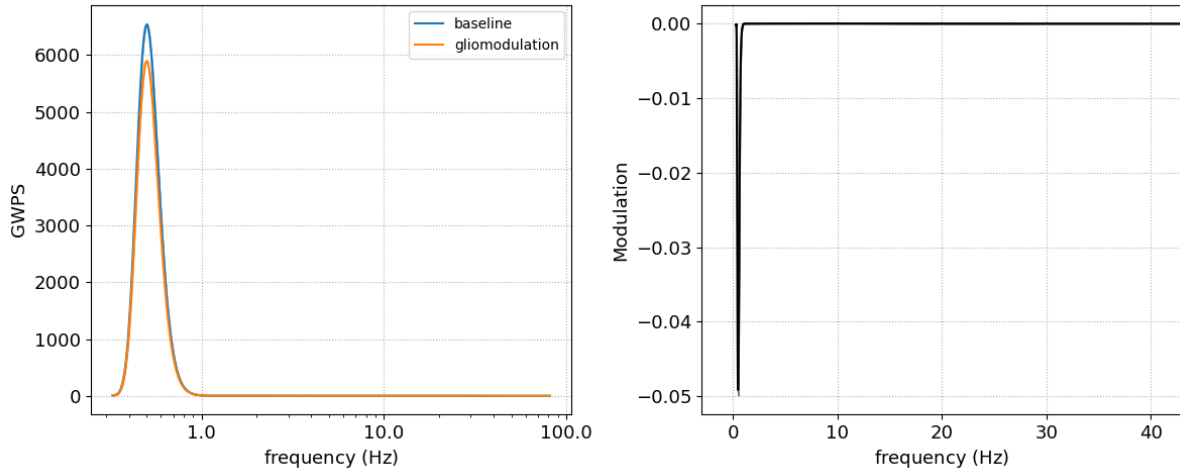


Figure 4.13: **Spectrum analysis for periodic external input.** (left panel) Spectrum analysis for baseline (blue) and gliomodulation (orange) signal. GWPS for 0.5 Hz, GWPS at baseline and signal of interest are respectively  $65.24 \pm 0.24 \cdot 10^2$  and  $58.94 \pm 0.19 \cdot 10^2$ . 5 different realizations of the same input are presented to the network. Neurons receives an input described by equation 4.10 coming from a single external neurons. Time simulation is 100 second with integration step of 0.05 ms for neurons and 0.01 s for astrocytes. Signal window: baseline 5 – 15 s; gliomodulation 50 – 90 s. Parameters:  $g = 0.25$ ,  $s = 1.00$ ;  $O_\beta = 3.2 \mu\text{M s}^{-1}$ ,  $O_\delta = 0.6 \mu\text{M s}^{-1}$ ;  $A = 763.2$  spk/s,  $\omega = 0.5$  Hz

The overall effect induced by glial cells regarding the amplitude of the periodic signal is presented in Figure (4.14). According to the above consideration regarding the modulation of constant stimulus and the presence of gliomodulation with periodic one, we can deduce a possible behaviour of power spectrum concerning the amplitude  $A$ :

- $A$  tends to 0: the periodic external stimulus tends to be a constant one, hence we do not expect modulation induced by persistent astrocytic activity;
- $A$  tends to  $\nu_0$ : the system tends toward its baseline condition for longer time simulation, hence we do not expect modulation.

Therefore, we can suppose that the functional relation between the modulation and the amplitude is represented by a "reverse bell-shape" curve with a peak in the region of gliomodulation. The right plot in Figure (4.14) well describes our consideration. For the selected frequency, the peak modulation occurs for the same amplitude value of the data in Figure (4.12),  $A = 763.2$  spk/s. Instead, for the last three investigated amplitude values ( $A > 3000$  spk/s), the percentage modulation is close to 0. It is important to stress that it vanishes (no difference between baseline and signal of interest) for extended time simulation.

We exploit the same procedure to investigate if the above type of modulation also occurs for higher input frequencies. In this sense, the data regarding a periodic input with

$\omega = 20$  Hz are collected in Figure (4.15). Interesting, in this condition, the percentage modulation is greater than the previous one. For instance, with  $A = 763.2$  spk/s the percentage decrease of the input frequency is circa 18 %.

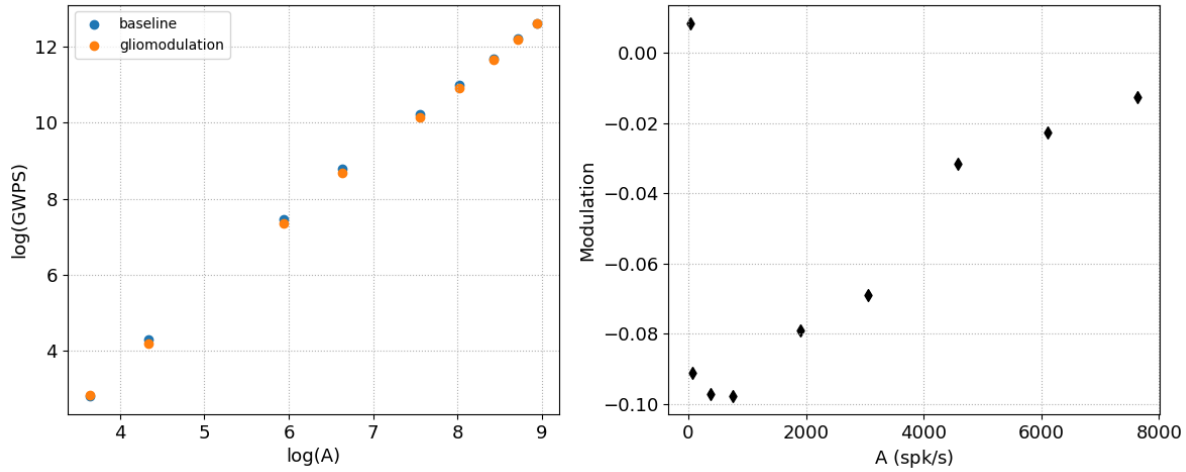


Figure 4.14: **Modulation of periodic signal for  $\omega = 0.5$  Hz.** (Left panel) GWPS for baseline (blue) and gliomodulation signal (orange) evaluate at 0.5 Hz. (Right panel) Percentage modulation regarding the amplitude values. Neurons receives an input described by equation 4.10 coming from a single external neurons. Time simulation is 100 second with integration step of 0.05 ms for neurons and 0.01 s for astrocytes. Signal window: baseline 5 – 15 s; gliomodulation 50 – 90 s. Parameters:  $g = 0.25$ ,  $s = 1.00$ ;  $O_\beta = 3.2 \mu\text{M s}^{-1}$ ,  $O_\delta = 0.6 \mu\text{M s}^{-1}$ ;  $\omega = 0.5$  Hz

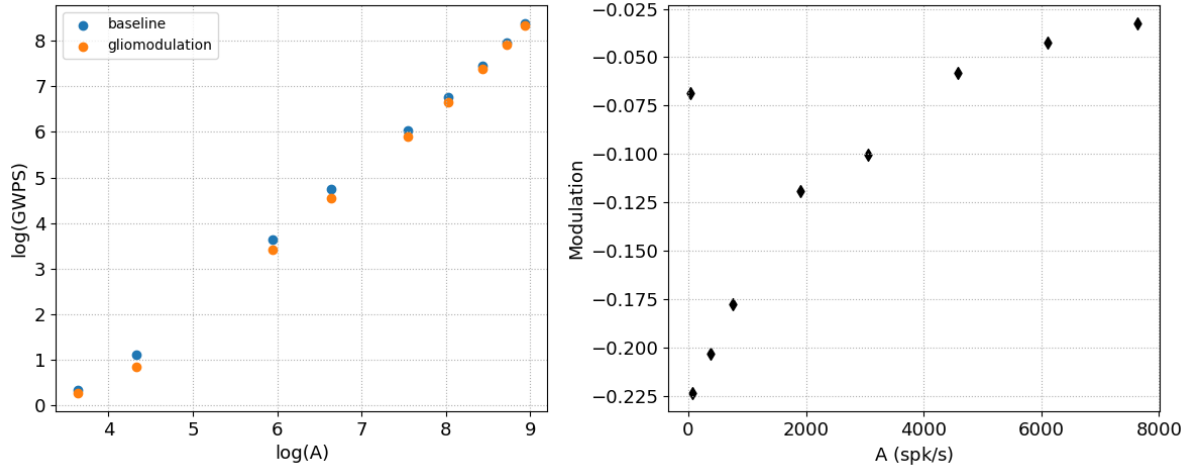


Figure 4.15: **Modulation of periodic signal for  $\omega = 20$  Hz.** (Left panel) GWPS for baseline (blue) and gliomodulation signal (orange) evaluate at 0.5 Hz. (Right panel) Percentage modulation regarding the amplitude values. Neurons receives an input described by equation 4.10 coming from a single external neurons. Time simulation is 100 second with integration step of 0.05 ms for neurons and 0.01 s for astrocytes. Signal window: baseline 5 – 15 s; gliomodulation 50 – 90 s. Parameters:  $g = 0.25$ ,  $s = 1.00$ ;  $O_\beta = 3.2 \mu\text{M s}^{-1}$ ,  $O_\delta = 0.6 \mu\text{M s}^{-1}$ ;  $\omega = 20$  Hz

We want to summarize the original and insightful results about the long-term effect of gliomodulation. We have identified persistent astrocytic activity as the main protagonist of the long-term gliomodulation effect. Indeed, the excitatory/inhibitory balance of the neural network depends on the presence or the absence of this dynamical regime (see

section 4.4). Nevertheless, the power spectrum analysis can partially shed light on the alteration induced by the glial cells. In this regard, we can appreciate the modulation of GWPS only at the frequency of periodic external input. On the other side, the encoding mechanism of constant external stimulus significantly highlight the presence of astrocytic dynamics in the network activity.

A possible explanation is found in the evaluation of LFP in equation (4.6). The network structure adopted for the original result provides an excitatory recurrent current 20 times lower than the inhibitory one (see values in Table 4.4 and the dynamical behavior in Figure (4.7)). Accordingly, despite the presence of modulation of the inner balance, the weight of recurrent excitation on LFP is lower than the inhibitory counterpart. Therefore, long-term gliomodulation leads to a moderate alteration in LFP that can be observed in power spectrum analysis. The attempt to validate this hypothesis was achieved by studying, with the same methods, the dynamics of balanced network with  $g = 5.0$  (see value in Table 4.1 and the dynamical behavior in Figure (4.5)). In this scenario, indeed, we expect a significant change in the spectrum analysis. However, the situation is not straightforward. As reported in Figure (4.6) the excitatory firing rate is too intense to sustain gliomodulation, thereby, the system does not show persistent astrocytic activity.

# Chapter 5

## CONCLUSIONS

The methods used in this thesis point out the variegated scenario of the complex interplay between neural and glial cells. We want to stress that further efforts in the computational and experimental fields are needed to improve our knowledge about this paramount functional coupling in the CNS.

The starting point of the analyses presented in this work concerns the reproduction of the current knowledge of tripartite synapses. In particular, the consideration of the heterogeneous connection allow us to set the right point of view for further analysis. In this context, indeed, the filter characteristic curve summarizes the dynamical features of this system and how the presence of astrocytes affects synaptic transmission. Therefore, starting from this evidence, the dynamical behaviour concerning the variation of the parameters and the qualitative bifurcation analysis spot the two mechanisms that regulate the gliomodulation: the depletion and the facilitation effects induced by the glial cells. With this procedures, we individuate the gliomodulation for the low frequencies range. This effect is the expression of the most significant aspect of the interplay between neuron and glia: the astrocyte dynamically regulates the transmission modality of synaptic input. Accordingly, we study how these dynamical regulations arise from the intensity of gliomodulation. Specifically, the increase of released gliotransmitters at each exocytosis event leads to dilating facilitation time window. In this modality, the release of neurotransmitters increases with the incoming action potential, which is an emerging feature not arising if we take into account only the neural and synaptic elements.

The above considerations bring to one of the most fascinating aspects of coupled nonlinear dynamical systems: a depletion mechanism does not necessarily provide decreasing effects. We want to highlight that in the field of neuroscience, "plus times minus is minus" is not always observed.

Nevertheless, nonlinearity and the large dimension of phase space remain the obstacles to finding an approximation solution. The importance of an analytical approximation description is not a mere mathematical exercise. The effort to extend the mean field derivation to the homosynaptic connection is justified by the attempt to bridge by a closed function the neural and astrocyte parameters. As we already described, our mean field derivation can reproduce the numerical data shape of the filtering curve only for a restricted range of parameters. The mathematical assumptions are restrictive from the point of view of the real physiology of tripartite synapse. The great limitation comes from the statistical independence between synaptic and astrocytic variables. In this way, we consider the two elements of the system completely disjointed. In other words, we neglect

the main aspect of bidirectional coupling. This leads to another important observation: all the features regarding the dynamical interactions are reflected in the biological guess function that relates the glial to synaptic activity. Accordingly, we estimate this function through a linear fit from numerical data. This suggests that, at least in this framework, the estimation from experimental observation might validate and/or improve our procedure.

The extension on the mesoscopic level of description is not straightforward. In this regard, we want to stress that the adopted model of the neuron-glia network suffers several limitations. Starting from the simple synaptic interaction, we deal with the well-described picture of glutamate regulation on the presynaptic pathway. However, other different neurotransmitters, including GABA, adenosine and endocannabinoid, could also be involved both in presynaptic and postsynaptic pathways of neuro-glia interactions. In addition, not only excitatory but also GABAergic interneurons can engage in astrocyte signalling [73]. In this sense, our model is quite general to be generalised also in the case of other neurotransmitter regulation (by taking into account the relative modulation of basal release probability and/or other synaptic variables) and the inhibitory synapses (by built tripartite synapses also with inhibitory signals).

From the point of view of astrocytes, instead, experimental evidence suggests that single astrocytic processes take part in several tripartite synapses with ongoing synapses from different neurons. In addition, astrocytes are organized in a network structure by gap junctions by which the  $IP_3$  can move from one cell to other. Specifically, this mechanism could deeply characterize the intracellular calcium level and the relative gliomodulation and, as pointed out in this thesis, the network dynamics.

Despite the aforementioned limitations of our modelling approach, we want to emphasize the original and insightful results presented in this thesis. The general framework adopted for the mesoscopic analysis consists to compare the dynamics of baseline condition and the dynamics of the full neuron-glia network. Accordingly, we emphasize the role of STP in the excitatory/inhibitory network. Interesting, the depletion induced by plasticity synapses does not drop the network's activity, contrary it provides an increase in both inhibitory and excitatory population firing rates. Therefore, also in this level of description, the results that come from common sense should lead to an inconsistent conclusion.

From the point of view of astrocytic activity, it is important to stress the consequences at the synaptic level. The sequence of depression and facilitation effects induced by glial activity characterizes the synaptic transmission from presynaptic to postsynaptic terminals. At the microscopic level of description, the activation and inactivation processes of presynaptic receptors make the synapses enable to carry the signal out only at a specific rate which is an emerging property due to the bidirectional coupling between neurons and astrocytes.

The natural question that we try to answer in this thesis is whether the presence of tripartite synapse could also be reflected at the network level. The results suggest that, at least for the adopted model, the introduction of an astrocytic population does not alter the dynamics of the network in terms of the mean quantities of firing rate and LFP. Therefore, in the first order level of analysis, we can not appreciate the role of astrocyte modulation. This is not a surprising result, indeed the models without glial elements well reproduce the mean firing rate of neuronal populations.

However, also at this point of analysis, we can notice an interesting observation concerning the long-term effect. The persistent astrocytic activity involves a consistent decrease in excitatory/inhibitory network balance. Notably, this regulation depends on the different rates of the depressing and facilitating mechanism of presynaptic receptors, as we point out in homosynaptic connection.

Strictly related to the balance regulation, the novel and insightful result is a prominent role of astrocytes in the encoding mechanism of an external periodic signal. Indeed, when we investigate the timing properties of LFP, namely the power spectrum (the second-order level of analysis), we notice that the external stimulus is encoded in a significantly different way in the presence of astrocytic activity. More specifically, we identify a glia-induced frequency filtering behaviour depending also on the amplitude of periodic external input. These original results put the astrocytes as a co-protagonist beside the neurons in the encoding of sensorial stimulus. Therefore, the results presented in this thesis suggest how the functional interplay between neural and non-neural cells in the CNS does not further neglect to obtain a mathematical description of the human brain as close as possible to the real physiological setting.

The general field of neuron-glia computational science, i.e. computational glioscience, is still at its early stage. However, we are tempted to speculate that the general procedure adopted in this thesis might shed light on both functional and pathological the activity of human brain domains that are not completely understood in the context of the classical neuron paradigm.

## Perspectives

The presented work lies in the project with the collaboration of Scuola Superiore Sant'Anna, the Roma Sapienza University and the Camerino University. The purpose of this project is to investigate the glioblastoma multiform and shed new light on the interactions among neurons, tumour cells and glial cells, leading to the identification of novel cellular and molecular therapeutic targets and the validation of non-invasive glioma therapies. The experimental setting is composed of syngeneic glioma cells and patient-derived GBM cells transplanted into the mouse visual cortex. The development of novel therapies requires a better understanding of the bidirectional communication between the tumour and the surrounding brain environment. From the computational perspective, the goal is to extend the present model of the mouse's primary visual cortex [74] to a neuronal-glial one both in healthy and pathological situations. By exploiting such models and comparing the simulated data with experimental ones, we might improve our knowledge of the underpinning physiological mechanisms that drive the development of the disease.

# Appendix A

## Mean field approximation

### A.1 Validity of Mean Field Description

The statistical independence assumption of the variables in mean field derivation induces an error. This approximation error has been estimated for bipartite synapses and heterosynaptic scenarios by the Cauchy-Swarz inequality of probability theory in [28, 15]:

$$\frac{|\langle ab \rangle - \langle a \rangle \langle b \rangle|}{\langle a \rangle \langle b \rangle} \leq \text{CV}_a \text{CV}_b \quad (\text{A.1})$$

$a$  and  $b$  are two generic random variables whereas  $\text{CV}_a$  and  $\text{CV}_b$  are, respectively, the coefficient of variation. Only if  $\text{CV}_a \text{CV}_b < 0.1$  provides a realistic description o synaptic dynamics. In the derivation of the mean field description of homosynaptic connection, the independence between astrocyte and synapses is embedded in the independence of  $u_S$  and  $u_0$ . The coefficient of variation of  $u_0$  with  $\alpha = 0$  is obtained from the equation 3.7

$$\text{CV}_{u_0}^2 = \frac{\langle u_0^2 \rangle - \langle u_0 \rangle^2}{\langle u_0 \rangle^2} = \frac{U_0^{*2}(\langle \Gamma_S^2 \rangle - \langle \Gamma_S \rangle^2)}{(U_0^* - U_0^* \langle \Gamma_S \rangle)^2} = \text{CV}_{\Gamma_S}^2 \frac{\langle \Gamma_S \rangle^2}{(1 - \langle \Gamma_S \rangle)^2} \quad (\text{A.2})$$

The self-consistency of the mean field derivation can now be checked by plotting the product of  $\text{CV}_{u_S}$  and  $\text{CV}_{u_0}$

$$\begin{aligned} \text{CV}_{u_S}^2 &= \frac{\Omega_f(1 - \langle u_0 \rangle)^2 \nu_S}{(\Omega_f + \nu_s)(2\Omega_f + \langle u_0 \rangle(2 - \langle u_0 \rangle)\nu_S)} \\ \text{CV}_{u_0}^2 &= \frac{\langle \Gamma_S \rangle^2}{(1 - \langle \Gamma_S \rangle)^2} \frac{\Omega_G^2}{(\Omega_G + (1 - \beta)\nu_A)(\Omega_G + (1 + \beta)\nu_A)} \end{aligned} \quad (\text{A.3})$$

where  $\beta = \exp - J_S U_A$ . In section 3.2.2 we have elucidated that the activation and deactivation process of presynaptic receptors regulate the modulation of  $u_0$ , accordingly these mechanisms handle the validity of statistical independence. Indeed, the reactivity of  $\Gamma_S$  dynamics for high values of the rates  $\Omega_G$  and  $\Omega_G$  leads to the coefficient of variation exceeding the 10% in the neighbour of  $\nu_S = 1.0$  spk/s as reported in Figure (A.1)

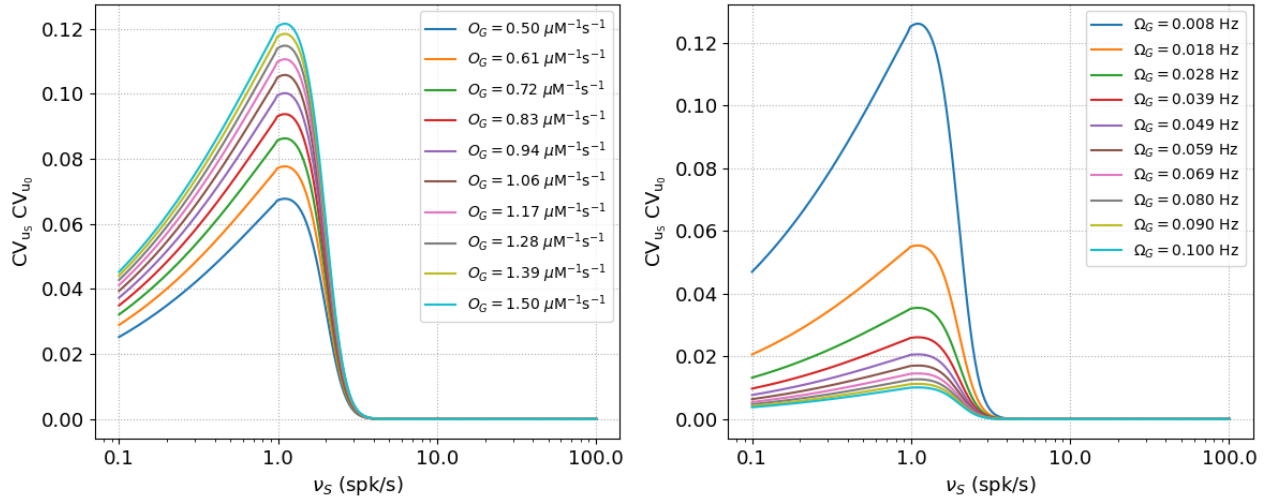


Figure A.1: **Validation of mean field approximation for homosynaptic scenario.** Validation of statistical independence with respect to  $O_G$  (left panel) and  $\Omega_G$  (right panel). Parameters: (left panel)  $\Omega_G = 0.0083 s^{-1}$ ,  $O_\beta = 3.2 \mu M s^{-1}$ ,  $O_\delta = 0.6 \mu M s^{-1}$ ; (right panel)  $O_G = 1.5 \mu M^{-1}s^{-1}$ ,  $O_\beta = 3.2 \mu M s^{-1}$ ,  $O_\delta = 0.6 \mu M s^{-1}$

# Appendix B

## Supplementary numerical material

In this appendix, we describe the adopted implementation procedure to generate and analyse the data. Then, we focus on the issues for the generation and the simulation of the neuron-glia network and the choice of integration step.

### B.1 Description of the code

We report in this appendix a brief sketch of implemented codes.

The codes are written in Python, exploiting the optimized function in common scientific packages. The time evolution of dynamical variables is implemented through the Brian2 simulator [16, 76]. Brian2 is an open-source python simulator for spiking neural networks, designed to be easy to learn and use, highly flexible and easily extensible. It allows the users to build their network with extensive elasticity, both at the structural level and in the choice of integration methods of single elements. Moreover, Brian2 optimizes the simulation of large networks of dynamical systems. We exploit this feature both for network simulation and bifurcation analysis.

From the point of view of computation, the neural network is a collection of objects that share several features. For instance, all the neurons share the dynamical model and parameters such as refractory time, reset and threshold value. Accordingly, in Brian2 neurons are represented by objects of *NeuronGroup*. Each *NeuronGroup* object models the activity of a group of neurons with identical dynamics, i.e. the same differential equation. In particular, the refractory and the reset condition defined the spiking activity. The connections between neurons are modelled by the *Synapses* class. Analogously to the *NeuronsGroup*, a synapse object is defined by the dynamics time course of the variable. The *on\_pre* keyword denotes the action that should be executed on the arrival of a presynaptic action potential. The random connectivity is provided by the *connect* method. The dynamics of the astrocyte's state variables can be implemented by a *NeuronGroup* object, exactly in the same way as neural variables. In terms of gliorelease, the astrocyte is an integrate and fire like element. Accordingly, the combination of the *threshold* and *reset* arguments provides the gliorelease event. Finally, the last step is connected by another synaptic object the astrocyte and the synapses to complete our description of the neuron-glial network in equation 4.4. In the same way, it is possible to build a network with a noninteracting element (uncoupled ordinary differential equations) that share the same dynamics with different value of selected control parameters. We exploit this method to optimize the bifurcation analyses.

Once obtained the network structure, the method *run* initializes the start of the sim-

ulation for the selected time duration. The recording step is provided by the Brian2 function *StateMonitor* and *PopulationRateMonitor*. The former allows the user to record the dynamical variables with a defined time step (that can be different from the integration step). The latter, instead, monitors the instantaneous population firing rate each time step. Any binning procedure is implemented after the record by the *smoothing* function.

The Fourier Transform and the Continuous Wavelet Transform are computed respectively by Scipy and PyWavelets packages. With SciPy has also been determined fit (*scipy.optimize.curve\_fit* function). The following methods and procedures are implemented by scratch using also Numpy ad Python built-in functions: bifurcation procedure and period evaluation,  $\chi^2$  test and standard error over different trials, modulation of power spectra. More precisely:

- Standard error. The error over 30 different trials for the mean value of monitored quantities is computed through the propagation of error,  $\Delta f = \sqrt{\frac{\partial f^2}{\partial x} \Delta x^2}$ . In the case of a few trials, 5 as section 4.5, we estimate the maximum error, i.e.  $(\text{Max} - \text{Min})/2$ . In both scenarios, we implemented the above formula using Numpy arrays. Given the sample and the mean field equation, we compute the  $\chi^2$  test exploit the Numpy arrays.
- Bifurcation. The adopted procedure used to compute the bifurcation plots is quite general and can be applied to general nonlinear dynamical systems. Here we describe the method used o reproduce the plots in Chapter 3. Let's consider a vector field:

$$\frac{d\mathbf{x}}{dt} = f(\mathbf{x}, \tilde{\mu}) \quad (\text{B.1})$$

where  $\mathbf{x} \in U \subset \mathbb{R}^n$  and  $\tilde{\mu} \in \mathbb{R}$  is the control parameter. To evaluate the qualitative changes induced by a small variation of  $\tilde{\mu}$ , we perform the following steps:

1. select the range of investigated control parameters:  $\tilde{\mu} \in [\tilde{\mu}_{min}, \tilde{\mu}_{max}]$ ;
2. built a *NeuronGroup* where each element, namely each ODE, is defined by the same equation (B.1) with a different value of  $\tilde{\mu}$ . In this way, we optimize the numerical solution of several systems;
3. monitor the time evolution of selected variables  $\mathbf{x}$  simultaneously for each  $\tilde{\mu}$ , such as  $C$  in the G-ChI model.
4. extrapolate from the signals the value of interest, such as minimum and maximum values of  $C$ ;
5. plot the values of interest regarding the respective control parameter.

In the case of a noisy system, we repeat this procedure 30 times for different noise realizations and report the values of interest as (mean  $\pm$  standard error). A similar procedure is adopted for the periods in section 2.1.3, in point 3 we monitor the time of presentation of the local maxima and, from this value, compute the period of the oscillation.

- Modulation. Let's consider a signal  $y(t)$  such as the LFP for the total time simulation in chapter 4. To evaluate the equation (2.49), we follow the above procedure:

1. we compute the CWT through PyWaletet packages to obtain a matrix  $P_{i,j}$ . The index  $i$  runs over the total investigated frequencies ( $i = 1, \dots, N_\omega$ ) and the index  $j$  runs over the total number of points in the numerical time grid ( $j = 1, \dots, T/h$ );
2. we evaluate the GWPS as the mean pf  $P_{i,j}$  over the selected time windows for the baseline and the signal of interest. Accordingly, we have two power spectra of the same shape;
3. we compute the modulation described in (2.49) using Numpy arrays.

## B.2 Neuron-glia network implementation and simulation

The adopted model of the neuron-glia network in section 4.1 is implemented by the general procedure described in the previous paragraph. The aim of Chapter 4 is to study the response of the neuron-glia network to external input. Therefore, we fixed the neuron-to-neuron and astrocyte-to-synapse connectivities for all the simulations. In Figure (B.1) we reported the size of the network both in terms of number of elements and connections, and the representation of connectivity matrix  $C_{i,j}$ .

$N_e$	3200
$N_i$	800
$N_{\text{exc syn}}$	639388
$N_{\text{inh syn}}$	639263
$N_a$	4000
$N_{\text{syn-to-astro}}$	639388
$N_{\text{astro-to-astro}}$	639388

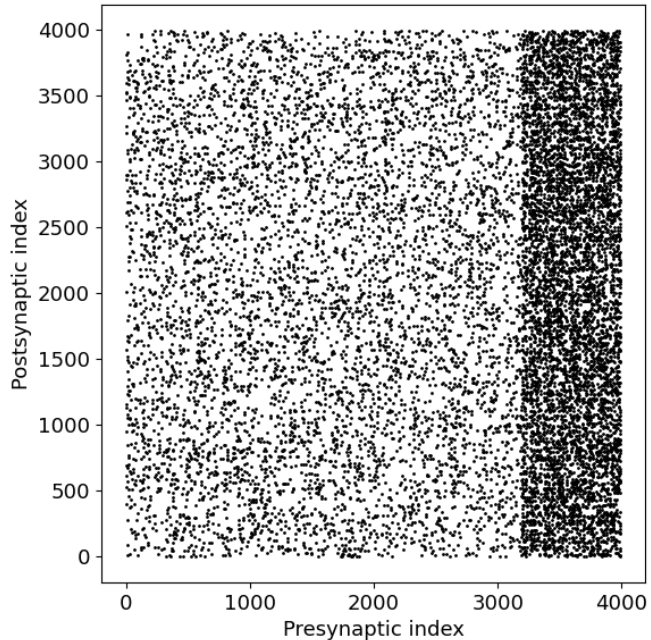


Figure B.1: **Neuron-glia network structure.** (Left) Table of elements in the network. (Right) Connectivity matrix  $C_{i,j}$ , the coupling of presynaptic neuron  $i$  with postsynaptic neurons  $j$  is represented as a black dot in the matrix. The different level of dot density in the matrix stands for the network balance between the ingoing excitatory and inhibitory recurrent connections. The plot illustrates the connectivity of 400 neurons. Parameters  $g = 0.25$ .

The realization of the connectivity between astrocytes and synapses  $A_{l,m_l}$  is more demanding. As reported in Figure (B.1) the matrix  $A_{l,m_l}$  is composed by  $N_a \cdot N_{\text{exc syn}}$  elements. This connectivity is built by the following procedure:

- each excitatory synapse is characterized by the index of its postsynaptic neurons;

- The coupling between the synapse and the astrocyte occurs when the index of the postsynaptic neuron is equal to the index of the astrocyte.

With this procedure, all the excitatory synapses ingoing to the neurons  $i$  take part in a tripartite synapse with the astrocyte  $i$  with  $i = 1, \dots, 4000$ , as reported in Figure (B.2).

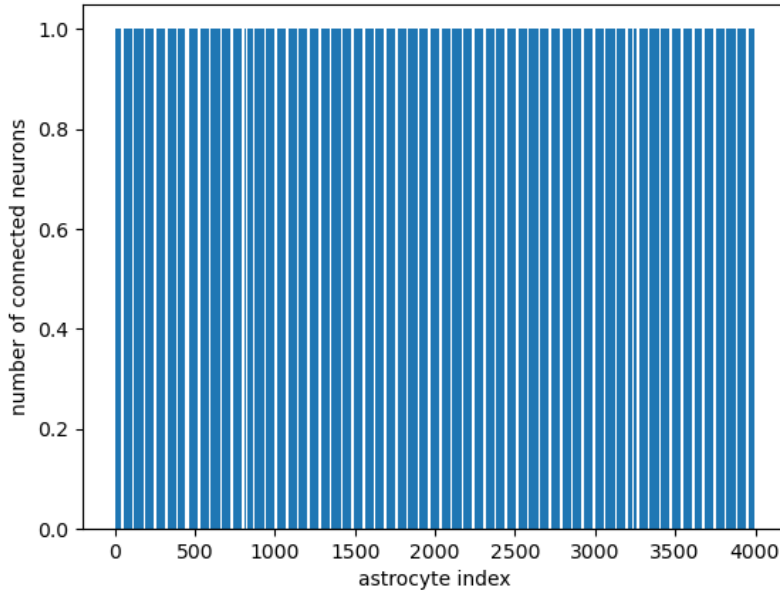


Figure B.2: **Astrocyte-to-Neuron connectivity distribution.** Connectivity distribution between astrocytes and neurons. According to the connectivity matrix  $A_{l,m_l}$ , each astrocyte is coupled with the ingong excitatory synapses of a single neuron.

The simulation of this network requires sustained computational efforts, especially for long-time simulation reported in section 4.4 and 4.5. The great issue is the allocation of several quantities concerning both neural (LFP and recurrent currents) and astrocytic (intracellular calcium concentration) quantities during the simulation. To avoid computational issues related to the limited memory, we exploit the Brian2 method to tackle this problem. The data for the long-term simulation are collected with this procedure:

- simulate the neuron-glia network for a window of 10 s long time;
- save the data;
- clear the memory;
- continue the simulation for the following time window.

The computational time for each time window is circa 55 min, thus each runs requires at least 9 hours<sup>1</sup>.

---

<sup>1</sup>This computational time refers to the simulation with the second-order Runge-Kutta method for the astrocytes. The simulation with the fourth-order method takes more than 4 hours for a single time window.

### B.3 Integration steps

In Chapter 3, the synaptic transmission is achieved by simulating The TM model of plasticity synapses, The G-ChI model of astrocytic activity and the time evolution of the fraction of presynaptic receptor  $\Gamma_S$ . The respective integration steps are chosen by looking at the time scale of their dynamical time course.

For the astrocytic model the integration steps is  $h_a = 0.01$  s, also in agreement with other simulation present in the literature [15, 16].

The characteristic time scale of TM variables  $u_S$  and  $x_S$  is settled by the depression and facilitation rate  $\Omega_d$  and  $\Omega_f$  in the order of seconds as reported in section C.1. Instead, the fraction of presynaptic receptor dynamics is characterized by the activation rate  $\Omega_G$  (order of tons of second) and the deactivation rate  $O_G G_A$ . For the values of the astrocytic activity in the range  $[10^{-3}, 10^1]$  gre/s, the mean values of  $G_A$  are given by the equation 2.30 and reported in Figure (B.3). Accordingly, the time scale related to decreasing (deactivation) is in order of seconds. The integration steps for TM variables and presynaptic receptors is  $h_s = 1$  ms, in agreement with similar analysis presented in [21, 16].

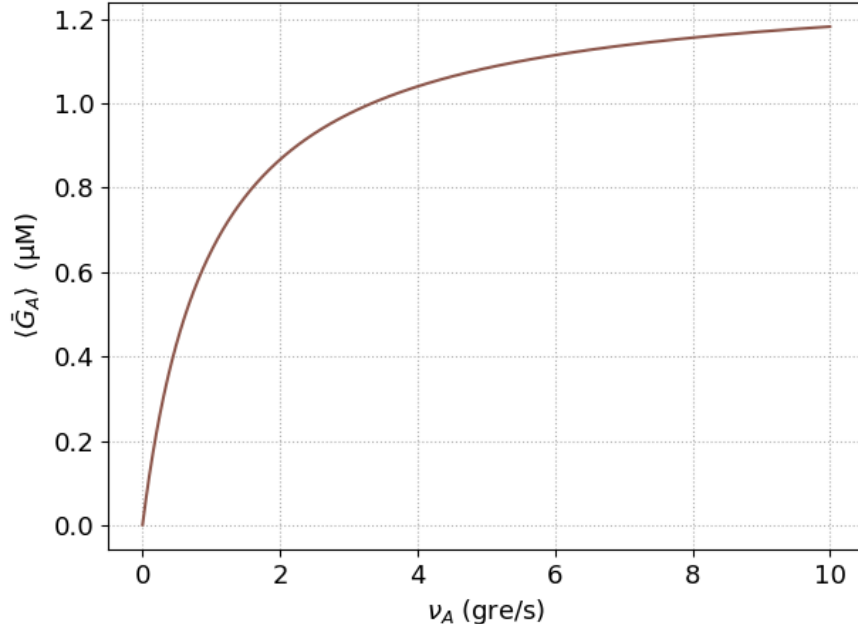
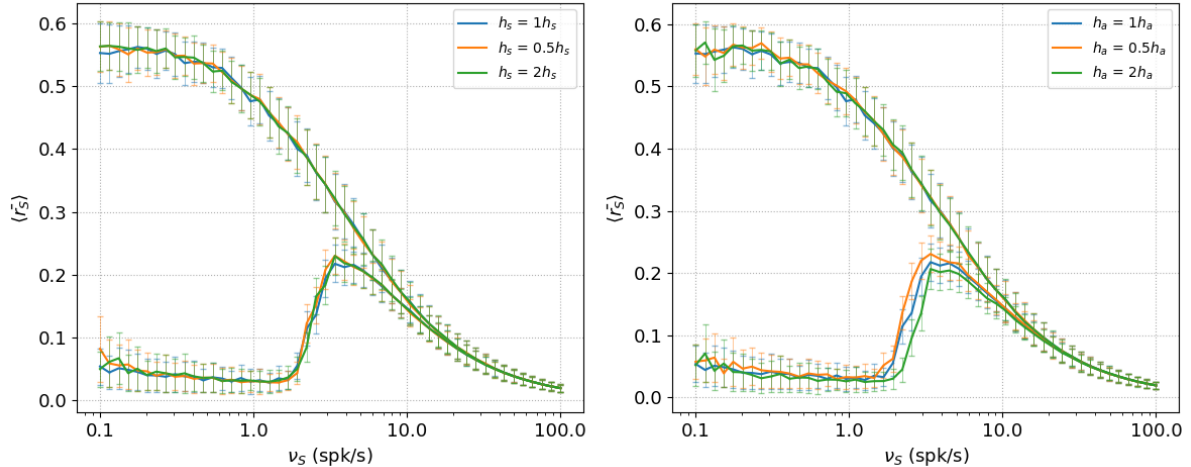


Figure B.3: **Average value of gliotransmitters concentration in the synaptic cleft.** The plots represent the relation  $\langle \bar{G}_A \rangle = \frac{\rho_e G_T}{\Omega_e} U_A \langle \bar{x}_A \rangle \nu_A$ . The time scale of the deactivation mechanism can be estimated by the product of  $\langle \bar{G}_A \rangle O_G$ . In particular for  $\nu_A = 0.2$  gre/s the rate is 108 mHz.

The robustness of synaptic transmission concerning the choice of integration steps is evaluated by simulating the characteristic curve with halving and doubling integration steps  $h_s$  and  $h_a$ . The result in Figure (B.4) elucidates that the qualitative behaviour does not change regarding the choice of integration step.



**Figure B.4: Validation of integration steps in synaptic transmission.** (Left panel) Characteristic curve concerning different  $h_s$  with  $h_a = 0.01\text{s}$ . (Right panel) Characteristic curve concerning different  $h_a$  with  $h_s = 1\text{ms}$ . Both plots elucidate that the qualitative behaviour of STP bipartite synapse and homosynaptic connection tripartite one is not affected by the choice of integration step. Mean value and standard error are computed over 10 different trials for each values of  $\nu_S$ .

More delicate is the evaluation of optimal integration step  $h_n$  for integrate and fire model. For this family of neural models, indeed, the choice of integration step has a crucial consequence on the neural firing rate [75]. To elucidate this point, let's consider a deterministic integrate and fire model with constant external input  $I_{ext}$ :

$$C_m \frac{dV}{dt} = g_l(E_l - V) + I_{ext}. \quad (\text{B.2})$$

The firing rate of this model is computed for  $h_n \in [0.01, 10]$  ms with second order Runge-Kutta integration scheme described in equation (2.2). As reported in left panel of Figure (B.5), the firing rate generated by the model with  $I_{ext} = 120$  pA is deeply influenced by the value of  $h_n$ . However, a close inspection points out that the firing rate converges with decreasing value of integration steps. The firing rate's dependence on the integration step is not a mere computational issue but involves also physiological properties like an input-output characteristic curve reported in right panel of Figure (B.5).

For our neuron-glia network, we chose  $h_n = 0.05$  ms according to the evidence that, in the neighbourhood of this value, the firing rate does not present dependence on integration steps. Also in this context, we evaluate the robustness of the original results presented in Chapter 4 regarding the integration step by simulating the dynamics with the same procedure of synaptic transmission. According to the above consideration, the qualitative behaviour of the neuron-glia network does not show any dependence on the integration step both in terms of recurrent balance (left panel) and power spectra modulation (right panel) as shown in Figure (B.6).

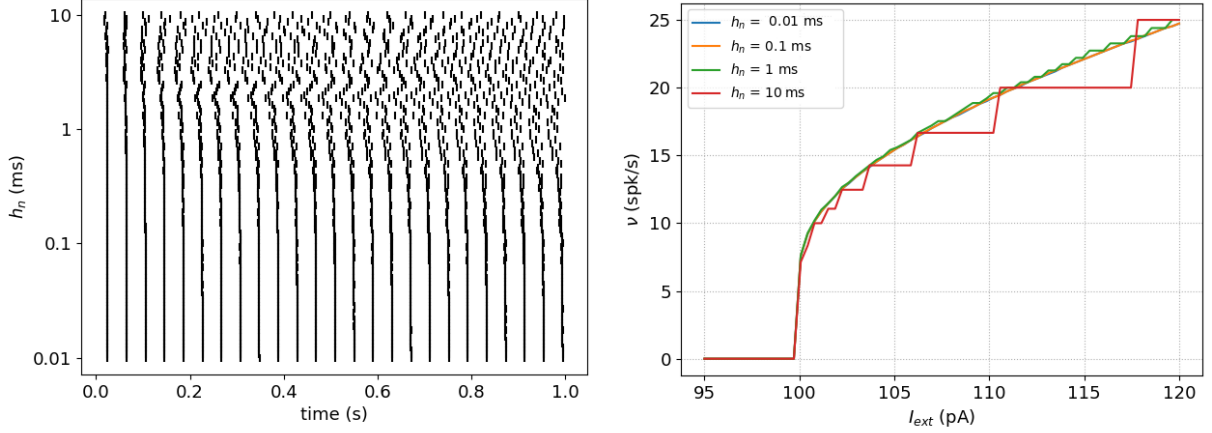


Figure B.5: **Validation of integration steps of Integrate and Fire model.** (Left panel) Raster plots of IF model with respect to integration step  $h_n$ , constant external input  $I_{ext} = 120$  pA. (Right panel) Input-output characteristic curve for 4 different values of  $h_n$ , time simulation is 15 s for each input  $I_{ext}$ .

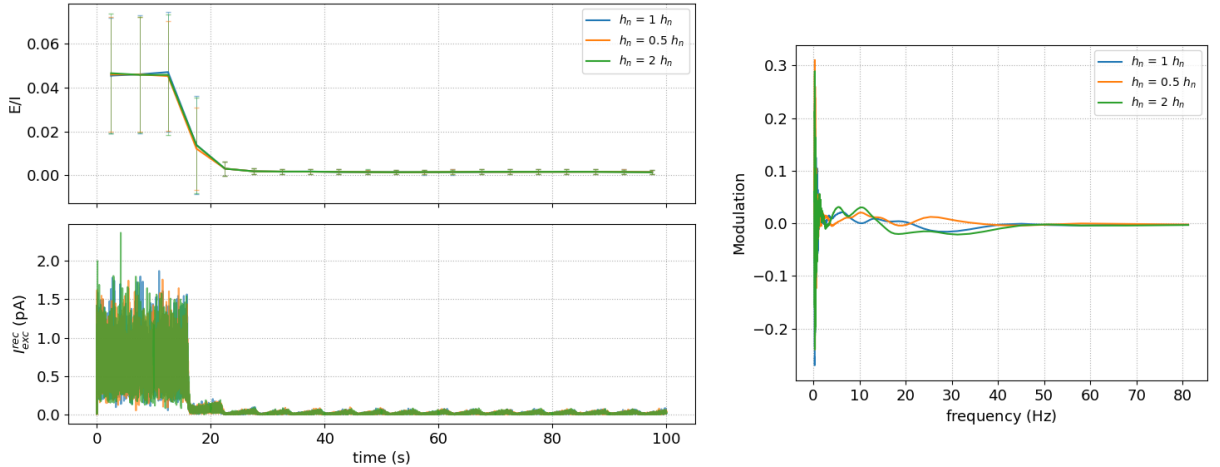


Figure B.6: **Validation of integration steps of neural-glia network.** (Left panel) E/I ratio (top) and excitatory recurrent current (bottom) with respect to integration step  $h_n$ . The data are computed with the same procedure of section 4.4 with the same external input. The qualitative behaviour is not affected by the choice of the integration step. (Right panel) Modulation of GWPS with respect to  $h_n$ . The data are computed with the same procedure in section 4.5. The qualitative behaviour is not affected by the choice of the integration step.

# Appendix C

## Parameters

Values of parameters used in the simulation are summarized the following tables. Parameters values are taken from previous published studies [17].

For instance,  $d_i$  for  $i = 1, 2, 3, 5$  where obtained from a reduction method that leads to Li-Rinzel model from De Young-Keizer one, for detailed derivation see [12]. Astrocytic parameters are taken from [19, 17].

### C.1 Neurons ans Synapses

Symbol	Name in code	Value	Units	Description
<i>Neuron parameters</i>				
$C_m$	C_m	198	pF	Membrane capacitance
$E_i$	E_i	-60	mV	Leak reversal potential
$g_l$	g_l	9.99	nS	Leak conductance
$V_r$	V_r	-60	mV	Reset potential
$V_\theta$	V_th	-50	mV	Firing threshold
$\tau_r$	tau_r	5	ms	Refractory period
<i>Synapses parameters</i>				
$\Omega_d$	Omega_d	2	s <sup>-1</sup>	Synaptic depression rate
$\Omega_f$	Omega_f	3.33	s <sup>-1</sup>	Synaptic facilitation rate
$Y_T$	Y_T	500	mM	Total vesicular neurotransmitter concentration
$\rho_c$	rho_c	0.005	-	Synaptic vesicle-to-extracellular space volume
$\Omega_c$	Omega_c	40	Hz	Synaptic vesicle-to-extracellular space volume
$U_0$	U_0	0.6	-	Resting synaptic release probability
$w_e$	w_e	50	pS	Excitatory synaptic conductance
$w_i$	w_i	1	nS	Inhibitory synaptic conductance
$\tau_e$	tau_e	5	ms	Excitatory synaptic time constant
$\tau_i$	tau_i	10	ms	Inhibitory synaptic time constant
$E_e$	E_e	0	mV	Excitatory synaptic reversal potential
$E_i$	E_i	-80	mV	Inhibitory synaptic reversal potential
<i>Presynaptic receptors</i>				
$O_G$	O_G	1.5	$\mu\text{M}^{-1}\text{s}^{-1}$	Activation rate per mole
$\Omega_G$	Omega_G	0.5	$\text{min}^{-1}$	Synaptic facilitation rate

## C.2 Astrocyte

Symbol	Name in code	Value	Units	Description
<i>Ca<sup>2+</sup>-induced Ca<sup>2+</sup> release</i>				
$C_T$	C_T	2	μM	Total cell free Ca <sup>2+</sup> content
$\rho_A$	rho_A	0.18	-	ER-to-cytoplasm volume ratio
$d_1$	d_1	0.13	μM	IP <sub>3</sub> binding affinity
$d_2$	d_2	1.05	μM	Ca <sup>2+</sup> inactivation dissociation constant
$d_3$	d_3	0.9434	μM	IP <sub>3</sub> dissociation constant
$d_5$	d_5	0.08	μM	Ca <sup>2+</sup> activation dissociation constant
$O_2$	O_2	0.2	μM s <sup>-1</sup>	IP <sub>3</sub> R binding rate for Ca <sup>2+</sup> inhibition
$\Omega_C$	Omega_C	6	s <sup>-1</sup>	Maximal rate of Ca <sup>2+</sup> release by IP <sub>3</sub> Rs
$\Omega_L$	Omega_L	0.1	s <sup>-1</sup>	Maximal rate of Ca <sup>2+</sup> leak from the ER
$O_P$	O_P	0.9	μM s <sup>-1</sup>	Maximal Ca <sup>2+</sup> uptake rate by SERCAs
$K_P$	K_P	0.05	μM	Ca <sup>2+</sup> affinity of SERCAs
<i>IP<sub>3</sub> signaling</i>				
$O_\beta$	O_beta	0.5	μM s <sup>-1</sup>	Maximal rate of IP <sub>3</sub> production by PLC $\beta$
$O_\delta$	O_delta	1.2	μM s <sup>-1</sup>	Maximal rate of IP <sub>3</sub> production by PLC $\delta$
$\kappa_\delta$	kappa_delta	1.5	μM	Inhibition constant of PLC $\delta$ by IP <sub>3</sub>
$K_\delta$	K_delta	0.1	μM	Ca <sup>2+</sup> affinity of PLC $\delta$
$O_{3K}$	O_3K	4.5	μM s <sup>-1</sup>	Maximum rate of IP <sub>3</sub> degradation by IP <sub>3</sub> -3K
$K_{3K}$	K_3K	1.0	μM	IP <sub>3</sub> affinity of IP <sub>3</sub> -3K
$K_D$	K_D	0.7	μM	Ca <sup>2+</sup> affinity of IP <sub>3</sub> -3K
$\Omega_{5P}$	Omega_5P	0.05	s <sup>-1</sup>	Maximal rate of IP <sub>3</sub> degradation by IP-5P
<i>Metabotropic receptor kinetics</i>				
$O_N$	O_N	0.3	μM <sup>-1</sup> s <sup>-1</sup>	Agonist binding rate
$\Omega_N$	Omega_N	0.5	s <sup>-1</sup>	Maximal inactivation rate
$K_{KC}$	K_KC	0.5	μM	Ca <sup>2+</sup> affinity of PKC
$\zeta$	zeta	10	-	Maximal reduction of receptor affinity by PKC
<i>Gliotrasmission</i>				
$C_\theta$	C_theta	0.5	μM	Ca <sup>2+</sup> threshold for exocytosis
$G_T$	G_T	200	mM	Total vesicular Gliotransmitter concentration
$\Omega_A$	Omega_A	0.6	s <sup>-1</sup>	Gliotransmitter recycling rate
$U_A$	U_A	0.6	-	Gliotransmitter release probability
$\rho_e$	rho_e	6.5 10 <sup>-4</sup>	-	Astrocytic vesicle-to-extracellular volume ratio
$\Omega_e$	Omega_e	60	s <sup>-1</sup>	Gliotransmitter clearence rate
$\alpha$	alpha	0	-	Gliotrasmission nature

# Bibliography

- [1] Verkhratsky A., Butt A. *Glial Neurobiology. A Textbook*, John Wiley Sons Ltd, 1rs eds. (2007)
- [2] De Pittà M. Neuron-Glia Interactions, In: Jaeger D., Jung R. (eds) *Encyclopedia of Computational Neuroscience*. Springer, New York, NY. (2020)
- [3] Somjen G.G. Nervenkitt: notes on the history of the concept of neuroglia. *Glia* vol.1, pp.2-9. (1988)
- [4] Virchow R. *Die Cellularpathologie in ihrer Begründung auf physiologische und pathologische Gewebelehre*. Berlin: August Hirschwald (1858).
- [5] Nave K.A. Myelination and support of axonal integrity by glia. *Nature* vol.468, pp.244-252. (2010)
- [6] Kettenmann H. et al. Physiology of microglia. *Physiological reviews* vol.91, pp.461-553. (2011)
- [7] Perea G. et al. Neuron-glia networks: integral gear of brain function, *Frontiers in Cellular Neuroscience* vol.8. (2014)
- [8] Hertz L. Possible role of neuroglia: a potassium-mediated neuronal-neuroglial-neuronal impulse transmission system. *Nature* vol.206, pp.1091-1094. (1965)
- [9] Amzica F. et al. Spatial buffering during slow and paroxysmal sleep oscillation in cortical networks of glial cells in vivo. *Journal of Neuroscience* vol.22, pp.1042–1053. (2002)
- [10] Berridge M. et al. The versatility and universality of calcium signalling, *Nat . Rev. Mol. Cell. Biol.* vol.1, pp.11-21. (2000)
- [11] De Pittà M., Berry H. A Neuron-Glia Perspective for Computational Neuroscience. In: De Pittà, M., Berry, H. (eds) *Computational Glioscience*. Springer Series in Computational Neuroscience. Springer, Cham. (2019)
- [12] Timofeeva J. Intracellular Calcium Dynamics: Biophysical and Simplified Models. In: De Pittà, M., Berry, H. (eds) *Computational Glioscience*. Springer Series in Computational Neuroscience. Springer, Cham. (2019)
- [13] De Pittà, M., Ben-Jacob, E., Berry, H. G Protein-Coupled Receptor-Mediated Calcium Signaling in Astrocytes. In: De Pittà, M., Berry, H. (eds) *Computational Glioscience*. Springer Series in Computational Neuroscience. Springer, Cham. (2019)

- [14] Lalloquette J. et al. Astrocyte Networks and Intercellular Calcium Propagation. In: De Pittà, M., Berry, H. (eds) *Computational Glioscience*. Springer Series in Computational Neuroscience. Springer, Cham. (2019)
- [15] De Pittà M., Gliotransmitter Exocytosis and Its Consequences on Synaptic Transmission. In: De Pittà, M., Berry, H. (eds) *Computational Glioscience*. Springer Series in Computational Neuroscience. Springer, Cham. (2019)
- [16] Stimberg M., et al. Modeling Neuron–Glia Interactions with the Brian 2 Simulator. In: De Pittà, M., Berry, H. (eds) *Computational Glioscience*. Springer Series in Computational Neuroscience. Springer, Cham. (2019)
- [17] De Pittà M., Brunel N. Modulation of Synaptic Plasticity by glutammatergic Glio-transmission: A Modeling Study, *Neural Plasticity* vol.2016. (2016).
- [18] De Pittà M. et al. Coexistence of amplitude and frequency modulations in intracellular calcium dynamics. *Phys Rev E Stat Nonlin Soft Matter Phys.* vol.77. (2008)
- [19] De Pittà M., Goldberg, M., Volman, V. et al. Glutamate Regulation of Calcium and IP<sub>3</sub> Oscillating and Pulsating Dynamics in Astrocytes. *J Biol Phys* vol.35, pp.383–411. (2009)
- [20] De Pittà M., Volman V., Berry H., Ben-Jacob E. A tale of two stories: astrocyte regulation of synaptic depression and facilitation. *PLoS Comput Biol.* vol.7. (2011)
- [21] De Pittà M., Brunel N., Volterra A. Astrocytes: Orchestrating synaptic plasticity? *Neuroscience* vol.323, pp.43-61. (2016)
- [22] Bergersen L.H., Gundersen V. Morphological evidence for vesicular glutamate release from astrocytes. *Neuroscience* vol.158, pp.260-265. (2009)
- [23] Santello M., Volterra A. Synaptic modulation by astrocytes via Ca<sup>2+</sup>-dependent glutamate release. *Neuroscience* vol.158, pp.253-259. (2009)
- [24] Bezzi P. et al. Astrocytes contain a vesicular compartment that is competent for regulated exocytosis of glutamate. *Nat Neurosci* vol.7, pp.613-20. (2004)
- [25] Chen X. et al. "Kiss-and-run" glutamate secretion in cultured and freshly isolated rat hippocampal astrocytes. *The Journal of Neuroscience* vol.25. (2005)
- [26] Gerstner W. et al. Theory and Simulation in Neuroscience. *Science* vol.338, pp.60-65. (2012)
- [27] Tsodyks M.V., Markram H. The neural code between neocortical pyramidal neurons depends on neurotransmitter release probability. *Proc Natl Acad Sci USA* vol.94, pp.719–723. (1997)
- [28] Tsodyks M.V., Pawelzik K., Markram H. Neural networks with dynamic synapses. *Neural Comput* vol.10, pp.821-835. (1998)
- [29] Tsodyks M.V. Activity-dependent transmission in neocortical synapses. In: Chow C, Gutkin B, Hansel D, Meunier C, Dalibard, J (eds) *Methods and models in neuro-physics* Ch.7, pp.245–265, Elsevier. (2005)

- [30] Brunel N. Dynamics of Sparsely Connected Networks of Excitatory and Inhibitory Spiking Neurons. *J Comput Neurosci* vol.8, pp.183–208 (2000).
- [31] Brunel N., Wang X.J. What determines the frequency of fast network oscillations with irregular neural discharges? I. Synaptic dynamics and excitation-inhibition balance. *J Comput Neurosci* vol.90, pp.415-30. (2001)
- [32] Mazzoni A., Panzeri S., Logothetis N.K., Brunel N. Encoding of naturalistic stimuli by local field potential spectra in networks of excitatory and inhibitory neurons. *PLoS Comput Biol* vol.4. (2008)
- [33] Einevoll G.T., Kayser C., Logothetis N.K., Panzeri S. Modelling and analysis of local field potentials for studying the function of cortical circuits. *Nat Rev Neurosci* vol.14, pp.770-85. (2013)
- [34] Cressman, J.R., Ullah, G., Ziburkus, J. et al. The influence of sodium and potassium dynamics on excitability, seizures, and the stability of persistent states: I. Single neuron dynamics. *J Comput Neurosci* vol.26, pp.159–170. (2009)
- [35] Ullah, G., Cressman Jr., J.R., Barreto, E. et al. The influence of sodium and potassium dynamics on excitability, seizures, and the stability of persistent states: II. Network and glial dynamics. *J Comput Neurosci* vol. 26, pp.171–183. (2009)
- [36] Savtchenko Leonid P., Rusakov Dmitri A. Regulation of rhythm genesis by volume-limited, astroglia-like signals in neural networks. *Phil. Trans. R. Soc. B* vol. 369. (2014)
- [37] Palmer Alexandra L. and Ousman Shalina S. Astrocytes and Aging. *Frontiers in Aging Neuroscience* vol 10. (2018)
- [38] Barone J., Rossiter H. Understanding the Role of Sensorimotor Beta Oscillations. *Front. Syst. Neurosci* vol.15. (2021)
- [39] M.P. Mattson. *Stress: Physiology, Biochemistry, and Pathology*. Ch.11, pp. 125-134. Academic Press. (2019)
- [40] Grech N., Dalli T., Mizzi S., Meilak L., Calleja N., Zrinzo A. Rising Incidence of Glioblastoma Multiforme in a Well-Defined Population. *Cureus* vol.12. (2020)
- [41] Poincaré H.J. Sur le problème des trois corps et les équations de la dynamique. *Acta Mathematica* vol.13, pp. 1-270. (1890)
- [42] Strogatz S.H. *Nonlinear Dynamics and Chaos. With Application to Physics, Biology, Chemistry, and Engineering* . CRC Press, 2nd eds. (2015)
- [43] Wiggins S. *Introduction to Applied Nonlinear Dynamical Systems and Chaos*. Springer, 2nd eds, (2003)
- [44] Meiss J.D. *Differential Dynamical Systems*. SIAM. (2008)
- [45] Izhikevich E. M. *Dynamical Systems in Neuroscience: The Geometry of Excitability and Bursting*. The MIT Press Cambridge. (2010)

- [46] Sterratt, D., Graham, B., Gillies, A., Willshaw, D. *Principles of Computational Modelling in Neuroscience*. Cambridge: Cambridge University Press. (2011)
- [47] Ermentrout G.B., Terman D.H. *Mathematical Foundations of Neuroscience*. Springer, Interdisciplinary Applied Mathematics vol. 35. (2010)
- [48] Gerstner W., Kistler W., Naud R., Paninski L. *Neuronal Dynamics: From Single Neurons to Networks and Models of Cognition*. Cambridge: Cambridge University Press, (2014)
- [49] Hodgkin A.L., Huxley A.F. A quantitative description of membrane current and its application to conduction and excitation in nerve. *The Journal of physiology* vol.117, pp.500–544. (1952)
- [50] Hodgkin A.L. The local electric changes associated with repetitive action in a non-medullated axon. *The Journal of Physiology* vol.107, pp.165–181. (1948)
- [51] Izhikevich E.M., FitzHugh R. FitzHugh-Nagumo model. *Scholarpedia* vol.1. (2006)
- [52] Morris C., Lecar H. Voltage oscillations in the barnacle giant muscle fiber. *Biophysical Journal* vol.35, pp. 193-213. (1981)
- [53] Burkitt A.N. A review of the integrate-and-fire neuron model: I. Homogeneous synaptic input. *Biol Cybern* vol.95, pp.1-19. (2006)
- [54] Faisal A.A., Selen L.P.J., Wolpert D. M. Noise in the nervous system. *Nature Reviews Neuroscience* vol.9, pp.292–303. (2008).
- [55] Softky W., Koch C. The highly irregular firing pattern of cortical cells is inconsistent with temporal integration of random EPSPs. *J Neurosci* vol.13, pp.334–350. (1993)
- [56] Skupin A., Falcke M. Statistical analysis of calcium oscillations. *Eur Phys J Spec Top* vol.187, pp.231–240. (2010)
- [57] Keizer J., De Young G.W. Two roles of Ca<sup>2+</sup> in agonist stimulated Ca<sup>2+</sup> oscillations. *Biophys J.* vol.61, pp.649-660. (1992)
- [58] Li Y.X., Rinzel J. Equations for InsP<sub>3</sub> receptor-mediated [Ca<sup>2+</sup>]<sub>i</sub> oscillations derived from a detailed kinetic model: a Hodgkin-Huxley like formalism. *J Theor Biol* vol.166, pp.461-73. (1994)
- [59] Tsodyks M.V., Markram H. The neural code between neocortical pyramidal neurons depends on neurotransmitter release probability. *Proc Natl Acad Sci U S A.* vol.94, pp.719-23. (1997)
- [60] Michaelis L., Menten M.L., et. al. The original Michaelis constant: translation of the 1913 Michaelis-Menten paper. *Biochemistry*. vol.50, pp.8264-9. (2011)
- [61] Araque A., Parpura V., Sanzgiri R.P., Haydon P.G. Glutamate-dependent astrocyte modulation of synaptic transmission between cultured hippocampal neurons. *Eur J Neurosci* vol.10, pp.2129-42. (1998a)
- [62] McKenna T.M., McMullen T.A., Shlesinger M.F. The brain as a dynamic physical system. *Neuroscience* vol.60, pp.587-605. (1994)

- [63] Richmond B.J. Information Coding. In: Jaeger, D., Jung, R. (eds) *Encyclopedia of Neuroscience* pp.137–144. (2009)
- [64] Destexhe A., Bedard C. Local Field Potential *Scholarpedia* vol.8. (2013)
- [65] Bushong A. et al. Protoplasmic Astrocytes in CA1 Stratum Radiatum Occupy Separate Anatomical Domains. *Society for Neuroscience* vol.22, pp.183-192. (2002)
- [66] Barardi A, Garcia-Ojalvo J, Mazzoni A. Transition between Functional Regimes in an Integrate-And-Fire Network Model of the Thalamus. *PLoS One* vol.11. (2016)
- [67] Hujian H., Jonas G.P. Fast-spiking, parvalbumin+ GABAergic interneurons: From cellular design to microcircuit function. *Science* vol.6. (2014)
- [68] Cannelli A. *Metodologie sperimentali in Fisica*. 3rd eds, EdiSES. (2010)
- [69] Aguiar-Conraria L., Joana Soares M. The Continuos Wavelet Transform: Moving Beyond Uni- and Bivariate Analysis. *Journal of Economics Surveys* vol.28, pp.344-375. (2013)
- [70] Pang T. *An Introduction to Computational Physics*. 2nd eds, Cambridge. (2010)
- [71] Gabbiani F., Cox S.J. *Mathematics for Neuroscientists*, Academic Press. (2010)
- [72] A. van der Schaaf, J.H. van Hateren. Modelling the Power Spectra of Natural Images: Statistics and Information. *Vision Research* vol. 36, pp.2759-70. (1996)
- [73] Mederos S., Perea G. GABAergic-astrocyte signaling: A refinement of inhibitory brain networks. *Glia* vol.67, pp.1842-1851. (2019)
- [74] Meneghetti N. et al. Narrow and Broad  $\gamma$  Bands Process Complementary Visual Information in Mouse Primary Visual Cortex. *eNeuro* vol.8 .(2021)
- [75] Harish G., Spigler G. et al. Convergence of regular spiking and intrinsically bursting Izhikevich neuron models as a function of discretization time with Euler method. *Neurocomputing* vol.350, pp.237-247. (2019)
- [76] <https://brian2.readthedocs.io/en/stable/>